CHAPTER IV

RESULTS AND DISCUSSION

4.1 Physical Properties of SBA-15

4.1.1 XRD Pattern of Pure SBA-15

XRD patterns of as-synthesized and calcined SBA-15 sample are shown in Figure 4.1. Assignment of those peaks are known as (100), (110), and (200) reflections, respectively, which are the characteristic pattern of hexagonal mesoporous structures [84]. Peak positions are located at quite low 2-theta values due to the lack of short-range order of its structure. After calcined in air at 550°C for 5 h, the XRD pattern shows that the hexagonal structure is still remained and peak intensity at (100) reflection increases which is resulted from the removal of triblock copolymer template from the pores of materials.

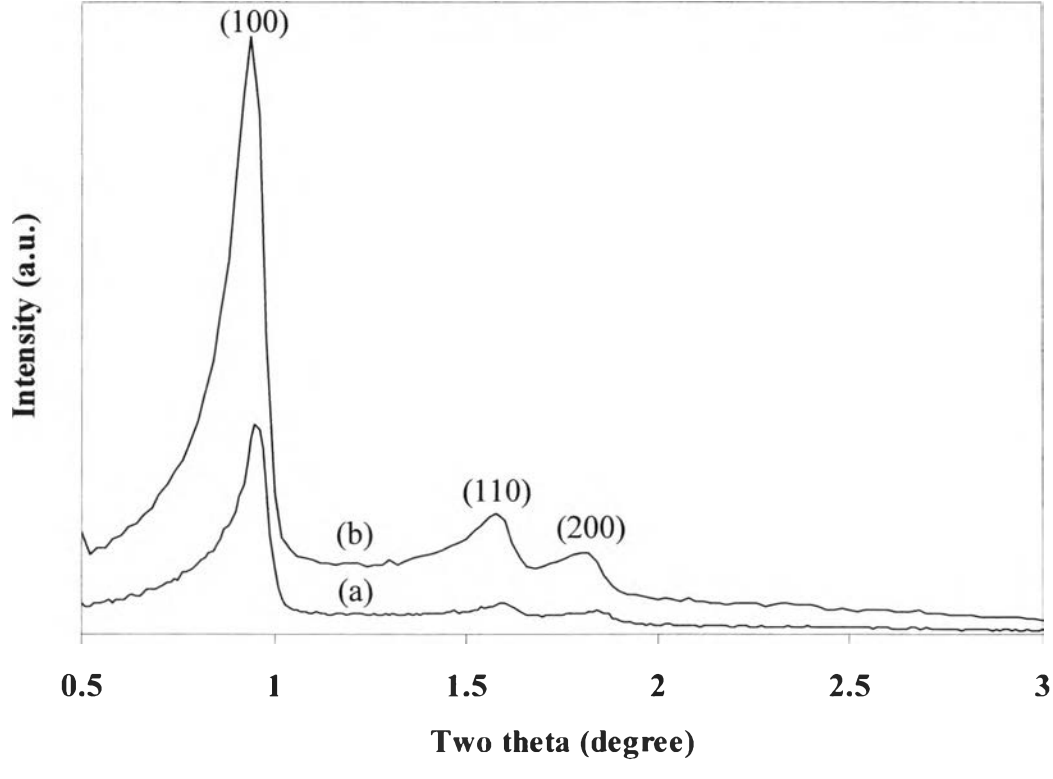

Figure 4.1 XRD patterns of (a) as-synthesized and (b) calcined SBA-15.

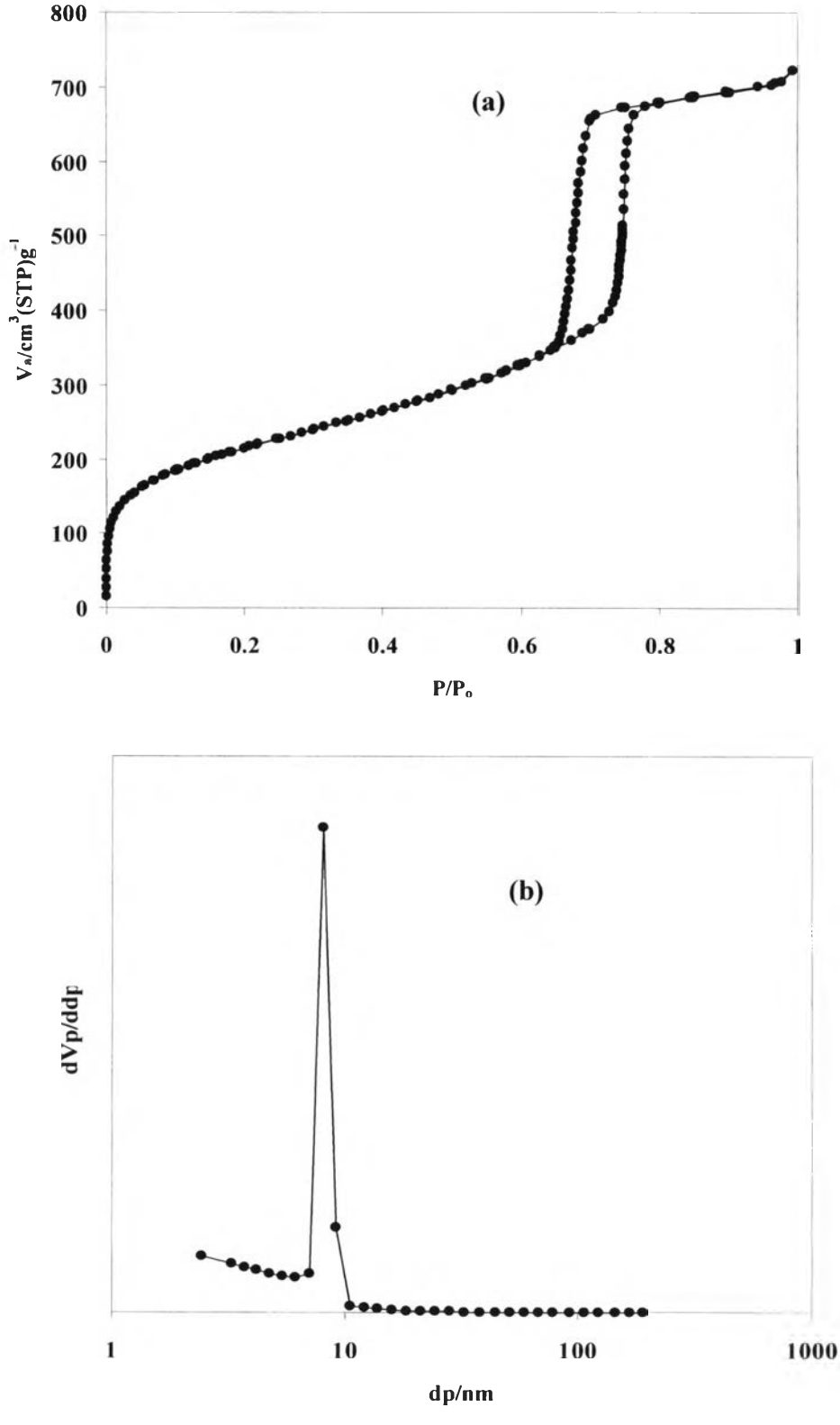

Figure 4.2 (a) Adsorption isotherm and (b) pore size distribution of SBA-15.

4.1.2 Sorption Properties of SBA-15

The adsorption isotherm and pore size distribution of calcined SBA-15 are shown in Figure 4.2(a). It exhibits a type IV adsorption isotherm which is a characteristic pattern of mesoporous materials. Considering the pore size distribution of resulted sample in Figure 4.2(b), narrow pore size distribution was found in SBA-15 at the pore diameter of 8.06 nm. The multipoint Brunauer, Emmett and Teller (BET) method was used in measuring total surface area of SBA-15, which was found at 797 m^2/g.

4.1.3 SEM Images of SBA-15

SEM images of calcined pure silica SBA-15 at different magnifications are shown in Figure 4.3. The SEM images reveal that the calcined SBA-15 consists of a bundle of rope-like particles with uniform size. The SEM images reveal that the calcined SBA-15 consists of small particle size of 50 x 110 nm, which aggregated into rope-like structure.

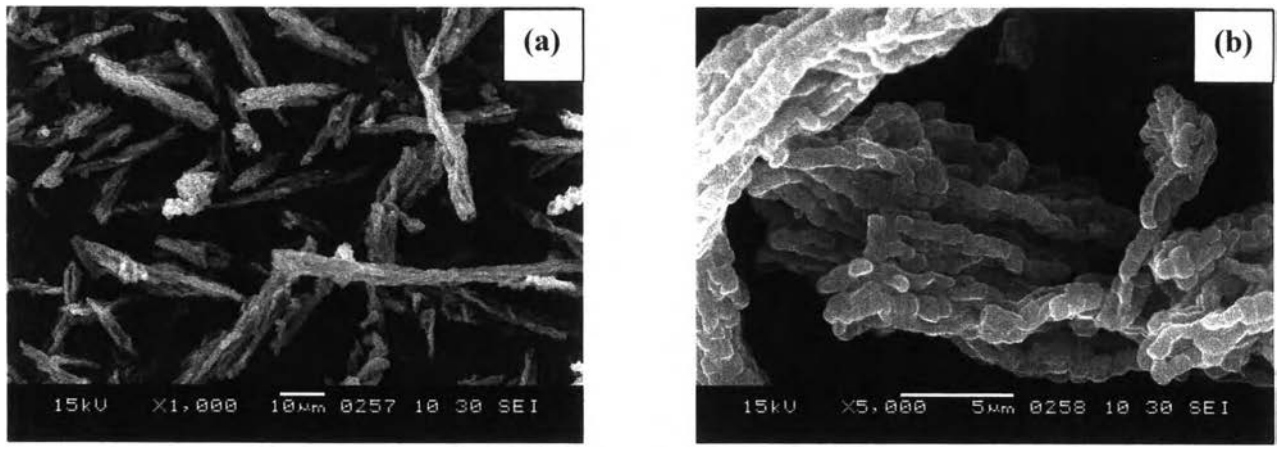

Figure 4.3 The SEM images of calcined pure Si- SBA-15 at different magnifications (a) x 1000 and (b) x 5000

Table 4.1 The summary of transformation products prepared from SBA-15 at various conditions.

Sample	Silica source	$TEAOH/SiO_2$ ratio	crystallization period (h)	yield[a] %	SBA-15/AlP ratio		SEM Particle size (nm)	BET Surface area (m^2/g)	Micropore volume (cm^3/g)	External[c] surface area (m^2/g)	Product phase	NH_3-TPD acidity (mmol/g)		
					In gel	In product[b]						weaker (170°C)	stronger (200°C)	total
Xerogel74	TEOS	-	-	-	-	-	10,000	333	-	313.6	amorphous	n/a	n/a	n/a
SBA-15	TEOS	-	-	-	-	-	50 x 110	797	-	-	SBA-15	n/a	n/a	n/a
Run No.1	SBA-15	0.39	6	n/a	60	n/a	n/a	n/a	n/a	n/a	α-quartz	n/a	n/a	n/a
Run No.2	SBA-15	0.39	12	10.7	60	19.6	128	609	0.29	111.1	BEA	n/a	n/a	n/a
Run No.3	SBA-15	0.39	24	26.9	60	19.9	147	775	0.28	75.7	BEA	n/a	n/a	n/a
Run No.4	SBA-15	0.39	48	42.4	60	20.3	116	765	0.28	84.8	BEA	n/a	n/a	n/a
Run No.5	SBA-15	0.26	48	71.8	60	18.6	215	781	0.31	43.4	BEA	0.71	0.23	0.94
Run No. 6	SBA-15	0.20	48	n/a	60	n/a	n/a	478	n/a	n/a	amorphous	n/a	n/a	n/a
Run No.7	SBA-15	0.10	48	n/a	60	n/a	n/a	430	n/a	n/a	distorted SBA-15	n/a	n/a	n/a
Run No.8	SBA-15	0.26	48	n/a	10	n/a	n/a	346	n/a	n/a	amorphous	n/a	n/a	n/a
Run No.9	SBA-15	0.26	48	79.8	30	13.9	173	782	0.3	106.9	BEA	1.09	0.12	1.21
Run No.10	SBA-15	0.26	48	6.0	90	25.1	211	455	0.51	41.1	BEA	0.51	0.28	0.8
Run No.11	Xerogel	0.26	48	6.7	60	23.2	165	784	0.31	67.9	BEA	n/a	n/a	n/a

[a] Gram of solid per 100 g starting material

[b] Si and Al were determined by XRF

[c] External surface area and micropore volume determined by application of the t-plot method

4.2 Physicochemical Properties of Synthesize Zeolite Beta

4.2.1 Effect of Crystallization Time on Transformation of SBA-15 into Zeolite Beta

4.2.1.1 Powder X-ray Diffraction

The time dependence of transformation of calcined SBA-15 into zeolite beta was studied by using the mixture containing SBA-15/AIP of 60 and $TEAOH/SiO_2$ of 0.39. Figure 4.4 illustrates XRD patterns of as-synthesized zeolite beta synthesized with the SBA-15/AIP in the reactant mixture of 60 and with various crystallization periods from 0-48 h. For the sample obtained after crystallization time of 6 h the characteristic XRD peaks of SBA-15 disappear and no peaks are observed in the whole range of Bragg angle from 0.5° to 40°. When the crystallization period was extended to 12 h, the characteristic XRD peaks were observed and the peak intensities became greater upon longer crystallization time. Therefore, SBA-15 decomposed initially to be an amorphous phase and subsequently transformed further to zeolite beta. For the calcined samples in Figure 4.5, the intensity of peak at 2θ of 7.7^{o} becomes much stronger than the peak at 2θ of 22.5^{o} indicating the effect of template removal from the zeolite beta channels, whereas the intensity of the peak at 2θ of 22.5 is extremely decreased showing that dealumination occur during the calcinations process. The XRD patterns of calcined samples consist of broad features, indicating the co-existence of both polymorph A and B. This common for zeolite beta and two polymorphs are always formed simultaneously and hardly separated. However, the XRD patterns of corresponding calcined products as shown in Figure 4.5 indicate the presence of α-quartz during the transformation of SBA-15 into zeolite beta within 6 h (Figure 4.5b), subsequently to the structure of BEA within 12 h (Figure 4.5c) and completely to the structure of BEA with in 24 h (Figure 4.5d). The phase of α-quartz was unrevealed in the XRD patterns of as-synthesized samples due to the presence of organic template. The zeolite crystallinity did not significantly change during crystallization for longer than 24 h. A parallel experiment was also carried out by conversion of silica xerogel to the structure of BEA. It is similar that the α-quartz phase was also observed during the transformation of silica xerogel to the BEA structure. These results suggest that SBA-15 is not transformed directly into zeolite beta but via the formation of an intermediate of α-quartz. It is in related to the

fact that high concentration of OH^- can cause formation of quartz during the synthesis of a silica rich zeolite. The transformation can be explained that SBA-15 firstly decomposed in an alkaline solution of TEAOH and transformed into a crystalline phase of α-quartz within 6 h and then subsequently to zeolite beta.

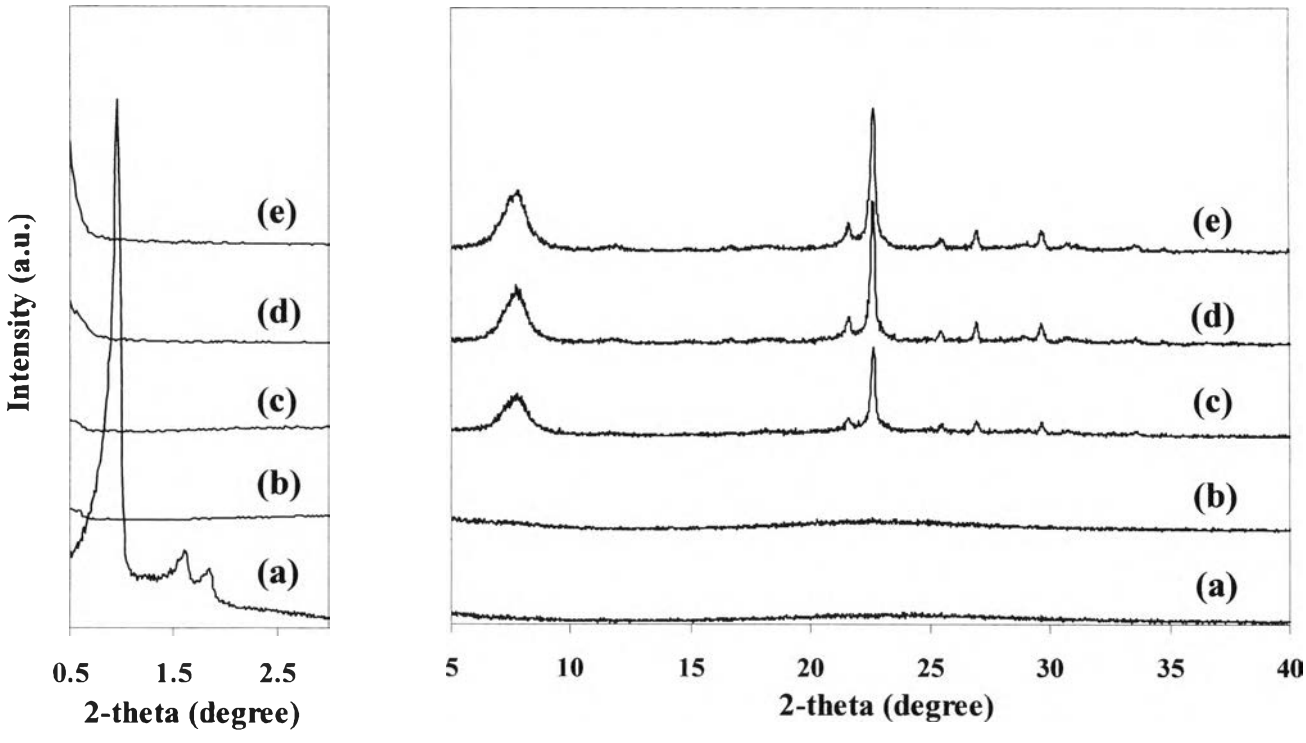

Figure 4.4 XRD patterns of as-synthesized products transformed from SBA-15 at various crystallization periods (a) 0 h; (b) 6 h; (c) 12 h; (d) 24 h and (e) 48 h.

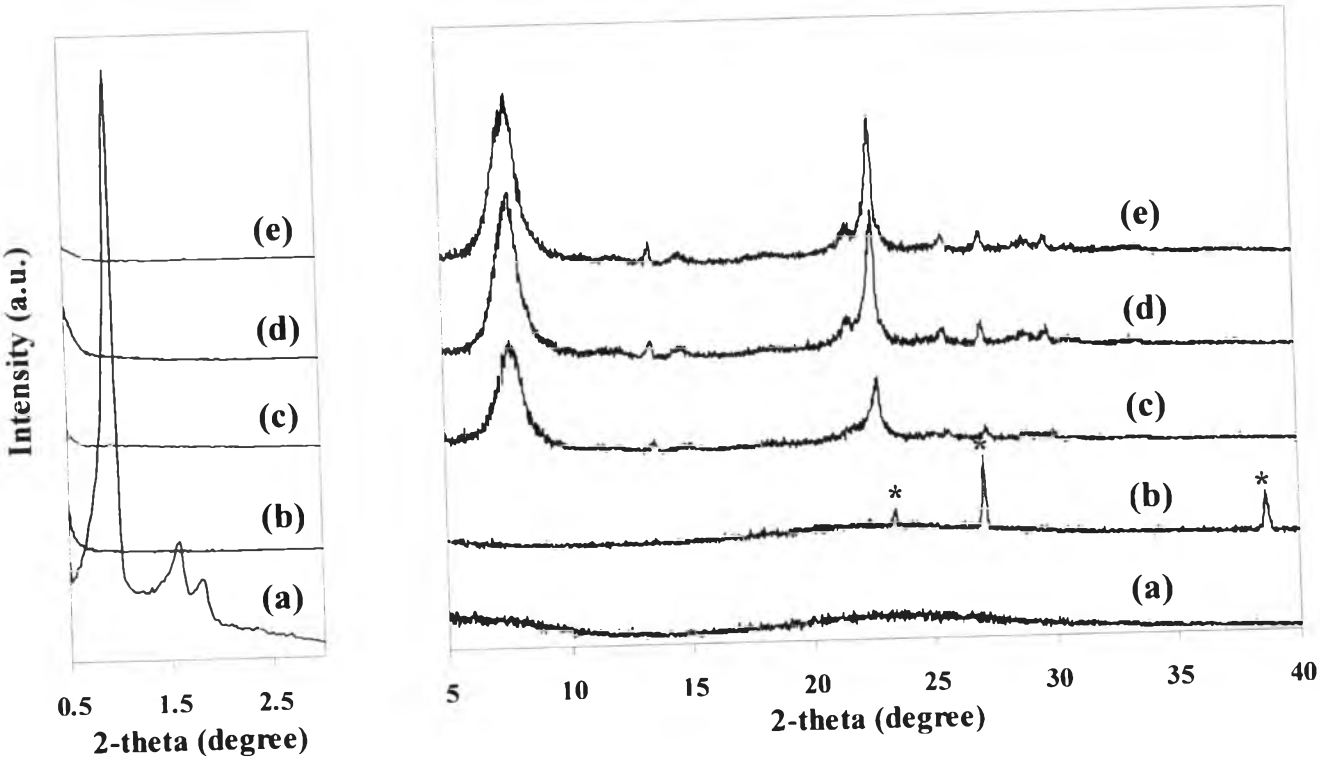

Figure 4.5 XRD patterns of calcined products transformed from SBA-15 at various crystallization periods (a) 0 h; (b) 6 h; (c) 12 h; (d) 24 h and (e) 48 h. (Note: * indicates the characteristic peaks of α-quartz.)

4.2.1.2 Element Analysis

Table 4.1 shows SBA-15/AIP mole ratios in gel and in catalyst of samples with various crystallization times. It was found that SBA-15/AIP ratios in catalyst of all samples were less than SBA-15/AIP ratios in gel which were calculated from reagent quantities. The large Al content determined by XRF technique is total content of both framework and non-framework Al species. The Si content was analyzed by XRF technique. In addition, there are no significant differences between the SBA-15/AIP ratios in catalyst for analogous samples synthesized from the same SBA-15/AIP ratio in gel. The SBA-15/AIP ratios in catalyst at crystallization time for 24 and 48 h are not different indicating the crystallization time at least 24 h are suitable to form zeolite beta structure.

4.2.1.3 SEM Images

Figure 4.6 shows SEM images of SBA-15 and the transformation products at various crystallization periods ranging from 0-48 h. The SEM image of the starting SBA-15 (Figure 4.6a) is different from all the rest. The particle shape of SBA-15 is the rope-like bundles of rods. In the presence of TEAOH and AIP, the SBA-15 rods disintegrate apart and recrystallize to form α-quartz crystals in shape of hexagonal prism (Figure 4.6b) after a period of 6 h. Upon prolongation of crystallization time, the hexagonal prisms disappear and the nano-sized particles of zeolite beta are found instead (Figures 4.6c-4.6e). The ranges of particle size are not quite different among the three samples of zeolite beta (116-147 nm) with crystallization time ranging from12-24 h. The zeolite particles are fairly spherical shaped and the surface is not smooth. From the expansion view of the SEM images, a trace of the aggregation of nano-sized (about 48 nm) crystals into a spherical particle can be suggested. However, the condition of 12-h crystallization gives the zeolite product at a very low yield while 24-h and 48-h crystallization periods give rise to 26.9% and 42.4 % yield, respectively. Therefore, 48-h crystallization period was selected for study the effect of TEAOH/SiO_2 ratio on the transformation of SBA-15 into zeolite beta.

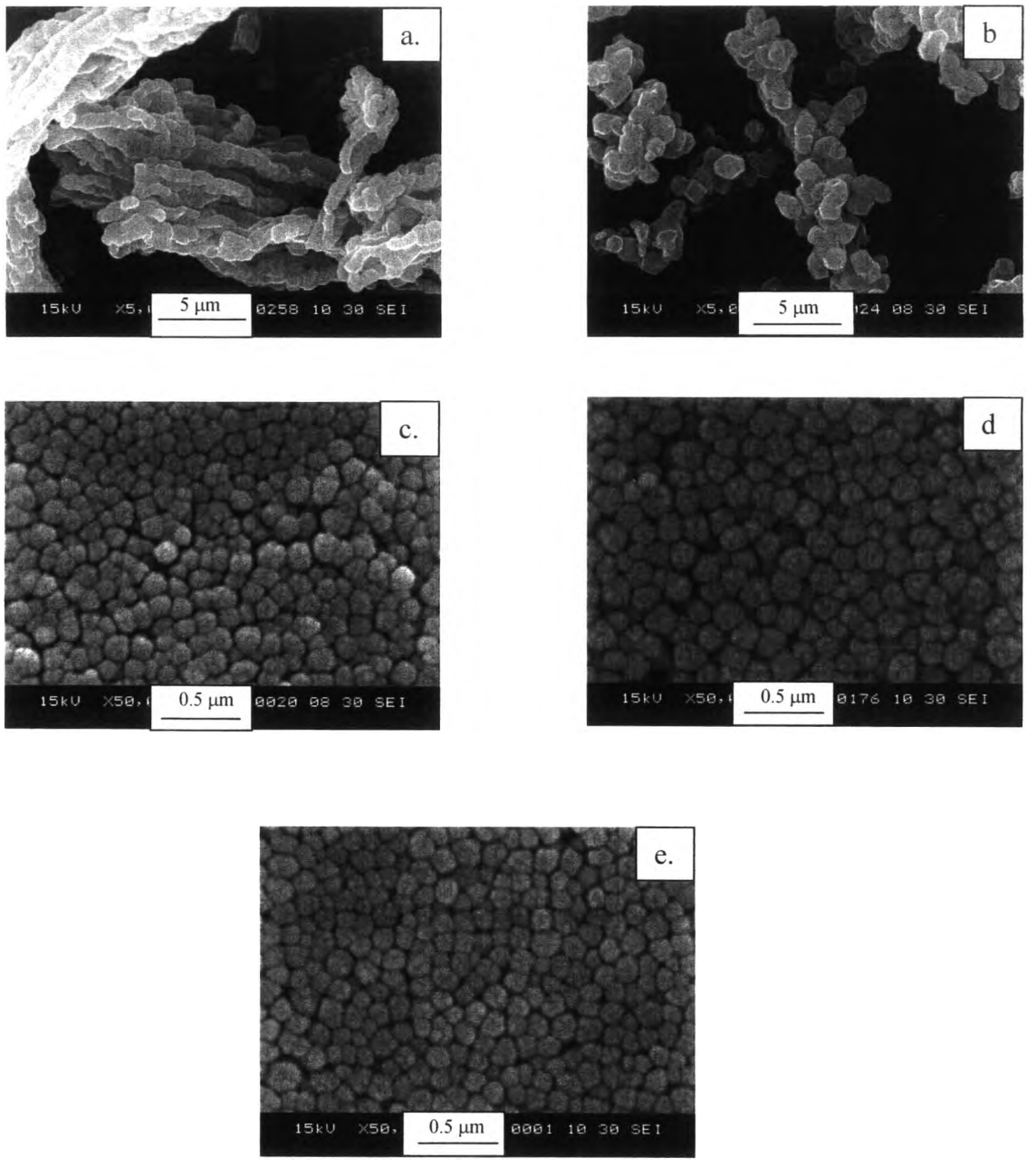

Figure 4.6 SEM images of calcined products after crystallization for various periods (a) 0 h; (b) 6 h; (c) 12 h; (d) 24 h and (e) 48 h

4.2.1.4 Nitrogen Adsorption-Desorption

Figure 4.7 shows the adsorption-desorption isotherms of the zeolite beta samples with various crystallization time. The adsorption-desorption isotherms show a type I isotherm which is typical for microporous material [131] after a crystallization time of 12 h. The sample crystallized for 12 h shows the both type microporous and mesoporous material, the mesoporous in the region of relative pressure around 0.3 to 0.8. The result is in agreement with the low crystallinity, related to decrease in order of the zeolite structure. Thus it can be confirmed by combining XRD and Adsorption isotherm that the product crystallized for 12 h not pure zeolite beta but contains the contamination of mesoporous phase which is not certainly SBA-15 because the characteristic peaks of SBA-15 was not observed in this sample. Each isotherm exhibits three different adsorption zones [132]. The first zone, adsorption at very low pressure corresponds to the nitrogen adsorption in micropore system. At the medium partial pressure, the second zone is created by the nitrogen adsorption on external surface. At high relative pressure ($P/Po > 0.8$), the third one rises steeply and presents hysteresis loop indicating the presence of interparticular porosity [132].

Pore size distribution was obtained from the adsorption data by mean MP method as shown in Figure 4.8. The distribution of micropore is quite narrow and similar for all samples. The pore size distribution peaks of the calcined zeolite beta samples are centered at 0.6 nm. Moreover, pore size distribution of sample crystallized for 12 h exhibits some distribution of mesoporous using the Barrett, Joyner and Halenda (BJH) method is shown as inset in Figure 4.8. The distribution peak of mesopores is broad and centered at about 7.05 nm. The result can be confirmed that mesoporous phase occurred is not SBA-15.

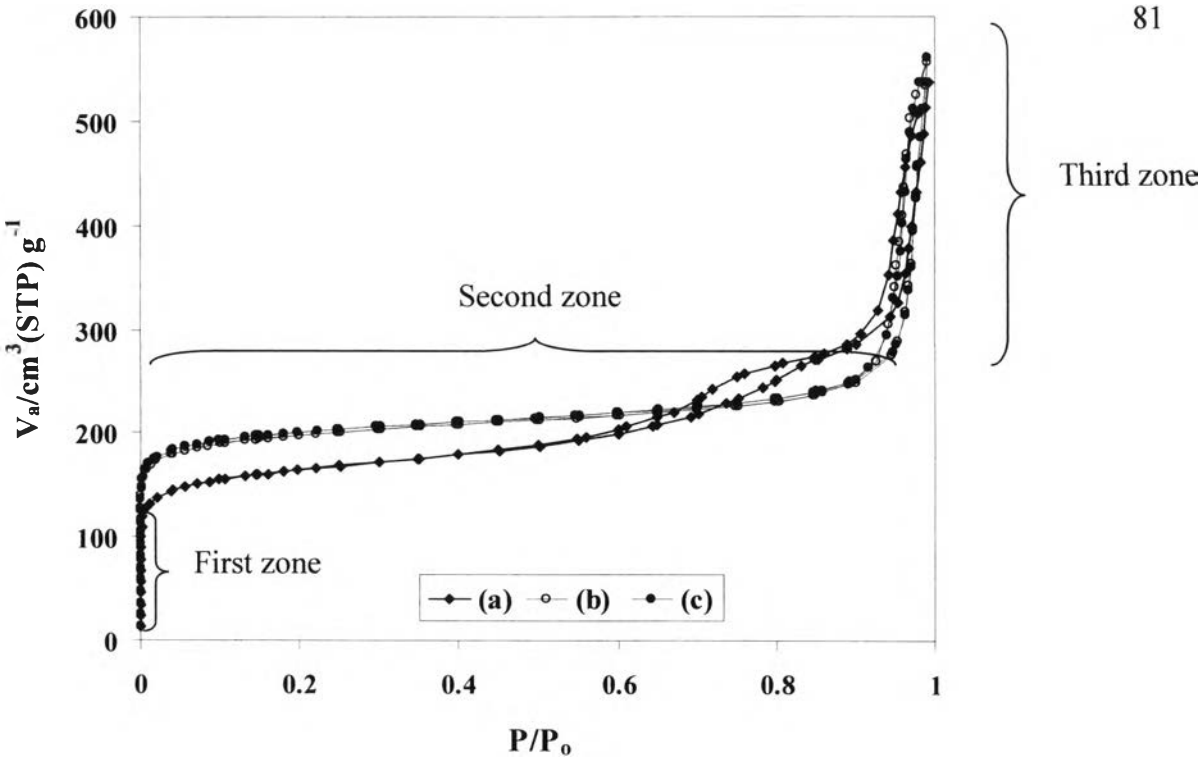

Figure 4.7 N_2 adsorption-desorption isotherm of zeolite beta samples with various crystallization periods (a) 12 h; (b) 24 h and (c) 48 h.

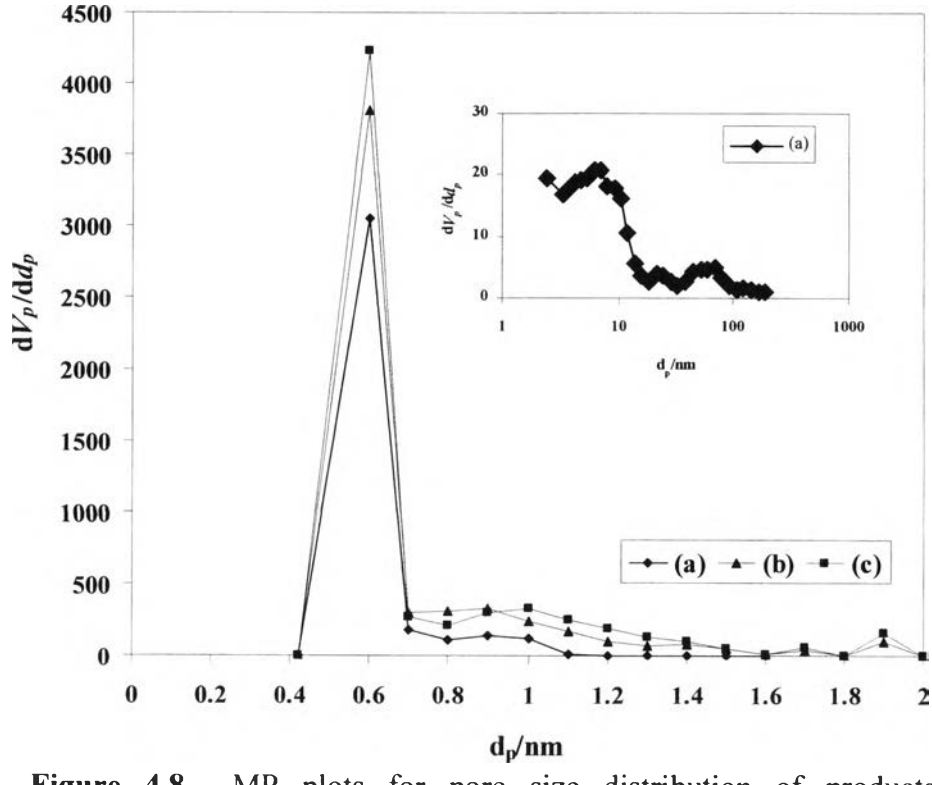

Figure 4.8 MP plots for pore size distribution of products with various crystallization periods (a) 12 h; (b) 24 h and (c) 48 h; inset BJH plot for products with crystallization periods (a) 12 h.

Table 4.1 shows textural properties of calcined zeolite beta samples with various crystallization time. The BET specific surface areas and external surface area of samples are in the range of 609 to 775 m^2/g and 75.7 to 111.1 m^2/g, respectively. Comparison of % product yield, Run No.4 gives a highest % product yield.

4.2.2 Effect of $TEAOH/SiO_2$ Ratios on Formation of Zeolite Beta

The quantity of TEAOH used as the organic template in the transformation of SBA-15 into zeolite beta needs to be carefully considered due to its important role on several properties of the zeolite in addition to the costly price. The alkalinity of the starting mixture is directly proportional to the amount of template. It would cause the formation of α-quartz if the extremely high alkalinity was used. It is noted herein that α-quartz was found during the transformation of SBA-15 into zeolite beta using the $TEAOH/SiO_2$ ratio of 0.39 indicating a highly excess of TEAOH was used. In addition, high alkalinity can cause the surface silanol group known as Q^3 of zeolite beta [32]. The more Q^3 group exists in the zeolite structure, the less stable by dealumination upon calcination zeolite beta is and that causes aluminum leaching from the tetrahedral site to the octahedral extra-framework site [32]

4.2.2.1 Powder X-Ray Diffraction

XRD pattern of as-synthesized and calcined zeolite beta samples with different $TEAOH/SiO_2$ ratios in catalyst are revealed in Figure 4.9 and 4.10. By varying the $TEAOH/SiO_2$ ratio in the starting mixture to 0.10, 0.20, 0.26, and 0.39, the small angle XRD patterns in Figure 4.10 (left) reveal the decrease in peak intensity of SBA-15 upon the increase in $TEAOH/SiO_2$ ratio. The high angle XRD patterns of calcined transformmation products in Figure 4.10 (right) shows that no crystalline product is observed when the $TEAOH/SiO_2$ ratio is lower than 0.26, *i.e.* SBA-15 partially transformed into an amorphous phase. The quartz phase is not observed for all samples. The $TEAOH/SiO_2$ ratio of 0.26 gave zeolite beta as the transformation product with the most remarkable crystallinity among all samples. If the $TEAOH/SiO_2$ ratio of 0.39 is used, the zeolite product with lower crystallinty is found. Incomplete coverage of the micelle by inorganic ions is accounted for the loss

of crystallinty. Thus it can be suggested that the SBA-15 be partially converted to an amorphous phase at the low amount of TEAOH and it is not successful to transform SBA-15 into zeolite beta due to not enough amount of template to form the cationic micelles which are the skeleton for surrounding inorganic ions to interact with the micelle and form aluminosilicate nucleation centers for further development to the zeolite framework structure. Reduction of crystallization period from 48 h to 24 h was also attempted and the XRD results in Figure 4.11 indicate the remarkable decrease in crystallinity of zeolite beta obtained. Thus, the crystallization time of 48 h is really required to obtain the zeolite with high crystallinity.

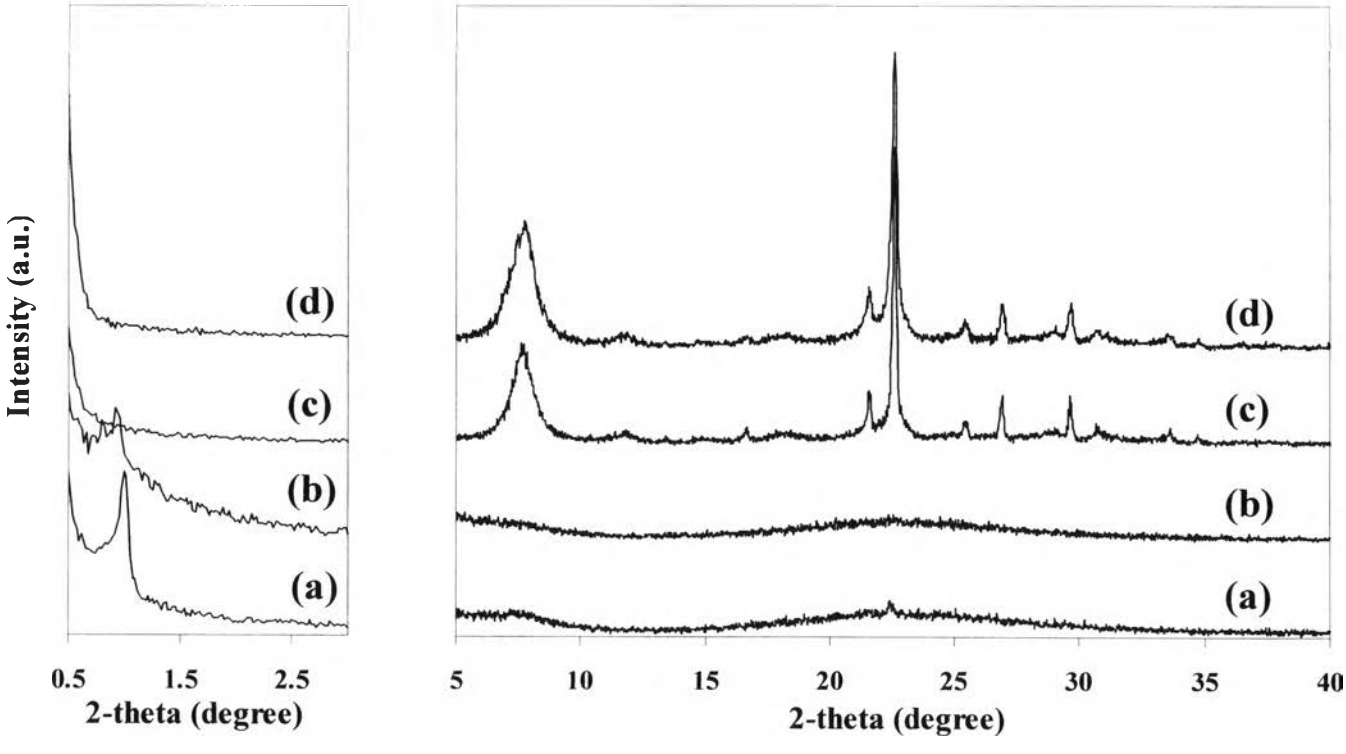

Figure 4.9 XRD pattern of as-synthsized zeolite beta with varied TEAOH/SiO_2 ratios: (a) 0.10; (b) 0.20; (c) 0.26 and (d) 0.39.

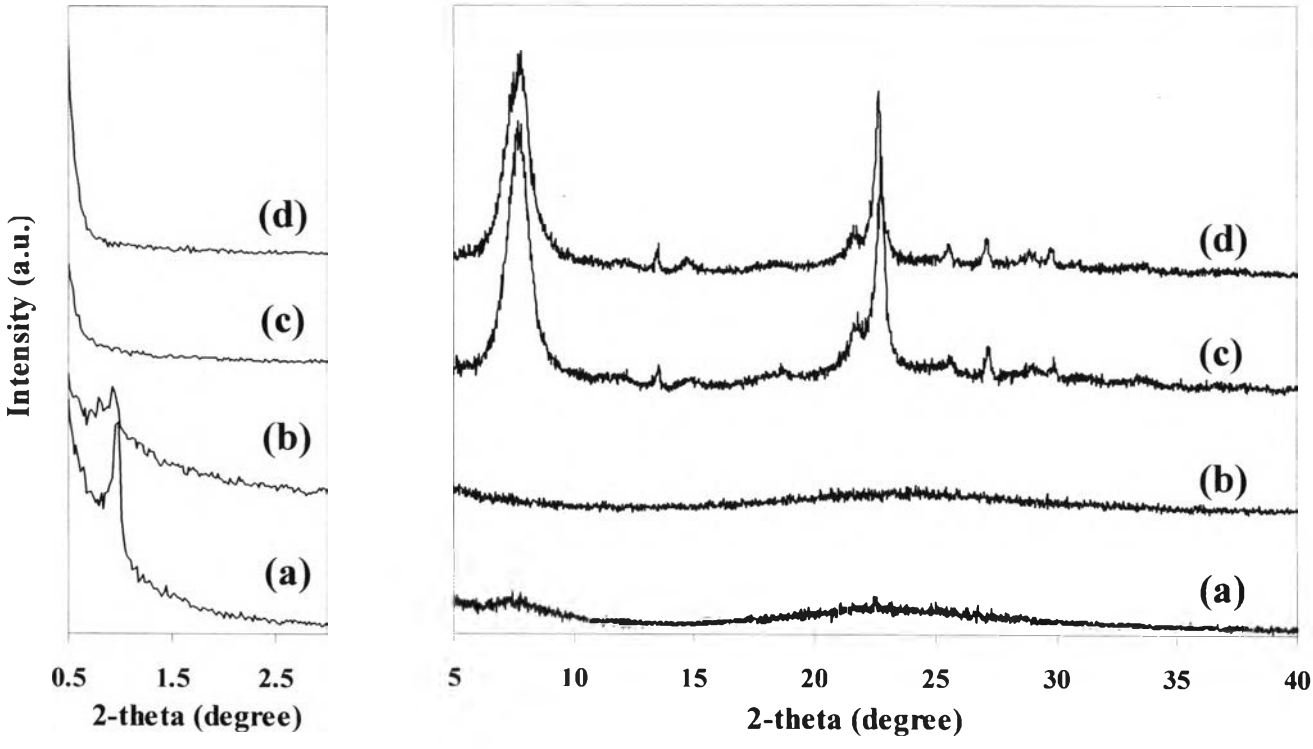

Figure 4.10 XRD pattern of calcined zeolite beta with varied TEAOH/SiO_2 ratios: (a) 0.10; (b) 0.20; (c) 0.26 and (d) 0.39.

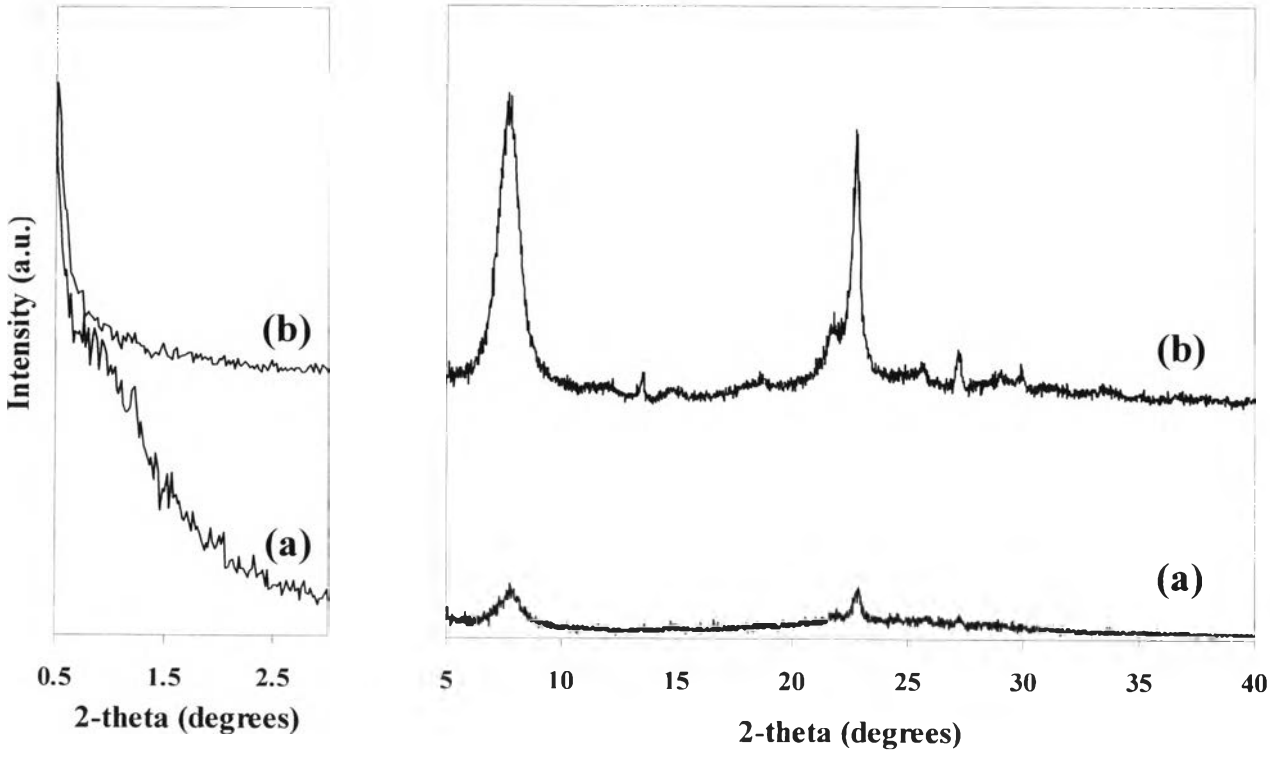

Figure 4.11 XRD pattern of calcined zeolite beta (TEAOH/SiO_2 ratio of 0.26) with varied crystallization periods: (a) 24 h and (b) 48 h.

4.2.2.2 Element Analysis

Table 4.1 shows SBA-15/AlP mole ratios in gel and in catalyst of samples with various TEAOH/SiO_2 ratios. It was found that SBA-15/AlP ratios in catalyst of all samples were less than SBA-15/AlP ratios in gel which were calculated from reagent quantities. The large Al content determined by XRF technique is total content of both framework and non-framework Al species. The Si content was analyzed by XRF technique. In addition, there are significant differences between the SBA-15/AlP ratios in catalyst for analogous samples synthesized from the same SBA-15/AlP ratio in gel. The TEAOH content increases with increasing the SBA-15/AlP ratio in catalyst. Due to a change in TEAOH/SiO_2 ratio implies a change in both the amount of TEA^+ cation as a structure-directing agent and the amount of OH^- anions. More template media give more high solubility of reactants and then high concentration; more silicon can dissolve in liquid phase and form zeolite beta framework more than small amount of template.

4.2.2.3 ^{27}Al-MAS-NMR Spectra

The ^{27}Al-MAS-NMR spectra after calcinations of all samples in Figure 4.12 exhibit the strong signal at 55 ppm is assigned to the tetrahedral coordination framework aluminum. The low signal of aluminum atoms at the framework site was observed at nearly 0 ppm is assigned to the octahedrally coordination non-framework site due to calcinations led to dealumination from tetrahedral site to extra-framework or octahedral site [32]. Table 4.2 shows O_h/T_d ratio of calcined product. The results show that the O_h/T_d ratios are not different although increasing the quantity of template.

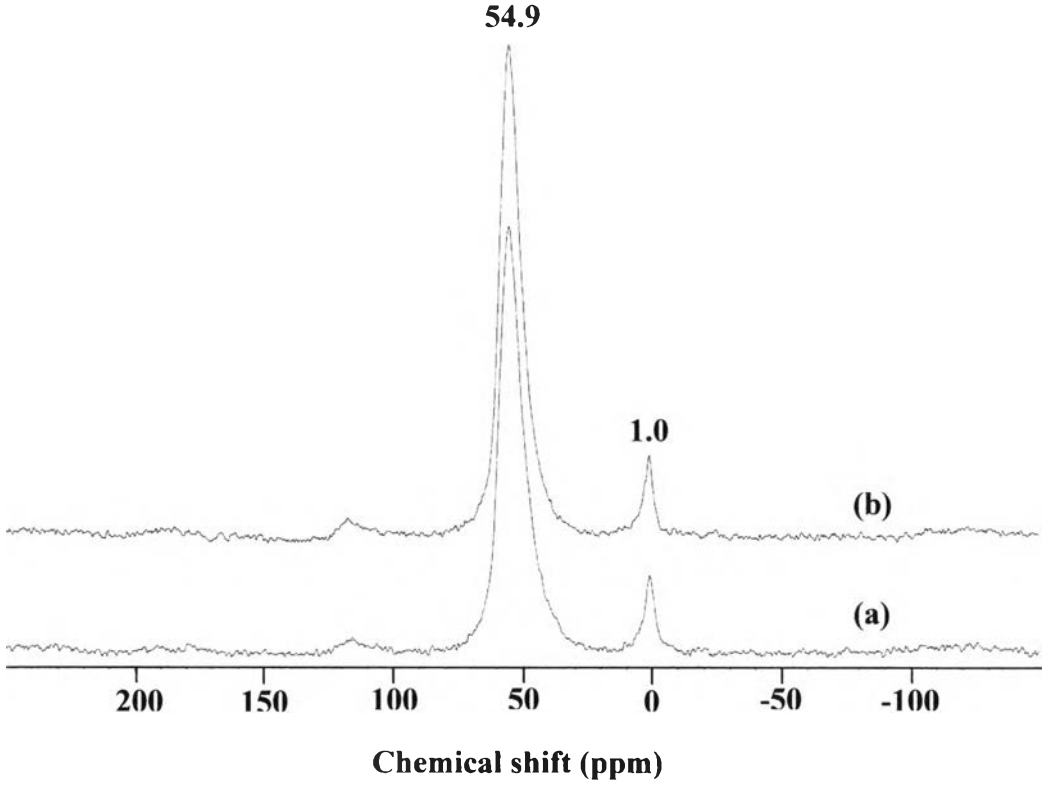

Figure 4.12 ^{27}Al-MAS-NMR spectra of calcined zeolite beta catalysts with different TEAOH/SiO_2 ratios (a) 0.26 and (b) 0.39.

Table 4.2 Comparison of O_h/T_d ratios in the calcined zeolite beta samples with different TEAOH/SiO_2 ratios

Catalyst	TEAOH/SiO_2 ratios	O_h/T_d
Run No.5	0.26	0.10
Run No.4	0.39	0.06

4.2.2.4 SEM Images

SEM images of the transformation products with different $TEAOH/SiO_2$ ratios are shown in Figure 4.13. The SEM image of product with $TEAOH/SiO_2$ ratio of 0.10 (Figure 4.13a) consists of only bundles of rope-like particles of SBA-15 without anything else. Confirmed by the XRD result in Figure 4.9 and the indication by adsorption isotherm of mesopore for this sample in Figure 4.14, the starting SBA-15 cannot be transformed if the $TEAOH/SiO_2$ ratio is not high enough. The SEM image of the sample with $TEAOH/SiO_2$ ratio of 0.20 shows large particles of amorphous phase with some particles of remaining SBA-15 as well as a hexagonal prism of quartz as displayed in Figure 4.13b. This result reveals the formation of α-quartz at a trace amount which is undetectable by XRD. The remaining SBA-15 is in agreement with the small angle XRD results in Figure 4.11b. It was found that zeolite beta is formed when the $TEAOH/SiO_2$ ratio of at least 0.26 was used and the particle size of zeolite beta decreased with increasing the $TEAOH/SiO_2$ ratio. The widely accepted crystallization mechanism assumes that inorganic anions interact with the template cations to form the structured aluminosilicate blocks, of which aggregates provide the basis for the growth of zeolite crystals. Thus, it is reasonable that concentrations of both silica and alumina in the liquid phase are highly related with crystal growth rate and crystal size, that is in agreement with Camblor *et al.* [32]. The template agent TEAOH provides not only alkalinity necessary for dissolution of silica and alumina sources, but also cations TEA^+, which are essential for the formation of inorganic-organic composite. A great deal of TEAOH provides rapid dissolution process and quickly develops to nucleation centers and finally zeolite crystals [133]. Ultimately, the crystal size of synthesized zeolite reduces as crystallization rate is fast. On the basis of the above reasoning, it is not surprising for the decrease of zeolite particle size with increasing template agent when the ratio of SBA-15/AIP is fixed. The results are in agreement with that of Jon *et al.* [29]. As a consequence the $TEAOH/SiO_2$ ratio of 0.26 is selected so as to study the effect of SiO_2/AIP in the starting mixture.

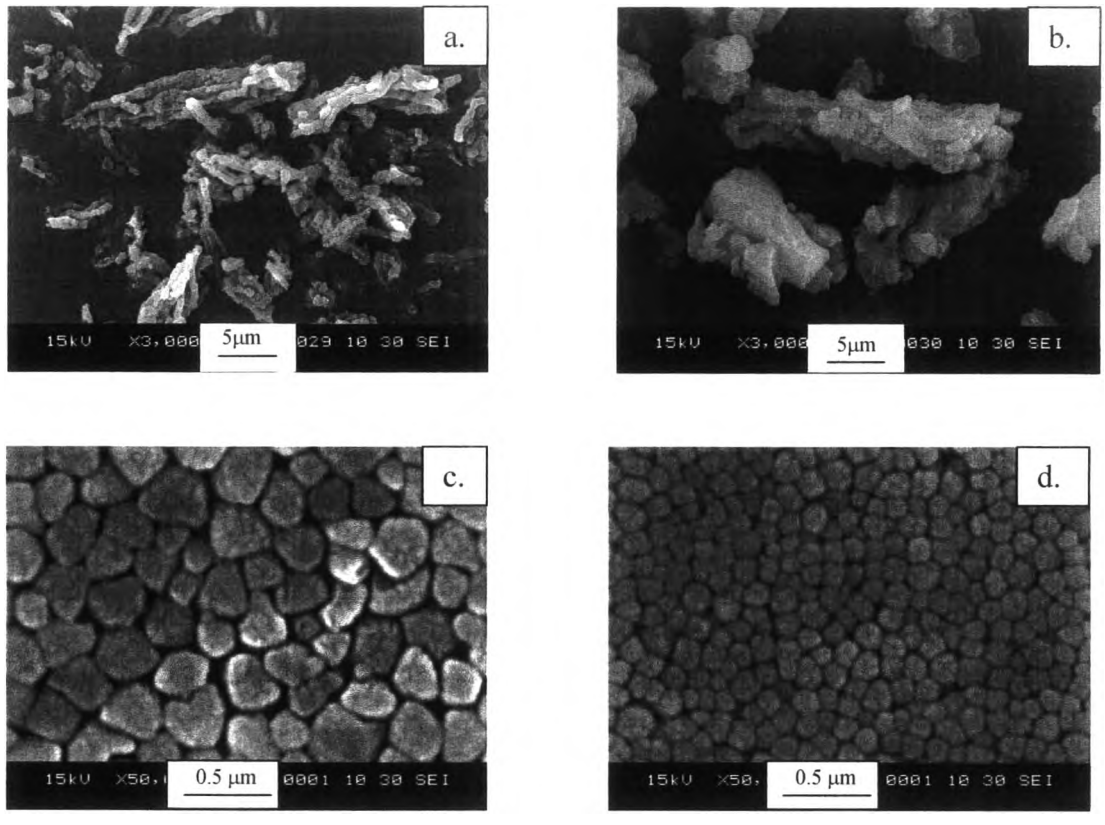

Figure 4.13 SEM image of calcined zeolite beta with various TEAOH/SiO_2 ratios of (a) 0.10; (b) 0.20; (c) 0.26 and (d) 0.39.

4.2.2.5 Nitrogen Adsorption-Desorption

Figure 4.14 shows the adsorption-desorption isotherms of transformation products with various TEAOH/SiO_2 ratios. SBA-15 exhibits a type IV adsorption isotherm which is a characteristic pattern of mesoporous material and its BET surface area is 797 m^2/g. The sample with the TEAOH/SiO_2 ratio of 0.10 also shows the type IV adsorption isotherm which is a characteristic pattern of mesoporous materials. This indicates the presence of the mesoporous system of SBA-15. This is really in accordance with the XRD and SEM results of this sample. Each of other samples obtained from the gel with the TEAOH/SiO_2 ratio ranging from 0.20 to 0.39 shows a Type I isotherm, the characteristic pattern of microporous material. However, the TEAOH/SiO_2 ratio of 0.20 provides a product with a low adsorbed amount of nitrogen, only one half of those adsorbed by two samples with higher TEAOH/SiO_2 ratios. The values of BET specific surface area are 430, 478, 781, and 765 m^2/g for

the samples with TEAOH/SiO_2 ratios of 0.10, 0.20, 0.26 and 0.39, respectively. It indicates that the structure of SBA-15 is somehow affected by TEAOH resulting in the tremendous decrease in BET specific surface area from 797 to 430 m^2/g. The data of pore size distribution obtained from the adsorption branch by MP calculation shows that the narrow distribution of micropore which is similar for the samples with TEAOH/SiO_2 ratio of 0.26 and 0.39. The pore size distribution peaks of both samples are centered at 0.6 nm, a typical value for zeolite beta while the samples with TEAOH/SiO_2 ratios of 0.10 and 0.20 exhibits both micropores of 0.6 nm and mesopores of 10.5 nm. The isotherms of zeolite beta obtained in this work exhibit an unusual large adsorbed amount of nitrogen at a very high relative pressure, P/P_o, near 1 due to the presence of high external surface area which is created by nanosized particles.

Table 4.1 shows the summary of transformation products prepared from SBA-15 at various conditions. It was also found that zeolite beta prepared from SBA-15 has higher yield than that prepared from silica xerogel at the same TEAOH/SiO_2 ratio (0.26) and crystallization time (48 h). The high yield of zeolite beta transformed from SBA-15 is accounted by the effect of surface area of silica sources: SBA-15 has much higher specific surface area than silica xerogel.

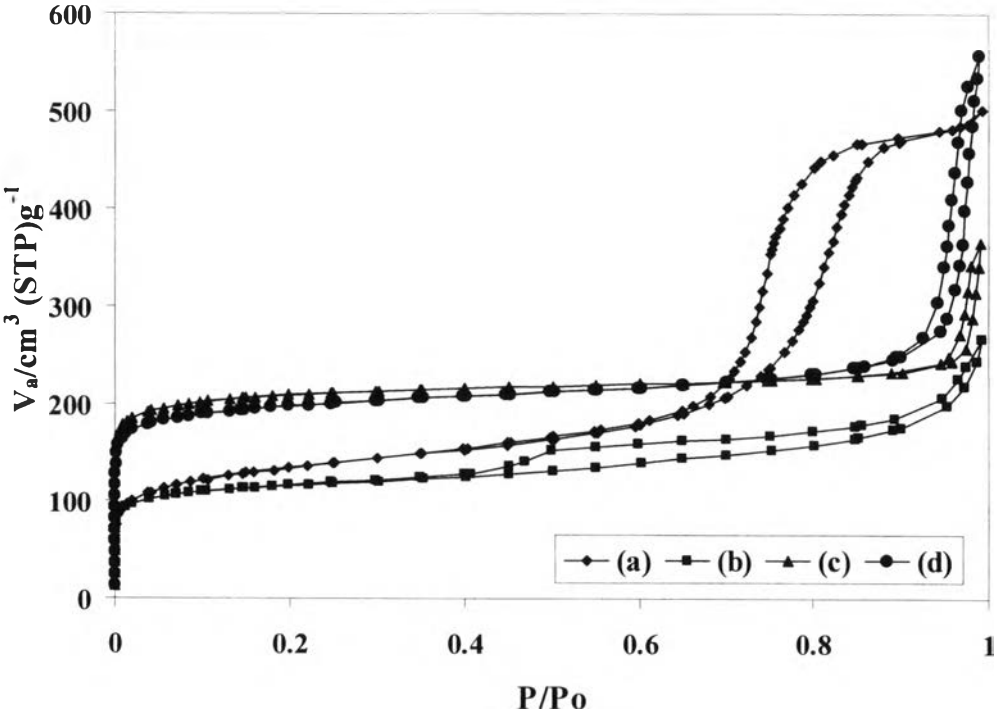

Figure 4.14 N_2 adsorption-desorption isotherm of zeolite beta samples with various TEAOH/SiO_2 ratios of (a) 0.10; (b) 0.20; (c) 0.26 and (d) 0.39.

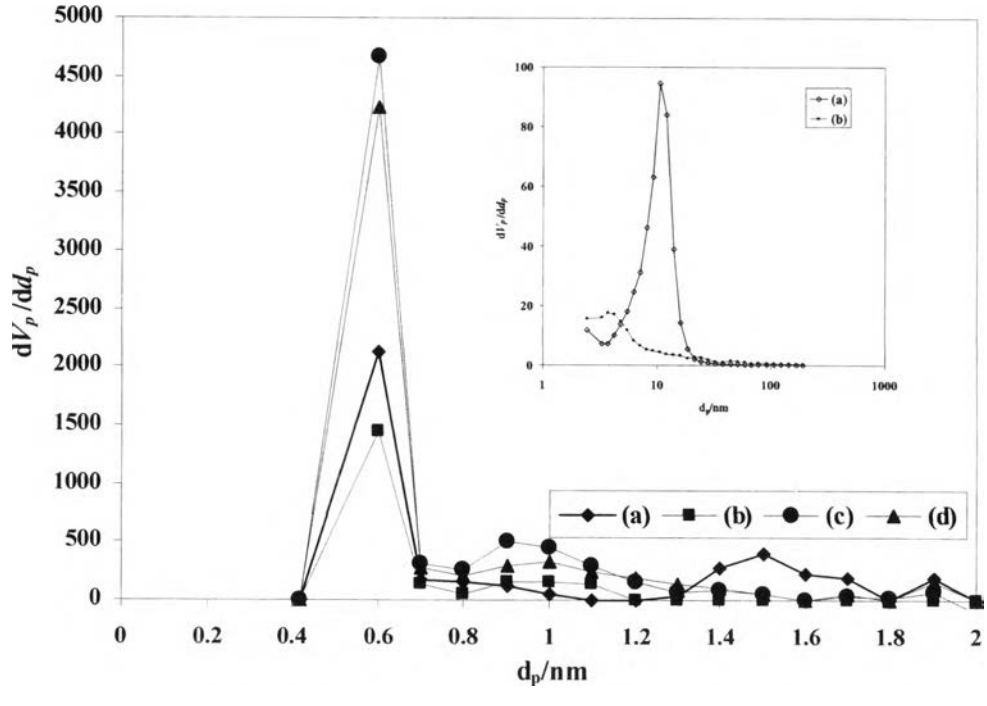

Figure 4.15 MP plots for pore size distribution of various TEAOH/SiO_2 ratios of (a) 0.10; (b) 0.20; (c) 0.26 and (d) 0.39; inset BJH plot for zeolite beta with TEAOH/SiO_2 ratios of (a) 0.10 and (b) 0.20.

4.2.3 Effect of SBA-15/AIP Ratio on Formation of Zeolite Beta

4.2.3.1 Powder X-Ray Diffraction

The XRD patterns of zeolite beta obtained from the starting mixture containing various SBA-15/AIP ratios are shown in Figure 4.16 and 4.17. The XRD peak intensities, indicating the zeolite crystallinity, are strongly affected by the SBA-15/AIP ratio in reactant mixture. At the SBA-15/AIP molar ratio of only 10, there is none of XRD peaks. Figure 4.17a shows the distorted structure of SBA-15 without formation of zeolite beta. The SEM image of this sample in Figure 4.18a shows particles of SBA-15 with shorter length of rope bundles. The distortion of SBA-15 is caused by incorporation of aluminum atoms into the structure of SBA-15 to form Al-SBA-15. Using high SBA-15/AIP ratios ranging from 30 to 60, zeolite beta with high crystallinity can be achieved as shown in Figures 4.17b and 4.17c. The latter XRD pattern exhibits higher crystallinity of zeolite beta while SBA-15 characteristic peaks are completely vanished. With further increasing the SBA-15/AIP ratio to 90, the intensities of characteristic XRD peaks of zeolite beta (Figure 4.18d) decrease.

It is obvious that the drastic decrease in crystallinity of high SBA-15/AIP ratio is not due to the effect of particle size. It indicates that the SBA-15/AIP ratio in reactant media can play an important role on the formation of the BEA structure by this synthesis method. For the SBA-15/AIP ratio as low as 10, the failure of formation of zeolite beta is owing to the amount of organic template, under the synthesis condition, acting as the skeleton for inorganic ions to adhere is not enough for all ions especially aluminum ionic species to form aluminosilicate building blocks. It seems that higher amount of $TEAOH/SiO_2$ is required for making the zeolite with low SBA-15/AIP ratio. Thus the excess amount of aluminum turns to be located at the extra-framework octahedral position instead of the framework tetrahedral site. This fact can be proven by ^{27}Al-MAS-NMR spectra of calcined SBA-15 and transformation products with different SBA-15/AIP ratios in Figure 4.21. The spectra of calcined products show the presence of an intense signal centered at around 55 ppm and small signal at about 0 ppm. The product at SBA-15/AIP ratios of 90 gives the signal at around 0 ppm with lower intensity than other samples. It indicates that the lower SBA-15/AIP ratio, the higher intensity of the peak assigned

for the octahedral aluminum site is found. As a result the SBA-15/AIP ratio of 10 is not suitable to prepare zeolite beta by this method. In other words, the large amount of AIP with the low SBA-15/AIP ratio can be account for the diminishing of the uniform of tetrahedral unit in the structure of zeolite beta.

For the SBA-15/AIP ratio of 30 or higher, the characteristic XRD pattern of SBA-15 is not observed. The presence of remained SBA-15 is thus neglected. Then what makes the zeolite product with the SBA-15/AIP ratio of 90 much less crystallinity although its particle size is the large. From SEM images, it can be said that the irregular shape and size of the particles is found the most for the sample with SBA-15/AIP ratio of 90. Some particles in a long granular shape are found in Figure 4.18d but hardly found in Figure 4.18b and 4.18c. However, all particles including the long granules still contain tiny crystals with similar sizes around 40 nm in diameter.

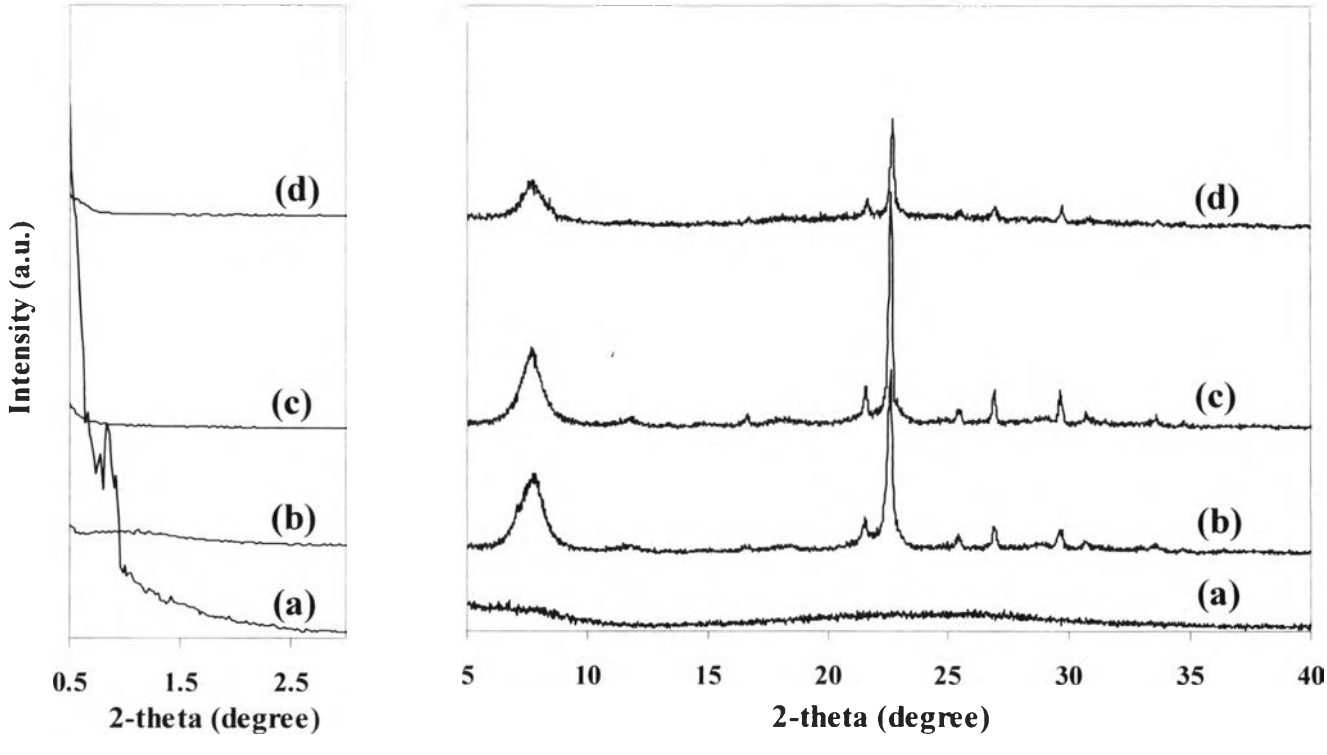

Figure 4.16 XRD patterns of as-synthesize zeolite beta (TEAOH/SiO_2 ratio of 0.26) with various SBA-15/AIP ratios: (a) 10; (b) 30; (c) 60; and (d) 90.

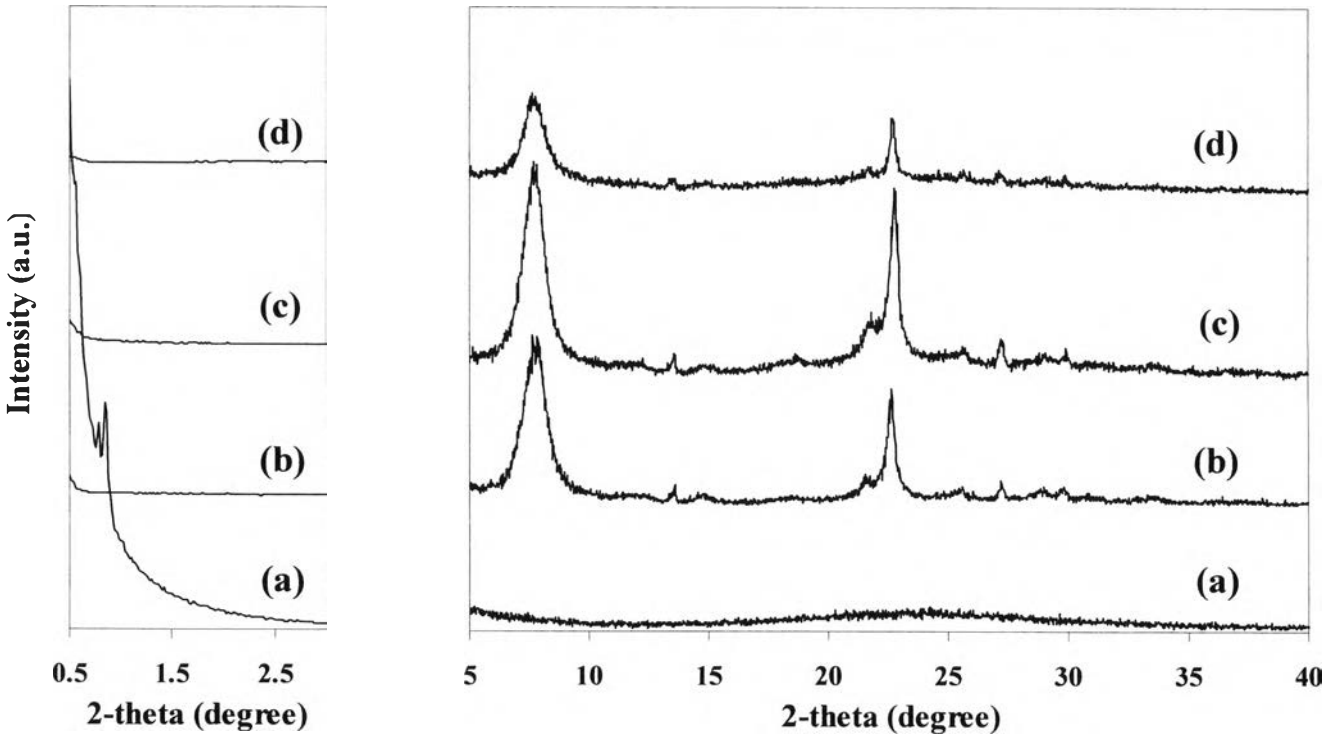

Figure 4.17 XRD patterns of calcined zeolite beta (TEAOH/SiO_2 ratio of 0.26) with various SBA-15/AIP molar ratios: (a) 10; (b) 30; (c) 60; and (d) 90.

4.2.3.2 Element Analysis

Table 4.1 shows the SBA-15/AIP ratios in gel and in catalyst of zeolite beta samples. It was found that the SBA-15/AIP ratios in catalyst of all samples that prepared from SBA-15 were less than the SBA-15/AIP ratios in gel which calculated from reagent quantities. In addition, the Al content increases with decreasing SBA-15/AIP ratio. The large Al content determined by XRF technique is total content of both framework and non-framework Al species. The data of Al content from XRF technique cannot exhibit the position of the Al species, whether it is located at tetrahedral framework or octahedral non-framework species, therefore data from ^{27}Al-NMR is needed for identification. The Si content is determined by XRF technique.

4.2.3.3 SEM Images

The SEM images of zeolite beta with various SBA-15/AIP ratios in the reactant mixture are illustrated in Figure 4.18. It is found that Figures 4.18 (b and c) shows the nanoparticles in like a skew quadrilateral shape with rough surface while Figure 4.18 (d) shows two phases together, *i.e.* the square shape spherical and the pentahedron particles with not an uniform size. It is consistent with XRD pattern having less order of structure for the corresponding sample obtained from the reactant mixture with the SBA-15/AIP ratio of 90. The ranges of particle size are not quite different among the three samples of zeolite beta (173-215 nm) with SBA-15/AIP ranging from 30 to 90.

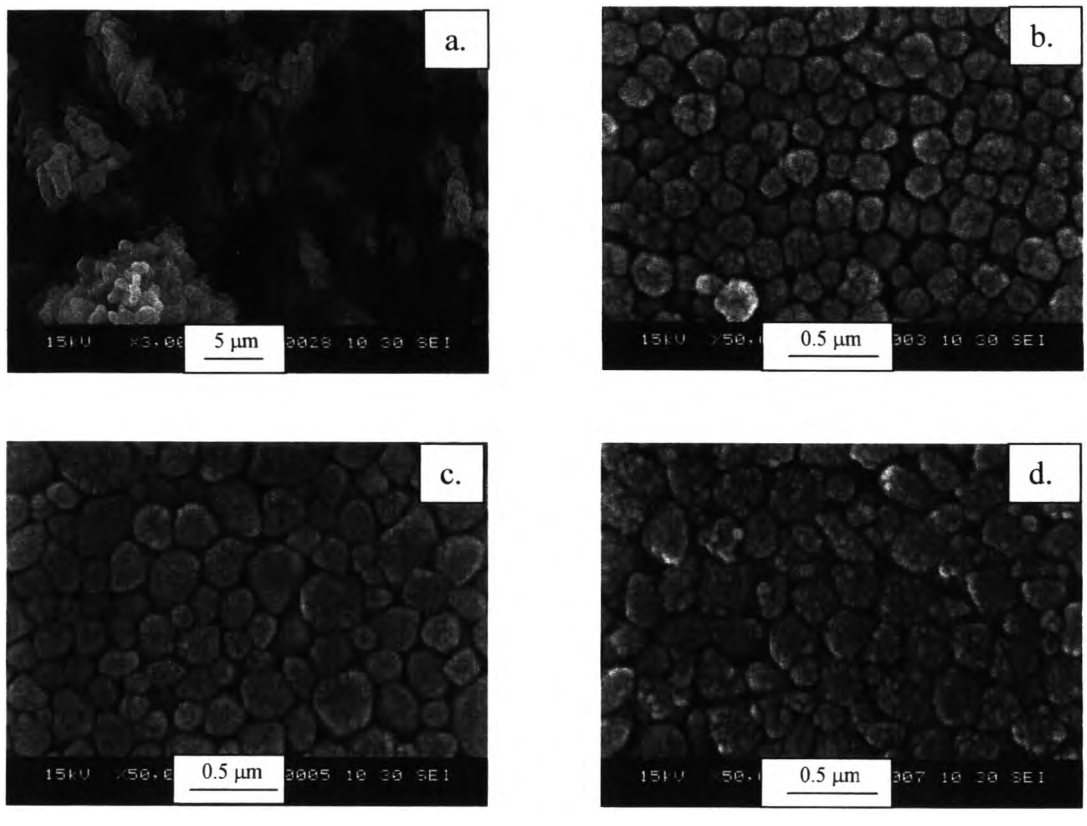

Figure 4.18 SEM images of calcined zeolite beta (TEAOH/SiO_2 ratio of 0.26) with various SBA-15/AIP ratios of (a) 10; (b) 30; (c) 60 and (d) 90.

4.2.3.4 Nitrogen Adsorption-Desorption

The nitrogen adsorption isotherms of calcined SBA-15 and transformation products with various SBA-15/AIP ratios are compared in Figure 4.19. The nitrogen adsorption isotherms of the products synthesized using the reactant mixture containing SBA-15/AIP ratios of 30-60 are the type I isotherms of microporous behavior. It is obvious that the SBA-15/AIP ratio of 30 provided with the sample with higher external surface area than the SBA-15/AIP ratio of 60. The increase in external surface area is affected by the particle nano-size. The transformation product obtained from the reactant mixture with the SBA-15/AIP ratio of 90 shows the hysteresis loop in the region of the relative pressure around 0.5-0.8 indicating the mesoporous behavior along with the microporous character at very low relative pressure. The result is in agreement with the low crystallinity, related to the decreased order of the zeolite structure. Thus it can be concluded by combining XRD, SEM and nitrogen adsorption isotherm that the product obtained from the reactant mixture with the SBA-15/AIP ratio of 90 is not normal zeolite beta but contains the mesopores which do not belong to SBA-15. We believe that it is a hybrid sample of mesoporous zeolite beta. This result has been occurred in synthesis of Ti-Beta/SBA-15 composite [39]. The BET surface areas are varied in the range between 455 and 782 m^2/g. The samples with high crystallinity exhibit higher BET specific surface areas and only the zeolite beta sample synthesized with SBA-15/AIP of 30 in the starting mixture shows the extremely high external surface area. The extremely high specific area of SBA-15 is the key role on the success of the synthesis of nanoparticle zeolite beta.

Pore size distribution was obtained from the adsorption data by mean MP method as shown in Figure 4.20. The distribution of micropore is quite narrow and similar for all samples. The pore size distribution peaks of the calcined zeolite beta samples are centered at 0.6 nm. Moreover, pore size distribution of sample SBA-15/AIP ratio of 10 and 90 exhibit some distribution of mesoporous using the Barrett, Joyner and Halenda (BJH) method is shown as inset in Figure 4.20. The distribution peak of mesopores is broad and centered at about 21.3 nm for sample SBA-15/AIP ratio of 10 and 7.05 nm for sample SBA-15/AIP ratio of 90. The result can be confirmed that mesoporous phase occurred is not SBA-15.

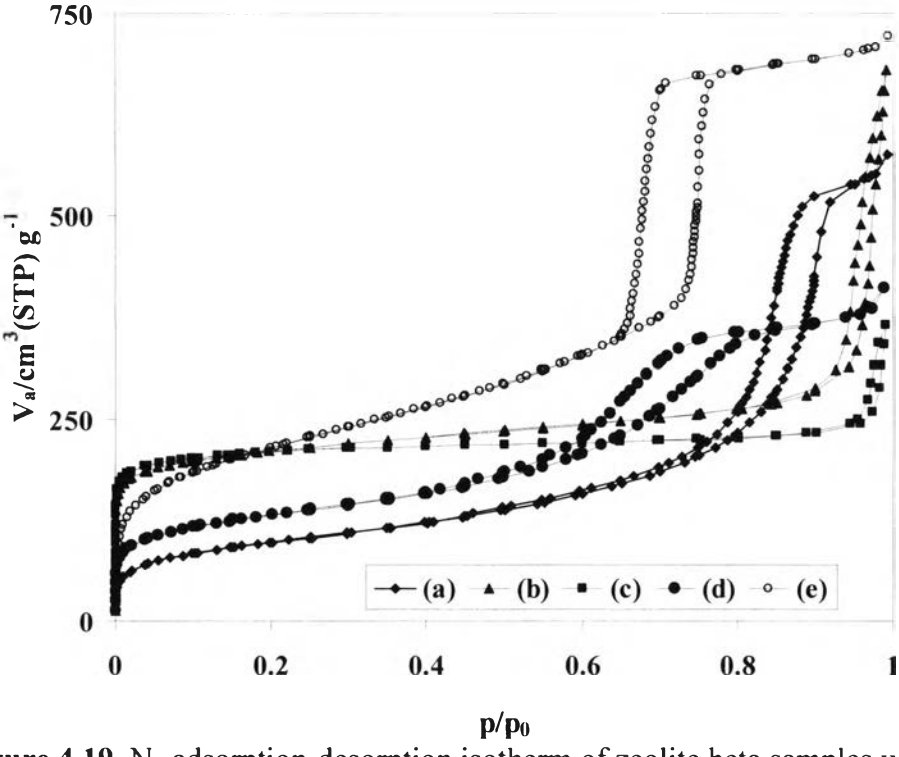

Figure 4.19 N_2 adsorption-desorption isotherm of zeolite beta samples with various SBA-15/AIP ratios of (a) 10; (b) 30; (c) 60, (d) 90 and (e) SBA-15.

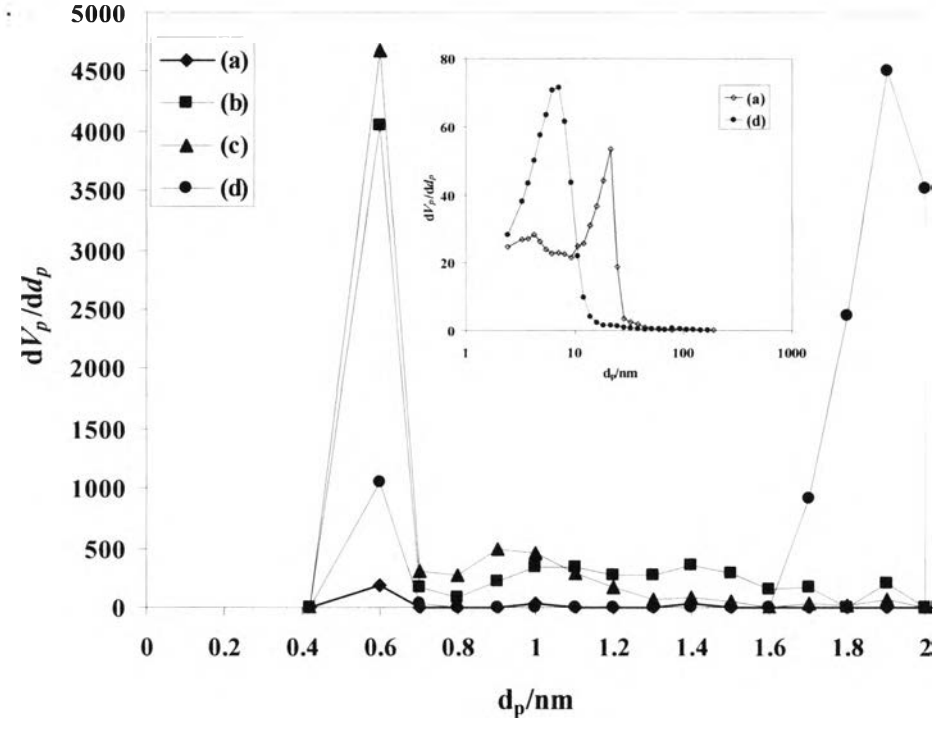

Figure 4.20 MP plots for pore size distribution of of calcined SBA-15 and transformation products using SBA-15/AIP ratios of (a) 10; (b) 30; (c) 60 and (d) 90; inset BJH plot for zeolite beta with SBA-15/AIP ratio of (a) 10 and (d) 90.

4.2.3.5 ^{27}Al-MAS-NMR Spectra

^{27}Al-MAS-NMR spectra of calcined zeolite beta samples with different SBA-15/AIP ratios are presented in Figure 4.21. The spectra of calcined products show the presence of an intense signal centered at around 55 ppm which corresponds to Al in tetrahedral (T_d) framework position and small signal at about 0 ppm that is assigned to octahedral (O_h) non-framework Al species. It was found that non- framework Al species were also generated during the calcinations process for the zeolite obtained. The intensity of signal at 55 ppm hardly changes when the Al content increases due to the saturation of number of framework site. However, sample Run No.10 gives the signal at around 0 ppm with lower intensity than other samples. It demonstrates Al incorporate into T_d framework and reduced dealuminatation from the framework site to non-framework site due to this sample content small amount of Al in gel. Table 4.3 shows O_h/T_d ratio of calcined zeolite beta. The zeolite beta with SBA-15/AIP ratio of 30 gives highest O_h/T_d ratio, indicating that Al content prefers incorporated into non-framework.

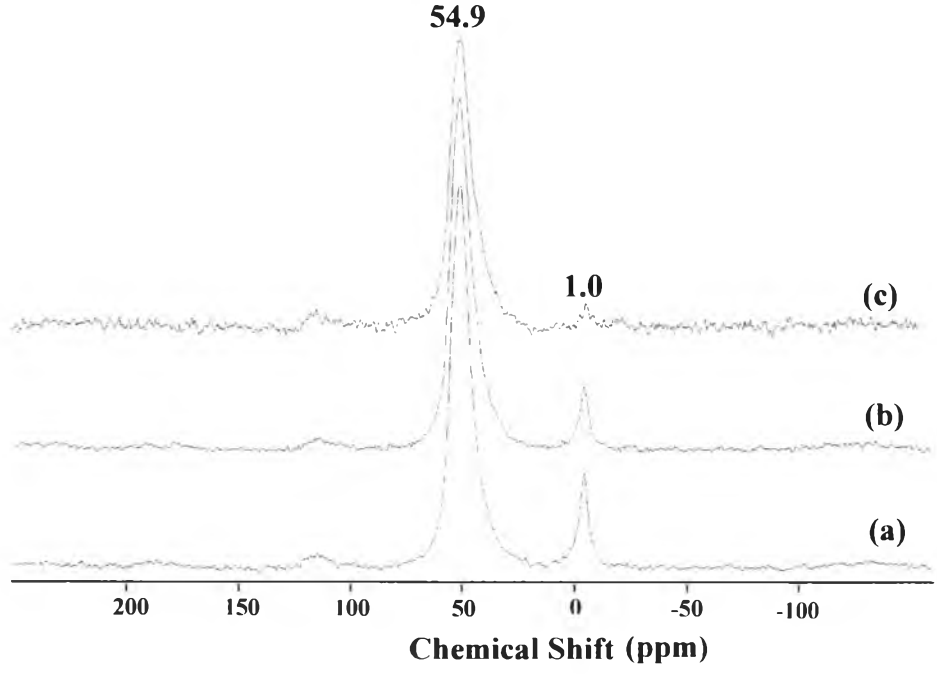

Figure 4.21 ^{27}Al-MAS-NMR spectra of calcined zeolite beta catalysts with differet SBA-15/AIP ratios in catalyst (a) 13.9; (b) 18.6 and (c) 25.1.

Table 4.3 Comparison of O_h/T_d ratios in the calcined zeolite beta samples with different SBA-15/AIP ratios

Catalyst	SBA-15/AIP ratios	O_h/T_d
Run No.9	30	0.12
Run No.5	60	0.10
Run No.10	90	0.04

4.2.3.6 NH_3-TPD Profiles

Figure 4.22 exhibits NH_3-TPD profiles of calcined SBA-15 and transformation products with different SBA-15/AIP ratios. The NH_3 desorption peak centered at 170°C is typically assigned to a weaker acid site, and the other one at 430°C is assigned to a stronger acid site. It is found that the peak at 170°C is more pronounced for all samples but in different extent. The acidities of the zeolite samples are concluded in Table 4.1. It is noted that the total acidity of the zeolite samples is inversely proportional to the SBA-15/AIP ratio used in the synthesis course. As usual, the lower the SBA-15/AIP ratio, the higher the acidity is. The $[AlO_2]^-$ tetrahedral units in the zeolite framework are accounted for the acidity of the zeolite samples. The results are similarity to A. Sakthivel *et al.* [134]. The product with the SBA-15/AIP ratio of 30 shows the highest number of acid sites.

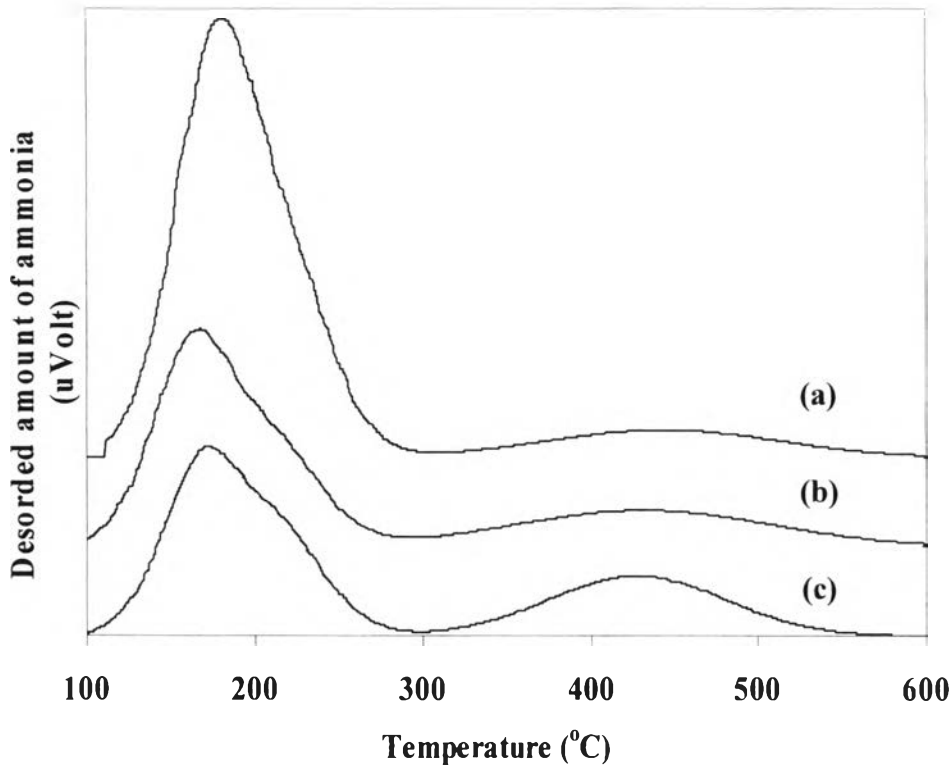

Figure 4.22 NH_3-TPD profiles of zeolite beta catalysts with various SBA-15/AIP ratios in catalyst of (a) 13.9; (b) 18.6 and (c) 25.1.

4.3 Activities of Various Zeolite Beta Catalysts in PP Waste Cracking

4.3.1 Effect of SBA-15/AIP Ratios

The effect of SBA-15/AIP ratios of 30, 60 and 90 (denoted Run No.9, Run No.5 and Run No.10) was tested in cracking of PP waste at low temperature of 350°C for 40 min with the catalyst amount of 10 wt% to plastic weight. The low temperature was used in order to avoid the competition of thermal cracking of PP waste. The results are compared in Table 4.4.

Table 4.4 Values of % conversion and % yield obtained by thermal cracking and catalytic cracking of PP waste over zeolite beta with various SBA-15/AIP ratios (Conversion: 10 wt% catalyst of plastic, N_2 flow of 20 cm^3/min. 350 °C and reaction time of 40 min).

	Thermal 350°C	**Run No. 9** (SBA-15/AIP = 30)	**Run No. 5** (SBA-15/AIP = 60)	**Run No. 10** (SBA-15/AIP = 90)
%conversion[a]	2.0	50.5	42.9	44.2
%yield				
1. gas fraction[b]	2.0	33.1	27.5	27.3
2.liquid fraction[c]	-	17.4	15.4	16.9
- distillate oil	-	14.8	12.7	13.1
- heavy oil	-	2.6	2.7	3.8
3. residue[d]	98.0	49.5	57.1	55.8
4. Total volume of liquid fraction (ml)	-	1.00	0.97	0.85
5. Liquid faction density (g/cm^3)	-	0.72	0.72	0.76

[a] *Deviation within 0.42%,* [b] *Deviation within 0.35%*
[c] *Deviation within 0.23%,* [d] *Deviation within 0.42%*

For thermal cracking at 350°C the liquid fraction was not obtained at all. The conversion of plastic is only 2.0% for thermal cracking but it is in the range from 42.9 to 50.5% for catalytic cracking over zeolite beta. The result indicates the difficulty in cracking of PP waste without catalyst at the low temperature about 350°C. Therefore, the total weight loss of plastic precursor after reaction is dedicated to gas fraction. The weight of white wax remained in the reactor after the reaction was included in the residue weight. In the presence of zeolite beta, the conversion drastically increase from 2.0 % to about 42-50%. The results indicate that the waxy residue decomposed into relatively lighter liquid hydrocarbons resulting in higher yield of liquid fraction than the case of thermal cracking. However, the SBA-15/AIP ratio of 30 gives the highest %conversion due to the influence of zeolite external surface area and strong acidity, determined by NH_3-TPD of zeolite beta. High external

surface area contains the great numbers of external acid sites, which may play an important role on the cracking of bulky molecule such as polymer [129]. The synergism of catalyst surface area, external surface area and acidity of zeolite beta SBA-15/AIP of 30 contributes to the PP waste conversion in the cracking process.

Figure 4.23 shows the accumulated volume of liquid fraction obtained by catalytic cracking of PP waste over zeolite beta with various SBA-15/AIP ratios at 350°C. The overall rates of liquid fraction formation are not different. That means the zeolite catalysts all have acidities in excess to catalyze the plastic cracking.

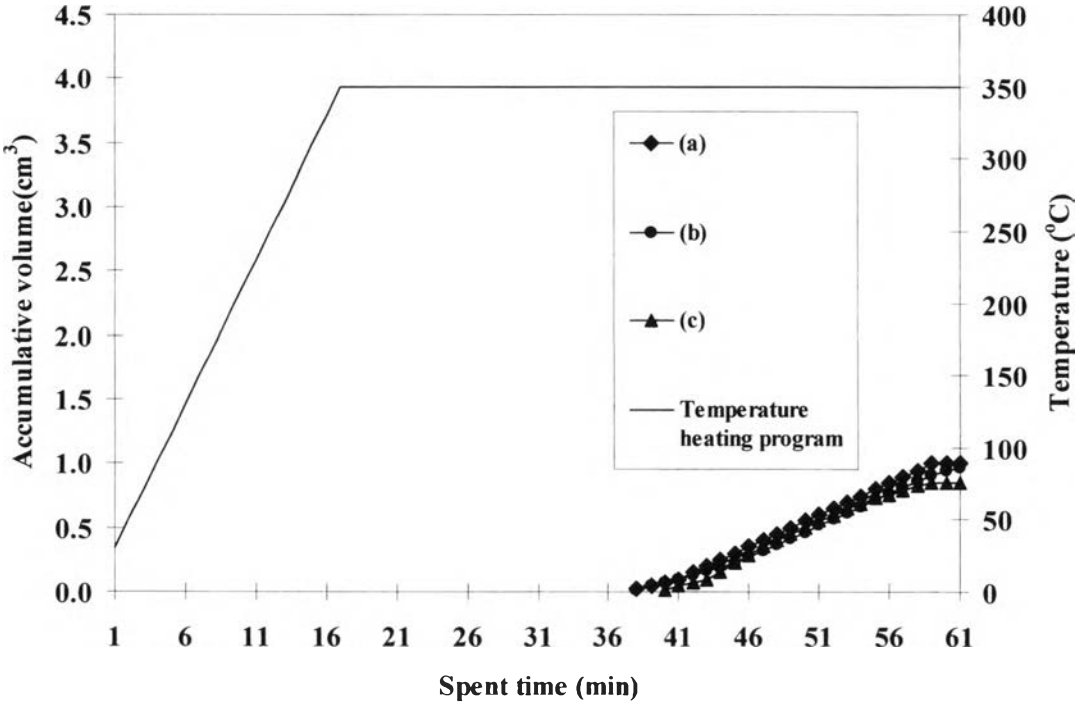

Figure 4.23 Accumulative volume of liquid fractions from catalytic cracking of PP waste over zeolite beta catalysts with different SBA-15/AIP ratios: (a) 30; (b) 60 and (c) 90.

Figure 4.24 shows distribution of gas fraction obtained by thermal cracking and catalytic cracking of PP waste over various zeolite beta catalysts at 350°C. For thermal cracking, propene, *n*-pentane and C_5^+ are the predominant products. In the presence of zeolite beta catalysts, the product distribution in gas fractions is different from that in the absence of catalyst or thermal cracking.

The main components in gas fractions from catalytic cracking are *n*-butane, *i*-butene and C_5^+.

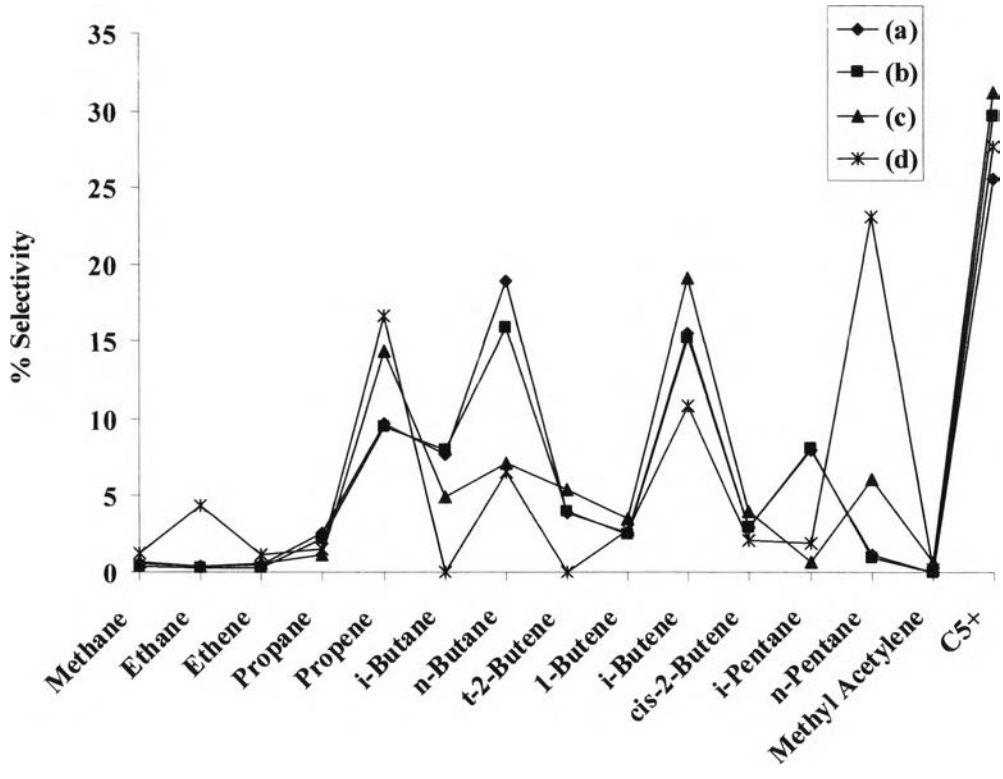

Figure 4.24 Product distribution of gas fractions obtained by catalytic cracking of PP waste using zeolite beta with various SBA-15/AIP ratios: (a) 30; (b) 60; (c) 90 and (d) thermal cracking at 350°C.

Figure 4.25 shows carbon number distribution of distillate oil obtained by catalytic cracking of PP waste over various zeolite beta catalysts at 350°C. The major liquid products for all SBA-15/AIP ratios are distributed in the range of C_7, C_8 and C_9. The selectivity of lighter hydrocarbon components increases with decreasing the SBA-15/AIP ratios in catalyst. The product distribution of SUPELCO standard gasoline fraction is shown in Figure 4.26 and the major components are C_7 and C_8. That is comparable to distribution of distillate oil obtained in this work based on the boiling point rang using n-paraffin as reference. In conclusion, the SBA-15/AIP ratio of 30 is a powerful catalyst and was selected for the study on the effect of temperature of reaction.

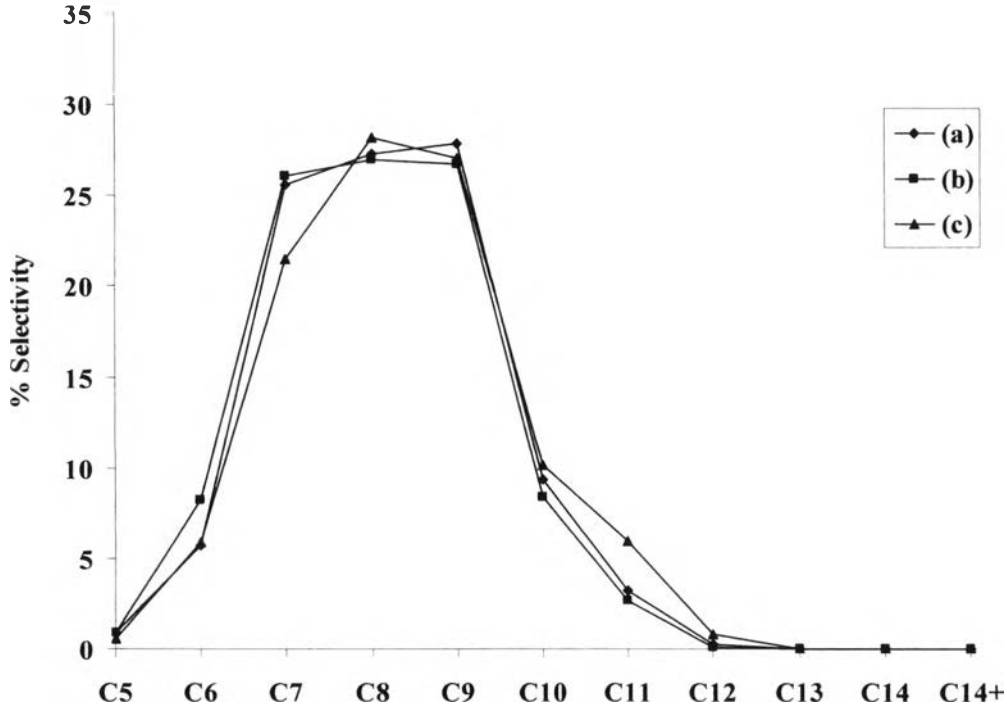

Figure 4.25 Carbon number distribution of liquid fractions from catalytic cracking of PP waste over zeolite beta with various SBA-15/AIP ratios: (a) 30; (b) 60 and (c) 90.

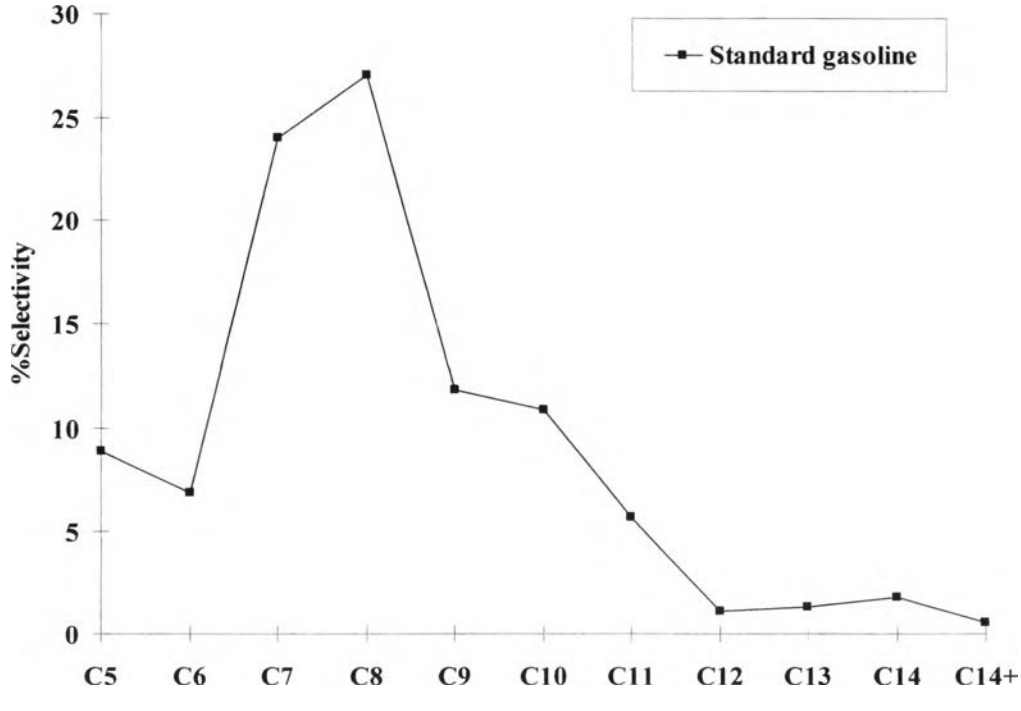

Figure 4.26 Carbon number distribution of commercial SUPELCO standard gasoline fraction.

4.3.2. Effect of Reaction Temperature

Zeolite beta with the SBA-15/AIP of 30 was used as a catalyst for studying the influence of temperature on its activity and the thermal cracking was tested in comparison. The values of %conversions and product distribution for thermal and catalytic cracking of PP waste at 350, 380, 400 and 420°C are shown in Table 4.5.

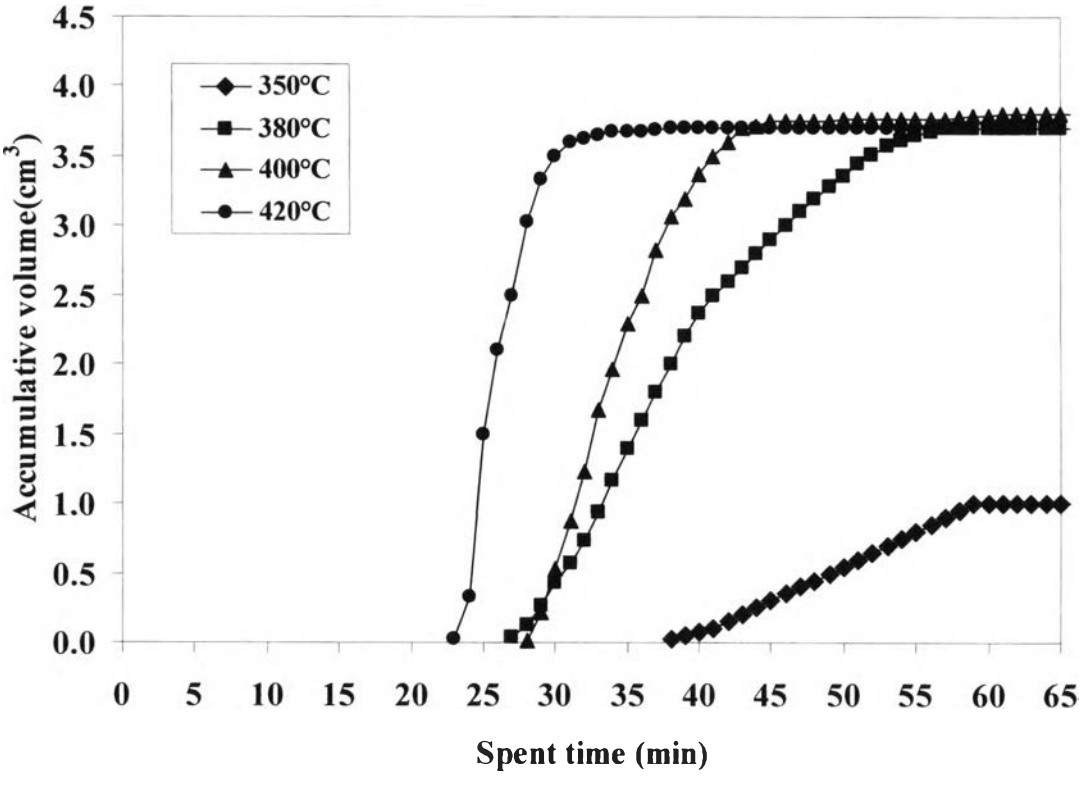

Figure 4.27 Accumulative volume of liquid fractions from catalytic cracking of PP waste over zeolite beta catalyst (SBA-15/AIP = 30, Run No.9) with various reaction temperatures.

Table 4.5 Values of % conversion and % yield obtained by thermal cracking and catalytic cracking of PP waste over zeolite beta (SBA-15/AIP = 30, Run No.9) various temperatures (Conversion: 10 wt% catalyst of plastic, N_2 flow of 20 cm^3/min. and reaction time of 40 min).

	350°C		380°C		400°C		420°C	
	catalytic	**thermal**	**catalytic**	**thermal**	**catalytic**	**thermal**	**catalytic**	**thermal**
%conversion[a]	50.5	2.0	95.5	21.2	96.0	60.0	96.1	93.3
%yield								
1. gas fraction[b]	33.1	2.0	42.9	14.3	42.6	25.2	44.5	41.1
2.liquid fraction[c]	17.4	-	52.6	6.9	53.4	34.8	51.5	52.2
- distillate oil	14.8	-	40.8	3.8	41.6	18.5	39.0	28.9
- heavy oil	2.6	-	11.8	3.1	11.8	16.3	12.5	23.3
3. residue[d]	49.5	98.0	4.5	78.8	4.0	40.0	3.9	6.7
- wax	-	-	2.75	-	2.33	-	2.31	-
- solid coke	-	-	1.75	-	1.67	-	1.59	-
4.Total volume of liquid fraction (ml)	1.00	-	3.70	0.33	3.80	2.30	3.70	3.40
5. Liquid fraction density (g/cm^3)	0.72	-	0.71	1.0	0.70	0.76	0.69	0.76

[a] Deviation within 0.20 [b] Deviation within 0.23
[c] Deviation within 0.30 [d] Deviation within 0.20

The activities of PP waste in term of %conversion and product distribution are very high up to 96% at all temperature from 380 to 420°C and are temperature independent. Below the temperature of 380°C the %conversion is affected by the temperature, the conversion decreases with decreasing the cracking temperature. The distribution of both gas and liquid products are also affected by temperature when the temperature was lowered than 380°C. Considering at temperature in the range 380°C to 420°C, the products are mainly in liquid fractions at the high yield about 51-53 % with minor product in gas fractions at the yield about 42-44 %. The distillated oil at 380°C and 400°C are not different. The effect of zeolite beta on PP waste cracking clearly observes at the residue of catalytic cracking dramatically reduces from 78.8% to 4.5% compared with thermal cracking. The liquid fractions have pale yellow color in all four temperatures.

The only difference is the initial rate of liquid formation as interpreted from Figure 4.27 which shows the plots of accumulative volume of liquid fractions versus lapsed time for PP waste cracking over zeolite beta with SBA-15/AIP ratio of 30 at various reaction temperatures. When the temperature is increased, the initial rate of liquid formation is faster. The rate of liquid formations is in the order of 420°C > 400°C > 380°C > 350°C.

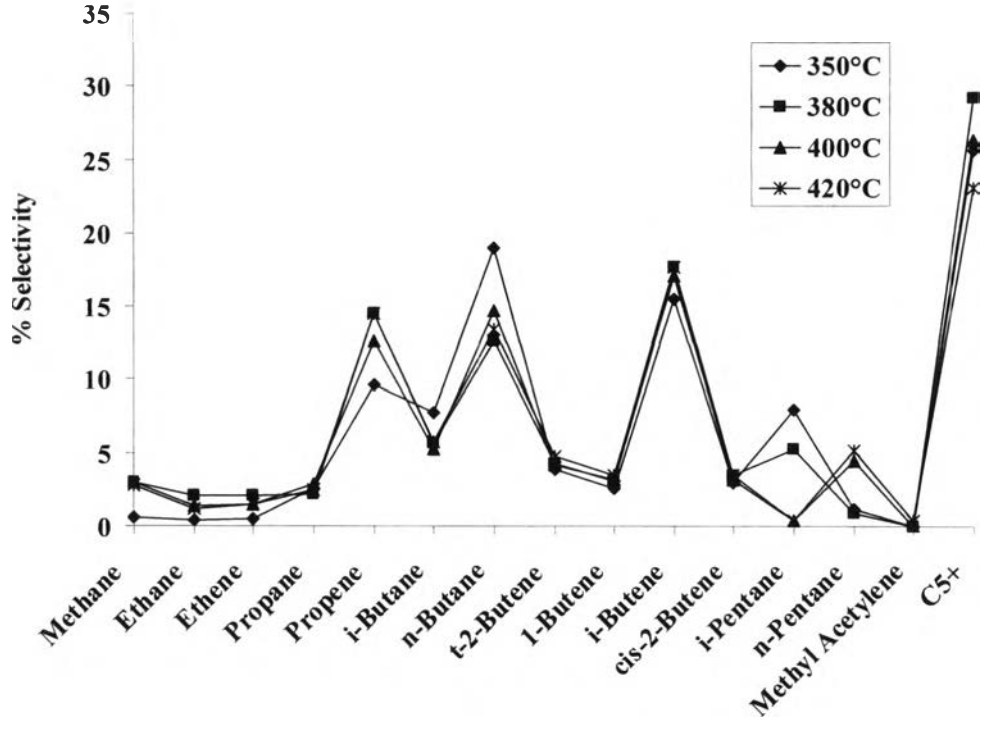

Figure 4.28 Product distribution of gas fractions obtained by catalytic cracking of PP waste using zeolite beta (SBA-15/AIP = 30, Run No.9) with various reaction temperatures.

Figure 4.28 and 4.29 shows distribution of gas fractions provided by catalytic cracking of PP waste over zeolite beta with the SBA-15/AIP ratio of 30 and thermal cracking at 350, 380, 400 and 420°C. The major component for catalytic cracking is propene, *n*-butane, *i*-butene and C_5^+. When the reaction temperature increases, lighter hydrocarbons (methane and ethane) increase. Considering of PP waste at ambient condition which are C_1 through C_5, major component for thermal cracking are propene and *n*-pentane. The growing yield of volatile components as function of temperature could be caused by the differences in the thermal stability of polymer chain, because hydrocarbon have reducing thermal stability with increasing temperature. Therefore, the C-C bonds were cracked more easily at 400 and 420°C than at lower temperature, and it resulted in higher yield of volatile products. Considering the gas selectivity of catalytic cracking of PP waste at 420°C are lower *n*-butane and higher *i*-pentane than 400°C due to the effect of thermal cracking with catalytic cracking.

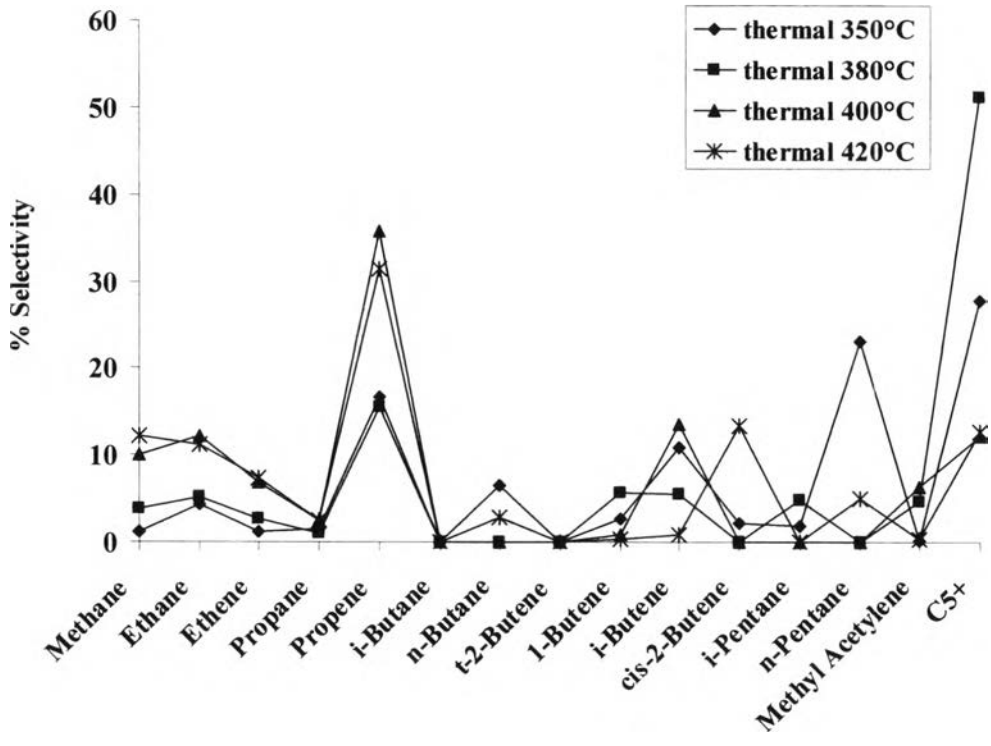

Figure 4.29 Product distribution of gas fractions obtained by thermal cracking of PP waste at various reaction temperatures.

Figures 4.30 and 4.31 show distribution of liquid fraction provided by catalytic cracking and thermal cracking of PP waste over zeolite beta with the SBA-15/AIP ratio of 30 at various temperatures. The major component for catalytic cracking is propene, *n*-butane, *i*-butene and C_5^+. When the reaction temperature increases, lighter hydrocarbons (methane and ethane) increase. The distillate oil components are mainly in the range of C_7 to C_9 for reaction temperatures at 380-420°C while C_8 and C_9 are major products at 350°C. This result indicates that liquid product distribution depends on temperature only at low temperature. The conversion and product distribution obtained at the temperatures of 380°C and 400°C are not different. As a result the temperature of 380°C is selected to be the test condition for further studies in this work. For thermal cracking at 380°C, the liquid fraction is rich of C_9. For the thermal cracking at 400 and 420°C, the liquid hydrocarbon fractions are distributed in a wide range of equivalent hydrocarbons from C_6 to C_9. It is well known that thermal cracking occurs by random scissoring of the

long polymeric chain and products of cracking are distributed in a wide range of molecular weights.

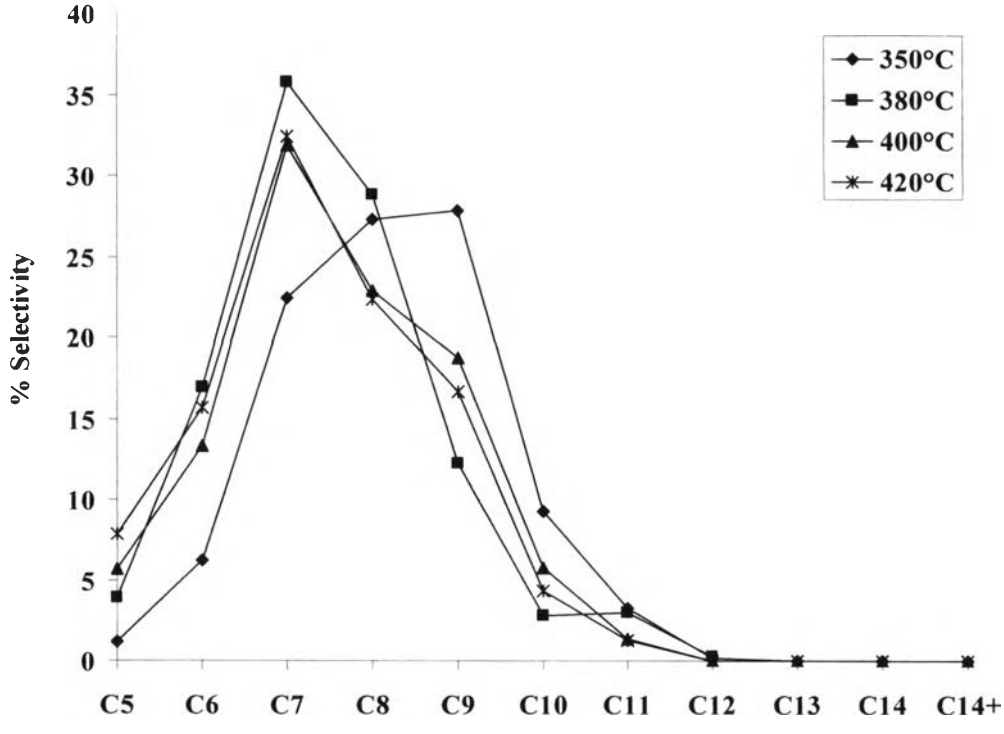

Figure 4.30 Carbon number distribution of liquid fractions from catalytic cracking of PP waste over zeolite beta (SBA-15/AIP = 30, Run No.9) with various reaction temperatures.

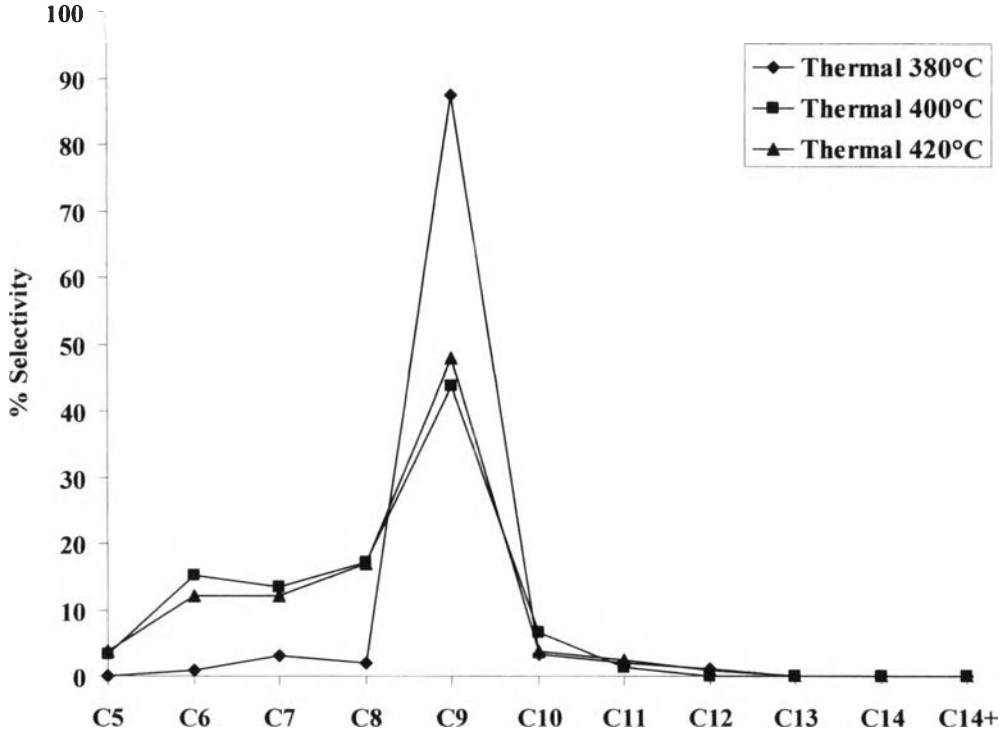

Figure 4.31 Carbon number distribution of liquid fractions from thermal cracking of PP waste at various reaction temperatures.

4.3.3. Effect of PP Waste to Catalyst Ratios

Values of conversion and product yield from PP waste cracking over zeolite beta with SBA-15/AIP ratio of 30 at 380°C with different catalyst amounts of 1, 3, 5 and 10 wt% to PP waste are shown in Table 4.6. The high conversion value of 95.8 and 95.5% are obtained in the cases of using 5 wt% and 10 wt% catalyst amounts but the conversion decreases to 85.9% in the case of using only 3 wt% catalyst amount. Reducing of catalyst amount to 1 wt% leads the %conversion drops to 49.3%, indicating that the conversion strongly depends on the catalyst content. The conversion strongly depends on the catalyst amount not exceeding 5%. However, % products yield the gas fraction yield decrease when the amount of catalyst reduces. Basically, the less catalyst amount, the less acidity resulting in the less gas fraction yield. However, there is no difference in liquid fraction yield. The amount of residue and the conversion are inversely related. The residue produced by using lower 5 wt% catalyst amount contains mainly wax to lower activity compared to using 5 wt%

catalyst. The lower acidity, the higher wax and residue is found. From the results that mention above, the optimum catalyst amount is the 5 wt% catalyst to PP waste due to the highest %conversion and lowest residue.

Table 4.6 Values of % conversion and % yield obtained by catalytic cracking of PP waste over zeolite beta (SBA-15/AIP of 30, Run No.9) various catalyst amounts at 380°C (Conversion: N_2 flow of 20 cm^3/min. and reaction time of 40 min).

	Catalyst amount			
	1%	**3%**	**5%**	**10%**
%conversion[a]	49.3	85.9	95.8	95.5
%yield				
1. gas fraction[b]	25.9	39.5	42.2	42.9
2.liquid fraction[c]	23.4	46.4	53.6	52.6
- distillate oil	19.2	36.7	39.0	40.8
- heavy oil	4.2	9.7	14.6	11.8
3. residue[d]	50.7	14.1	4.2	4.5
- wax	-	-	3.1	2.7
- solid coke	-	-	1.1	1.8
4.Total volume of liquid fraction (ml)	1.41	3.05	3.70	3.70
5. Liquid faction density (g/cm^3)	0.71	0.72	0.71	0.71

[a] *Deviation within 0.30* [b] *Deviation within 0.40%*
[c] *Deviation within 0.35* [d] *Deviation within 0.30%*

Figure 4.32 shows the kinetic rate in catalytic cracking of PP waste over various amounts of zeolite beta catalyst at 380°C. The initial rates of liquid fractions in the reaction using 5 wt% and 10 wt% catalyst content are faster than that over using 3 wt% and 1 wt% catalyst amount, indicating the predominant competitive rate of dissociation of liquid molecules to gas molecules compared to the rate of liquid formation.

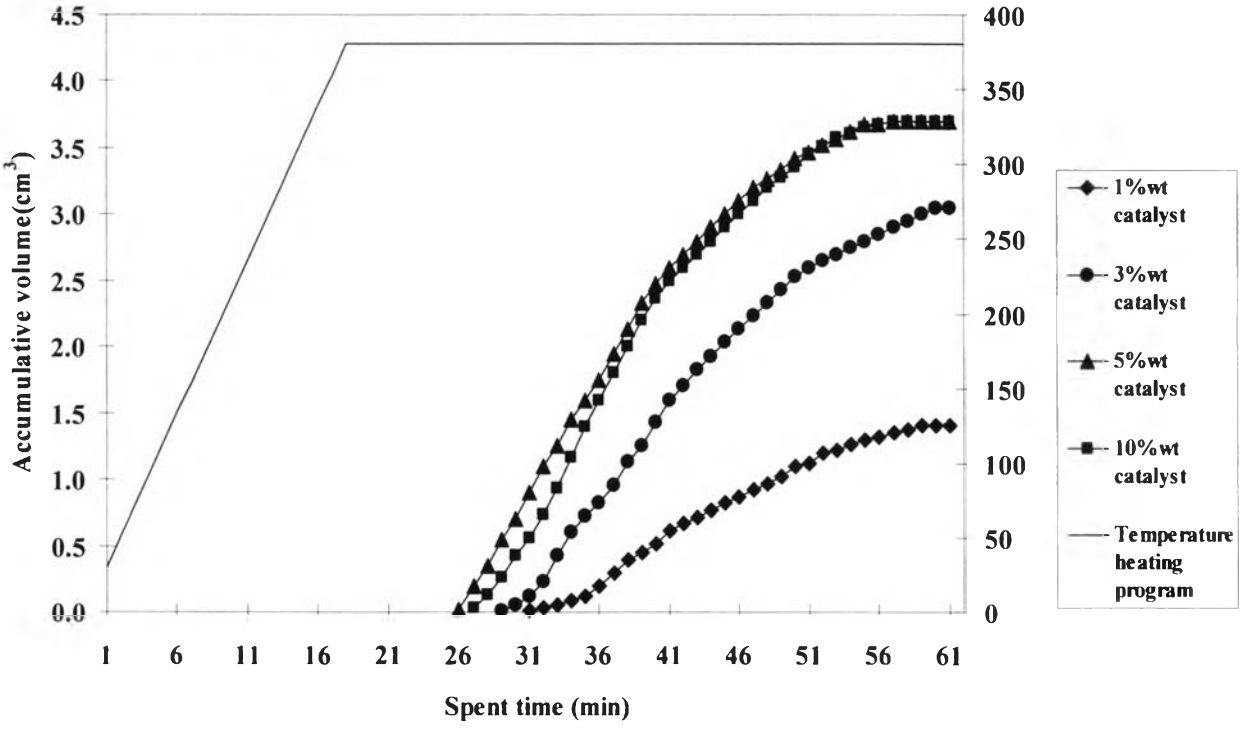

Figure 4.32 Accumulative volume of liquid fractions from catalytic cracking of PP waste over zeolite beta catalyst (SBA-15/AIP = 30, Run No.9) with various catalyst amounts.

Figure 4.33 shows distribution plots of gas fractions obtained by catalytic cracking of PP waste over zeolite beta with SBA-15/AIP ratio of 30 catalyst with different catalyst amount at 380°C. The favored gaseous products are propene, *i*-butene and C_5^+. The selectivity of gas fraction for 5% and 10% catalyst amounts are similar but different from that for the 1 and 3 wt% catalyst amounts.

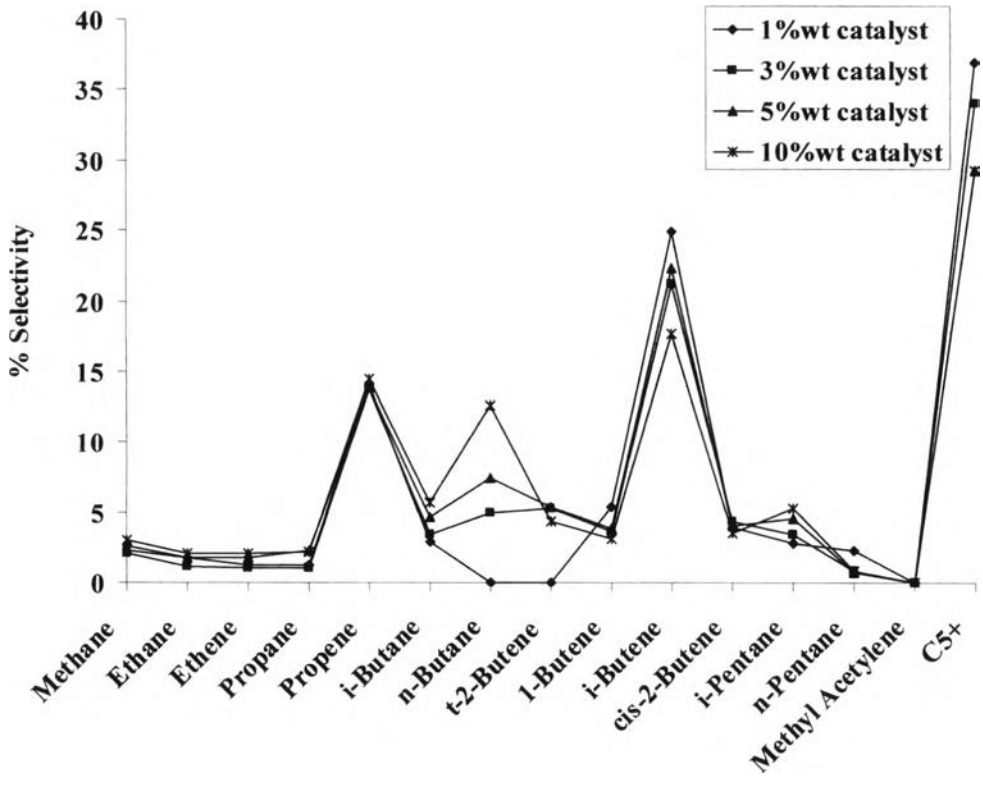

Figure 4.33 Product distribution of gas fractions obtained by catalytic cracking of PP waste using zeolite beta (SBA-15/AIP = 30, Run No.9) with various catalyst amounts.

The product distributions of light oil obtained by catalytic cracking of PP waste over zeolite beta catalysts with different catalyst amounts at 380°C are shown in Figure 4.34. The product distributions in liquid phase for 1, 3, 5 and 10 wt% catalyst amount are different. For 3, 5 and 10 wt% catalyst content, the major products are in the range of C_7 and C_8 while C_7 to C_9 are dominant for 3 wt% catalyst content. When catalyst amount is reduced, the liquid products distributed in the range of C_6 and C_7 increases while the selectivity to C_9 and C_{10} components decrease. In this work, the choice is using 5 wt% catalyst amounts due to it gives high % conversion and used small amount of catalyst.

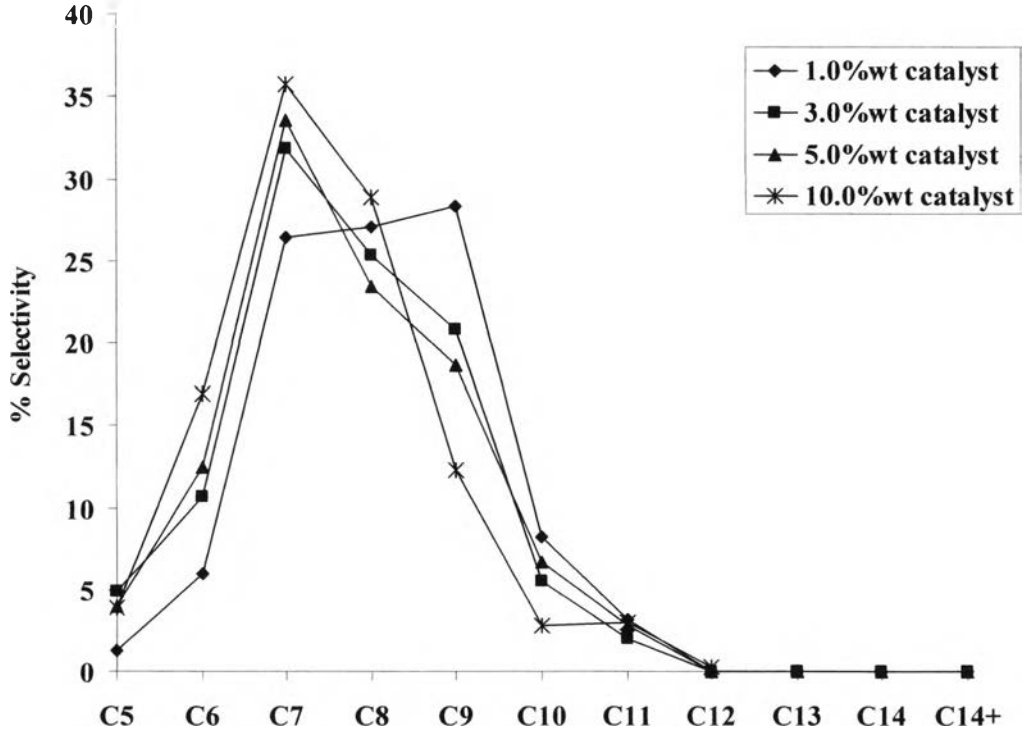

Figure 4.34 Carbon number distribution of liquid fractions from catalytic cracking of PP waste of using zeolite beta (SBA-15/AIP = 30, Run No.9) with various catalyst amounts.

4.3.4 Activities of Regenerated BEA in PP Waste Cracking

The values of %conversion and %yield obtained by the PP waste cracking using fresh and regenerated zeolite beta with SBA-15/AIP ratio of 30 catalysts at 380°C are shown in Table 4.7. The values of %conversion are not different from fresh catalyst. The regenerated catalyst provided relatively lower yield of gas fraction and higher residue comparing to the fresh catalyst. Relatively more amount of residue, especially in form of wax was remained in the reactor of the regenerated catalyst rather than that of fresh catalyst. This result suggests the regenerated catalysts have less specific surface area and acidity than the fresh catalyst.

Table 4.7 Values of % conversion and % yield obtained by catalytic cracking of PP waste using the fresh and the regenerated catalysts (SBA-15/AIP = 30, Run No.9) at 380°C (Conversion: 5 wt% catalyst of plastic, N_2 flow of 20 cm^3/min. and reaction time of 40 min).

	Fresh Run No.9	**1st Regenerated Run No.9**	**2nd Regenerated Run No.9**	**3rd Regenerated Run No.9**
%conversion[a]	95.8	95.1	93.5	85.6
%yield				
1. gas fraction[b]	42.2	40.5	37.7	36.6
2. liquid fraction[c]	53.6	54.6	55.8	49.0
- distillate oil	39.0	39.8	42.2	36.8
- heavy oil	14.6	14.8	13.6	12.2
3. residue[d]	4.2	4.8	6.5	14.4
- wax	3.1	3.09	3.92	7.53
- solid coke	1.1	1.76	2.16	6.87
4. Total volume of liquid fraction (ml)	3.70	3.73	3.80	3.12
5. Liquid faction density (g/cm^3)	0.71	0.71	0.71	0.72

[a] *Deviation within 0.68%* [b] *Deviation within 0.98%*
[c] *Deviation within 0.42%* [d] *Deviation within 0.68%*

Figure 4.35 shows the accumulated volume of liquid fraction in the graduated cylinder. The initial rate of liquid formation is not significantly different on matter using the fresh or regenerated 1 to 2 cycles. For the third regenerated, the initial rate is slow and gives small amount of total liquid fractions, indicating the efficiency of catalyst is limited.

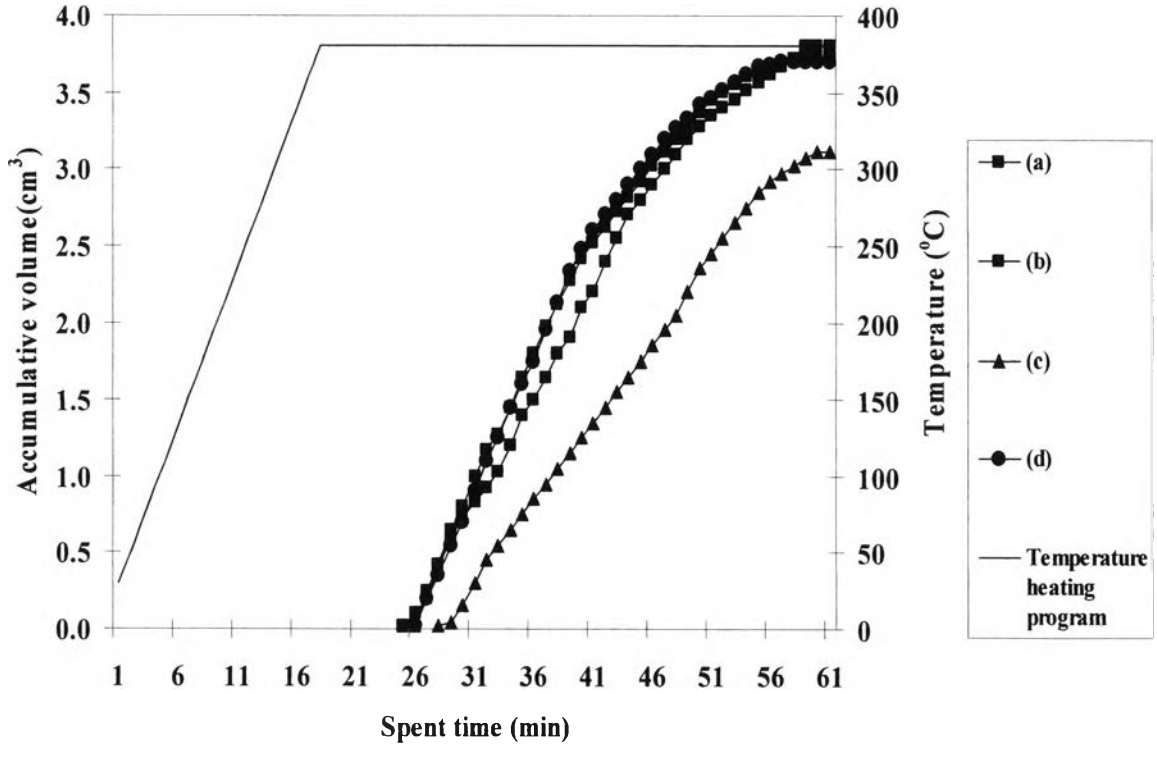

Figure 4.35 Accumulative volume of liquid fractions from catalytic cracking of PP waste over the fresh and the regenerated catalysts (SBA-15/AIP = 30, Run No.9): (a) the 1st regenerated; (b) 2nd regenerated; (c) 3rd regenerated catalyst and (d) fresh catalyst.

Figure 4.36 shows distribution of gas fractions obtained by catalytic cracking of PP waste using the fresh and regenerated zeolite beta with SBA-15/AIP ratio of 30 catalysts at 380°C. The gas fraction composes the same product distribution. There is no difference in selectivity in gas fraction between four catalysts.

The product distribution of liquid fraction obtained by catalytic cracking of PP waste using the fresh and regenerated zeolite beta with SBA-15/AIP ratio of 30 catalysts at 380°C are shown in Figure 4.37. Both fresh, regenerated 1 and 2 cycles catalysts provide mainly C_7 and C_8 while C_8 and C_9 are mainly product for third regenerated, indicating the acidity of catalyst at the third regenerated is reduced by several calcinations before used.

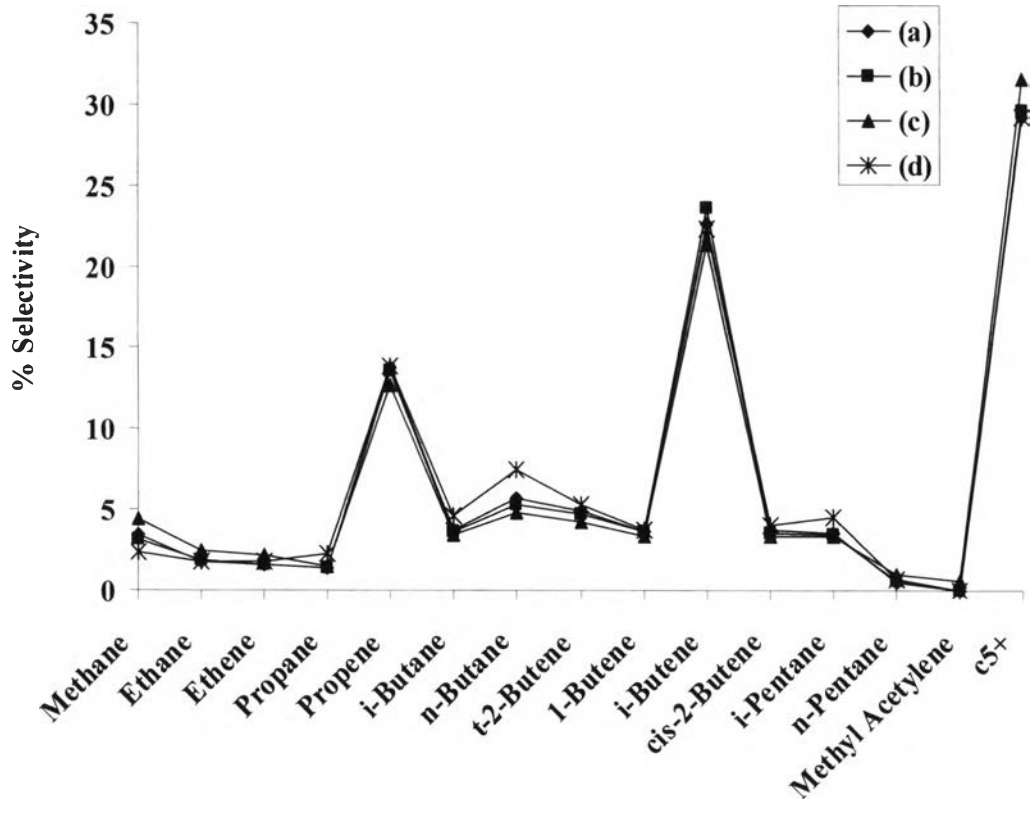

Figure 4.36 Distribution of gas fraction obtained by catalytic cracking of PP waste using the fresh and the regenerated Run No.9 catalysts (SBA-15/AIP = 30, Run No.9): (a) the 1st regenerated; (b) 2nd regenerated; (c) 3rd regenerated catalyst and (d) fresh catalyst.

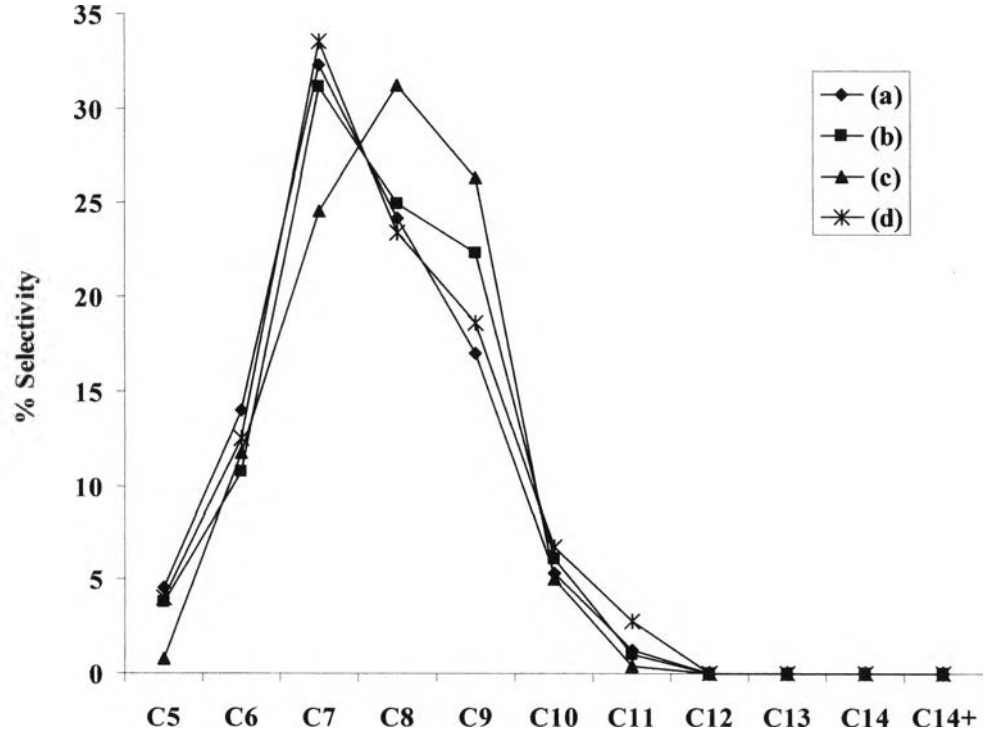

Figure 4.37 Distribution of liquid fraction obtained by catalytic cracking of PP waste using the fresh and the regenerated (SBA-15/AIP = 30, Run No.9): (a) the 1st regenerated; (b) 2nd regenerated; (c) 3rd regenerated catalyst and (d) fresh catalyst.

4.3.5 Regenerated Catalyst (PP)

4.3.5.1 XRD Results

The used zeolite beta with SBA-15/AIP ratio of 30 catalysts became black after use due to coke deposit on the surface and pore. However, it easily turned to white after regeneration by calcinations in muffle furnace at 550°C for 5 h. XRD patterns of the calcined unused and regenerated zeolite beta with SBA-15/AIP of 30 catalysts are shown in Figure 4.38. After catalytic run, the structure of zeolite beta was still remained for the 1st regenerated (firstly regenerated), 2nd regenerated (secondly regenerated) and 3rd regenerated (thirdly regenerated) catalysts with almost the same crystallinity as the unused catalyst.

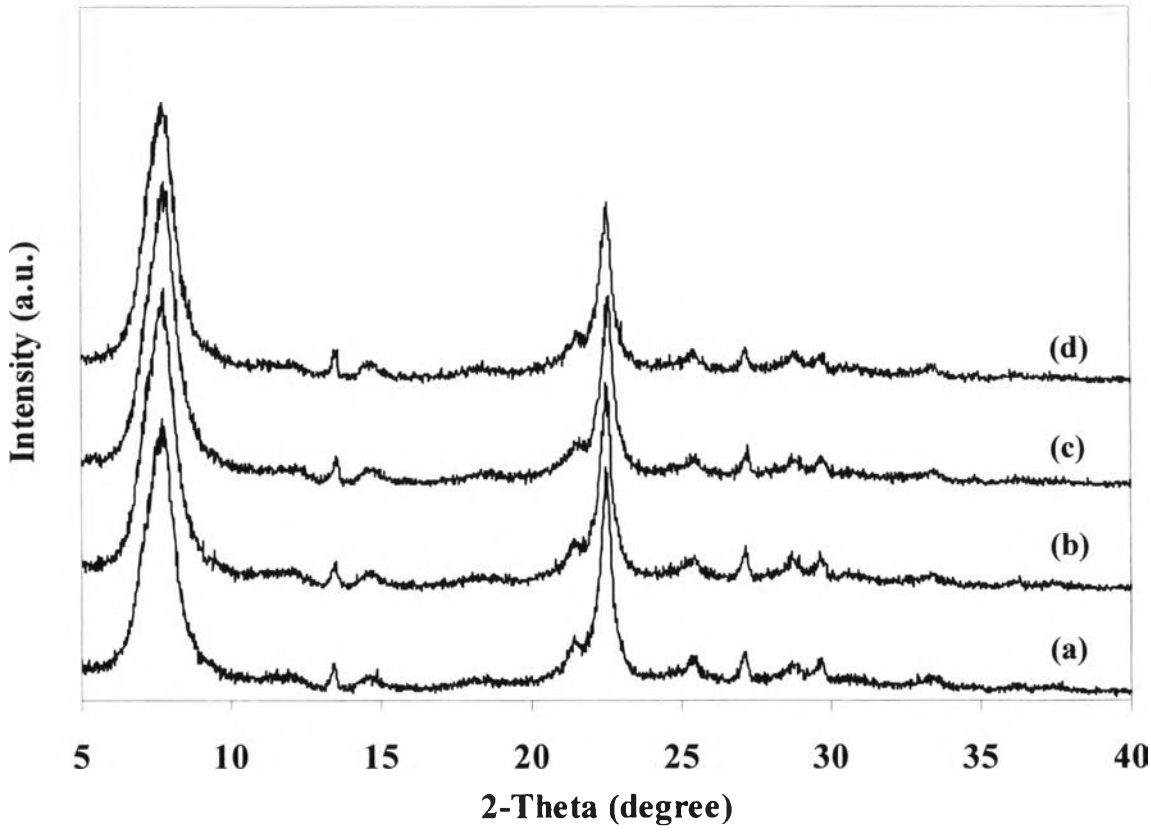

Figure 4.38 XRD pattern of (a) the calcined unused; (b) the 1st regenerated; (c) 2nd regenerated and (d) 3rd regenerated catalyst.

4.3.5.2 SEM Images

Figure 4.39 shows SEM images of the 3rd regenerated catalyst with different magnification. After the third regenerated catalytic run, it is obvious that the regenerated catalyst particle are not changed morphology with similar particle size compared to the fresh catalyst picture of which has been shown in Figure 4.20(a).

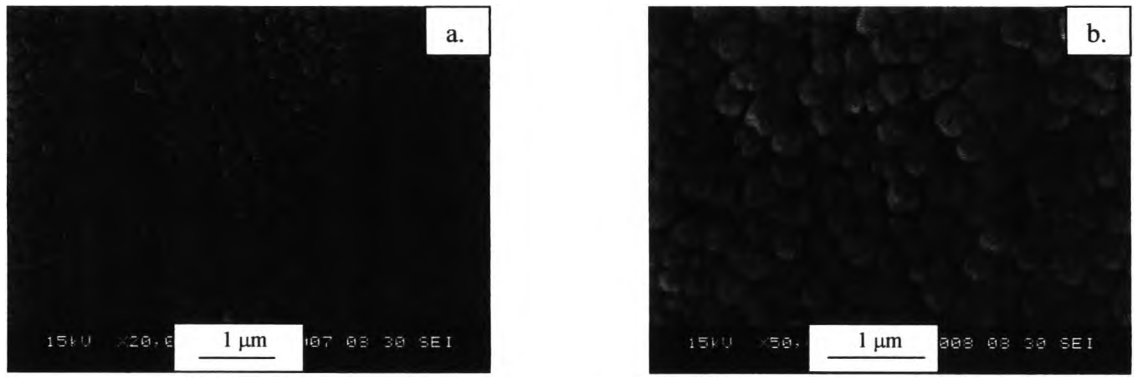

Figure 4.39 SEM images of 3rd regenerated Run No.9 sample with different magnification (a) x20,000 and (b) x 50,000.

4.3.5.3 Nitrogen Adsorption-Desorption

The adsorption-desorption isotherms of fresh and regenerated catalysts are shown in Figure 4.40. The calcined unused, 1st regenerated, 2nd regenerated, 3rd regenerated and fresh catalyst exhibits the characteristic isotherm of microporous material with the specific surface area of 724, 679, 648 and 782 m^2/g. It was sharply decreased compared with the fresh catalyst.

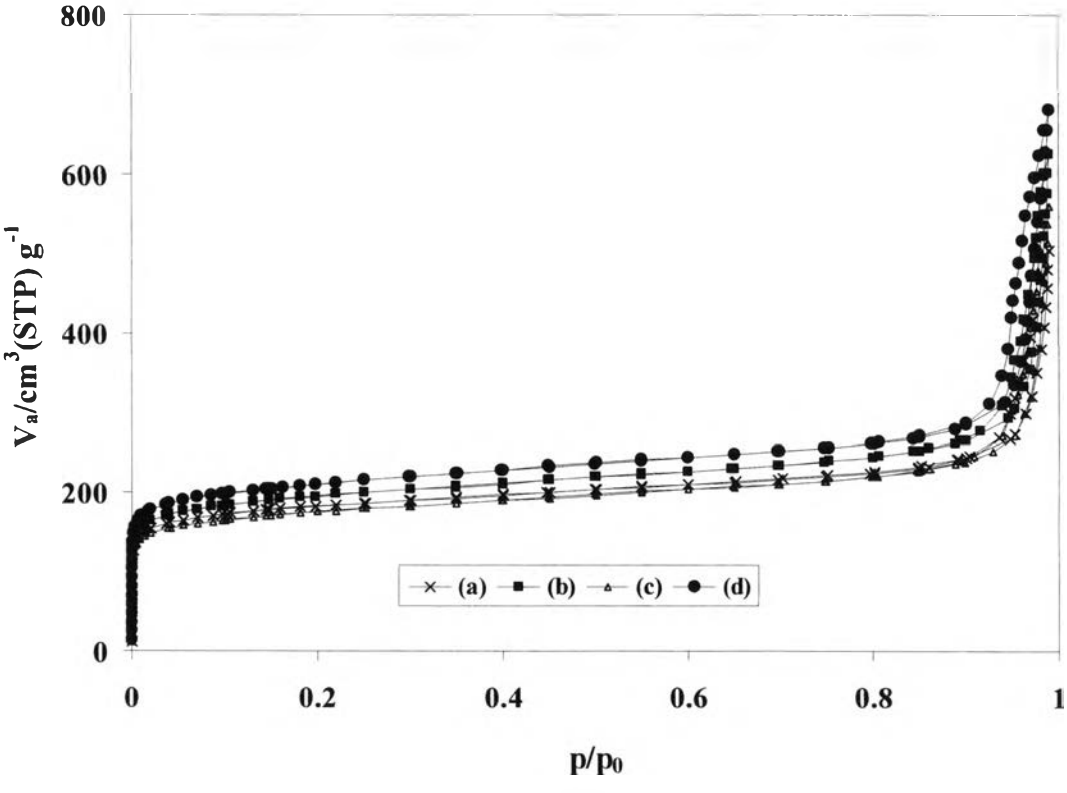

Figure 4.40 N_2 dasorption-desorption isotherms of the regenerated and fresh catalyst: (a) the 1st regenerated; (b) 2nd regenerated; (c) 3rd regenerated catalyst and (d) fresh catalyst.

4.4 Activities of Various Zeolite Beta Catalysts in HDPE Waste Cracking

4.4.1 Effect of SBA-15/AIP Ratios

The values of %conversion and product yield obtained by the thermal cracking catalytic cracking of HDPE waste over zeolite beta catalysts with different SBA-15/AIP ratios at 380°C are compared in Table 4.8. The %conversion for catalytic cracking is extremely higher than thermal cracking. The result shows that the cracking of HDPE wastes at low temperature of 380°C hardly occur without presence of catalyst. The % conversions are in the range from 79.4 to 88.0%. Zeolite beta with SBA-15/AIP ratio of 60 gives highest % conversion and light oil due to that gives a highest stronger acidity. Furthermore, zeolite beta with SBA-15/AIP ratio of 90 shows the higher %conversion than SBA-15/AIP ratio of 30 because of the higher total

acidity of SBA-15/AIP ratio of 90. The result indicates that the acidity of those catalysts is more dominant than its specific surface area and external surface area. Considering the catalytic cracking of HDPE waste is lower than that PP waste at the same temperature owing to the enhanced reactivity associated to the structure of these polymers. HDPE waste is formed by linear macromolecule, whereas PP waste is characterized by a certain degree of branching. The presence of tertiary carbon in PP waste molecules provides favorable position for the initiation of polymer chain cracking since their activation requires weaker conditions than the secondary carbon activation does [132].

Table 4.8 Values of % conversion and % yield obtained by thermal cracking and catalytic cracking of HDPE waste over zeolite beta with various SBA-15/AIP ratios (Conversion: 10wt% catalyst of plastic, N_2 flow of 20 cm^3/min. 380°C and reaction time of 40 min).

	Thermal 380°C	**Run No.9** (SBA-15/AIP = 30)	**Run No. 5** (SBA-15/AIP = 60)	**Run No. 10** (SBA-15/AIP = 90)
%conversion[a]	0.3	79.4	88.0	82.4
%yield				
1. gas fraction[b]	0.3	40.4	39.6	35.3
2.liquid fraction[c]	-	39.0	48.4	47.1
- distillate oil	-	27.6	37.2	34.6
- heavy oil	-	11.4	11.2	12.5
3. residue[d]	99.7	20.6	11.9	17.6
- wax	-	18.6	9.9	13.9
- solid coke	-	2.0	2.0	3.7
4.Total volume of liquid fraction (ml)	-	2.38	3.15	2.98
5.Liquid faction density (g/cm^3)	-	0.73	0.72	0.72

[a] *Deviation within 0.30%,* [b] *Deviation within 0.34%*
[c] *Deviation within 0.30%,* [d] *Deviation within 0.30%*

Figure 4.41 shows accumulated volume of liquid fraction in graduated cylinder in case of normal zeolite beta with various SBA-15/AIP ratios. The initial rate of zeolite beta with SBA-15/AIP ratio of 60 is faster than zeolite beta with SBA-15/AIP ratio of 30 and 90. That confirms the acidity effect of Al incorporated in the zeolite beta structure can play important role on activity of catalysts in cracking of HPDE waste.

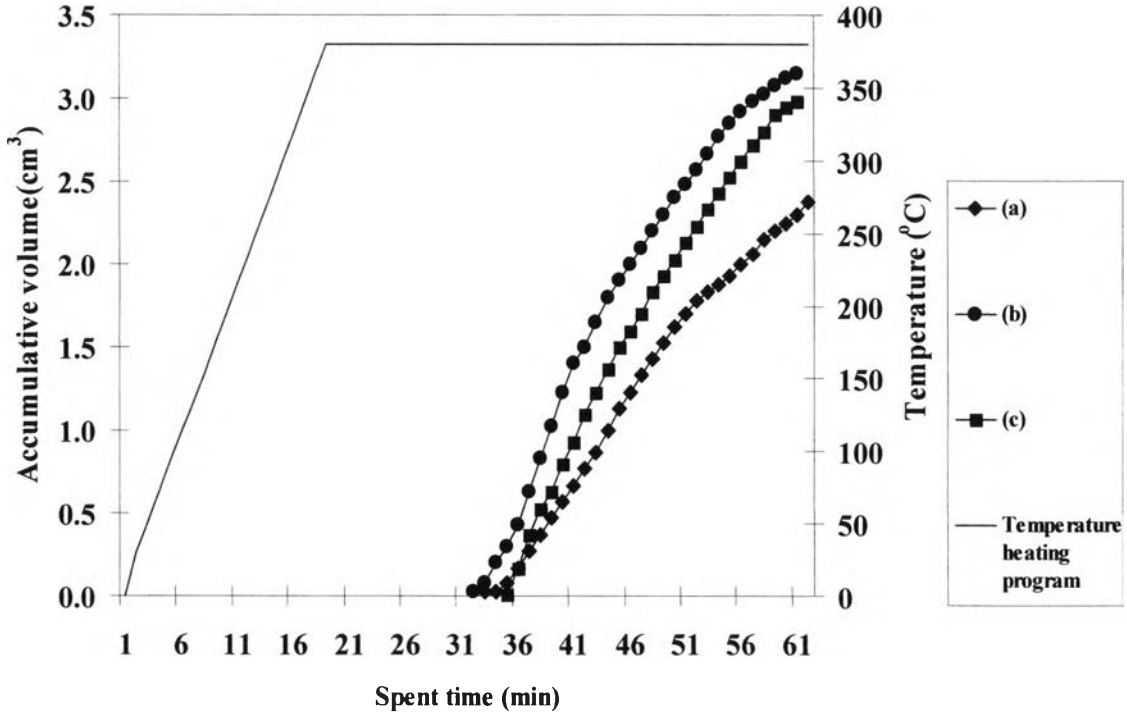

Figure 4.41 Accumulative volume of liquid fractions from catalytic cracking of HDPE waste over zeolite beta with various SBA-15/AIP ratios: (a) 30; (b) 60 and (c) 90.

Figure 4.42 shows distribution plot of gas fractions obtained by thermal cracking and catalytic cracking of HDPE waste at 380°C. The main products of thermal cracking are propene, *i*-butene and C_5^+ whereas gas fractions of catalytic cracking consists of mainly propene, *n*-butane, *i*-butene and C_5^+. The product distribution in gaseous phase is slightly different upon changing the SBA-15/AIP ratio in catalyst. Figure 4.43 shows product distribution of distillate oil obtained by the catalytic cracking of HDPE waste with different SBA-15/AIP ratio. For the HDPE

waste cracking over all catalysts, liquid fraction is rich of C_7 and C_8. That is very similar to a commercial SUPELCO standard gasoline.

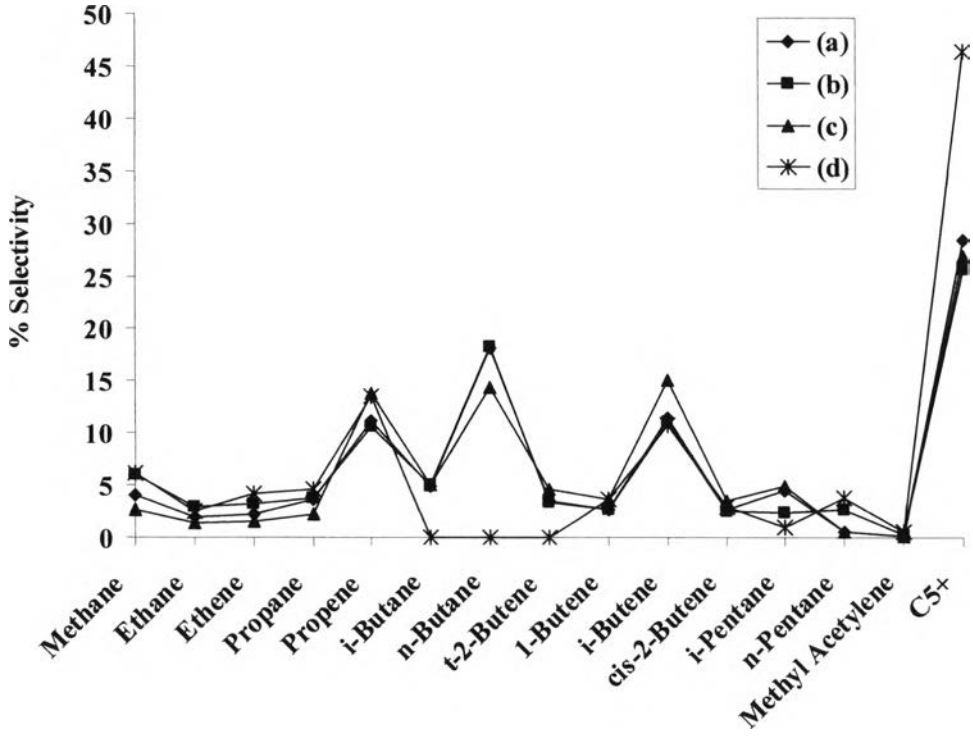

Figure 4.42 Product distribution of gas fractions obtained by catalytic cracking of HDPE using zeolite beta with various SBA-15/AIP ratios: (a) 30; (b) 60; (c) 90 and (d) thermal cracking at 380°C.

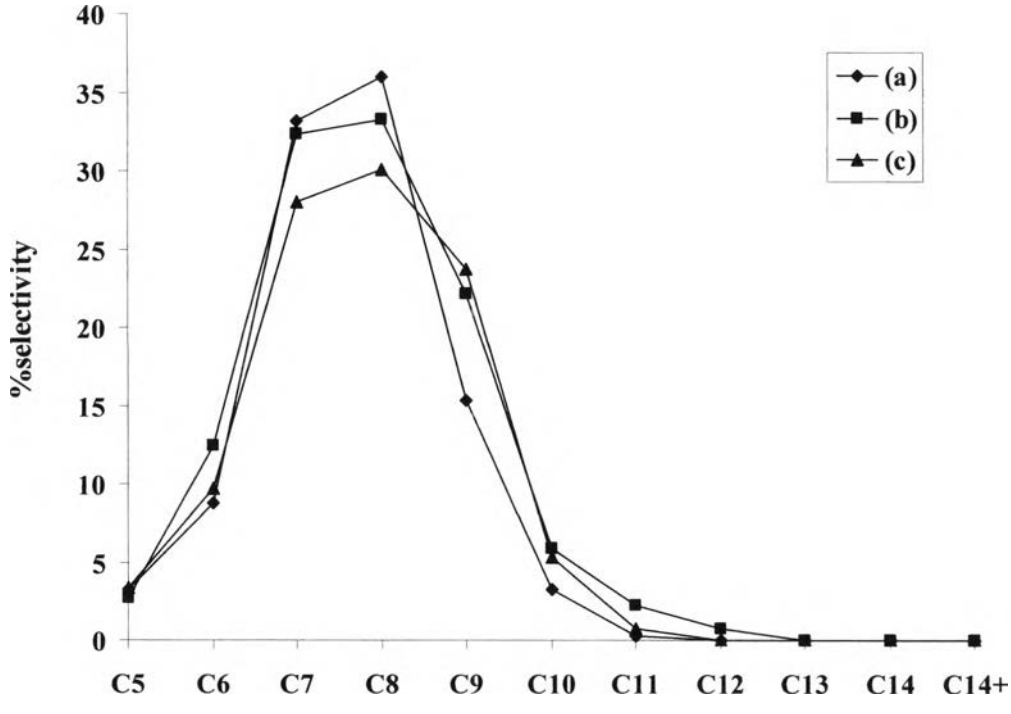

Figure 4.43 Carbon number distribution of liquid fractions from catalytic cracking of HDPE over zeolite beta with various SBA-15/AIP ratios: (a) 30; (b) 60 and (c) 90.

4.4.2 Effect of Reaction Temperature

Table 4.9 shows the value of % conversion and % yield obtained by thermal cracking and catalytic cracking of HDPE waste over zeolite beta with SBA-15/AIP ratio of 60 catalysts at different reaction temperature. The catalytic cracking gives the %conversion and %yield greatly higher than the thermal cracking due to the high acidity of catalyst. Increasing temperature from 380°C and 400°C resulted in significant higher % conversion and %yield. That indicates both conversion and yield of liquid products are affected by temperature of cracking. The %conversion and %yield of zeolite beta at 400°C and 420°C are not different. The increase of product yields (gases, liquids) as function of temperature could be caused by the differences in the thermal stability of polymer chain, since hydrocarbons have reducing thermal stability with increasing temperature.

Table 4.9 Values of % conversion and % yield obtained by thermal cracking and catalytic cracking of HDPE waste over zeolite beta (SBA-15/AIP = 60, Run No.5) various temperatures (Conversion: 10wt% catalyst of plastic, N_2 flow of 20 cm^3/min. and reaction time of 40 min).

	Thermal 380°C	380°C	Thermal 400°C	400°C	Thermal 420°C	420°C
%conversion	0.3	88.1	2.4	95.5	75.2	96.2
%yield						
1. gas fraction	0.3	39.6	2.4	37.9	67.8	36.9
2.liquid fraction	-	48.4	-	57.6	7.4	59.3
- distillate oil	-	37.2	-	41.7		41.6
- heavy oil	-	11.2	-	15.9		17.7
3. residue	99.7	11.9	97.6	4.5	24.8	3.8
- wax	-	9.9	-	2.8	-	2.3
- solid coke	-	2.0	-	1.7	-	1.5
4.Total volume of liquid fraction	-	3.15	-	4.05	0.40	4.18
5.Liquid faction density (g/cm^3)	-	0.72	-	0.71	0.77	0.71

[a] *Deviation within 0.11%,* [b] *Deviation within 0.23%*
[c] *Deviation within 0.30%,* [d] *Deviation within 0.20%*

Figure 4.44 show the volume of liquid fractions accumulated in the graduated cylinder. The initial rate of 420°C is much faster than 400°C and 380°C. That is due to the temperature dependence of kinetic effect. Therefore on the purpose of conversion of plastic to liquid fuel, the temperature of 400°C was selected for the rest of work on the catalytic cracking of HDPE waste.

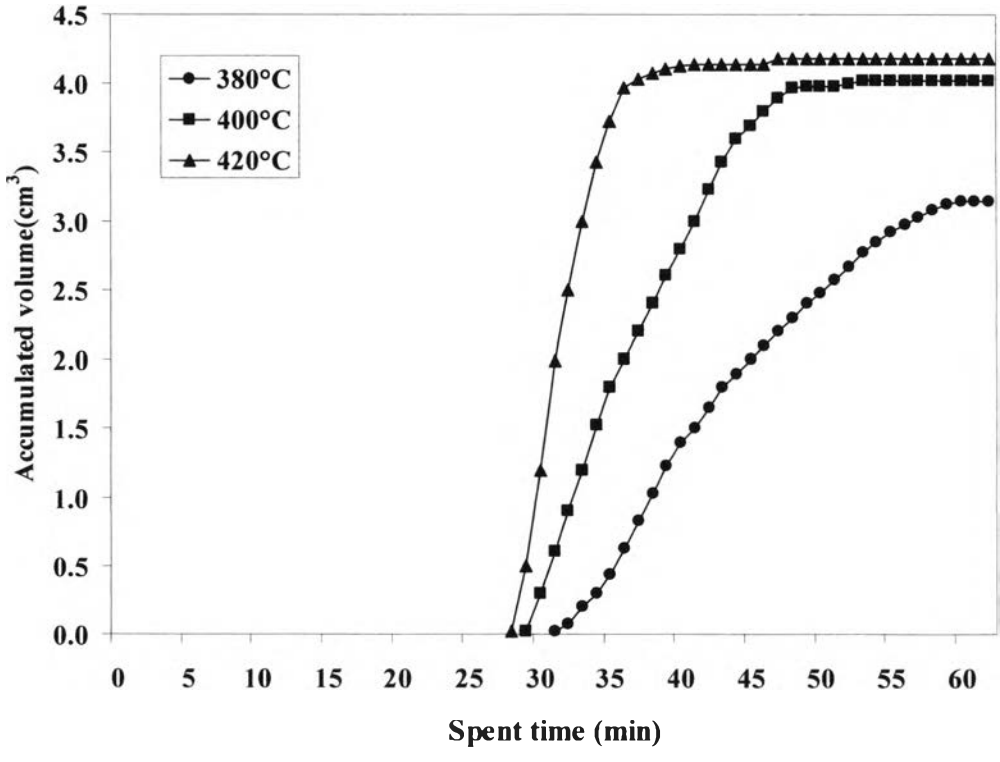

Figure 4.44 Accumulative volume of liquid fractions from catalytic cracking of HDPE waste over zeolite beta (SBA-15/AIP = 60, Run No.5) various temperatures.

Figure 4.45 and Figure 4.46 shows the component of gases formed in catalytic cracking reactions and thermal cracking of HDPE waste using zeolite beta with SBA-15/AIP ratio of 60 at 380, 400 and 420°C. In catalytic cracking, the main products are to propene, *n*-butane, *i*-butene and C_5^+. While in the thermal cracking, the distribution in gas fractions is mainly ethane, propene, *n*-butane, *i*-butene and C_5^+. It is indicating good catalytic activity for producing light hydrocarbon gases. The temperature also affected the composition of gases, because it was found that the concentration of products of HDPE waste catalytic cracking (propene, *n*-butane and

i-butene) increased, while that of C_5^+ decreased with increasing temperature. Changing of gasous component also presents in thermal cracking.

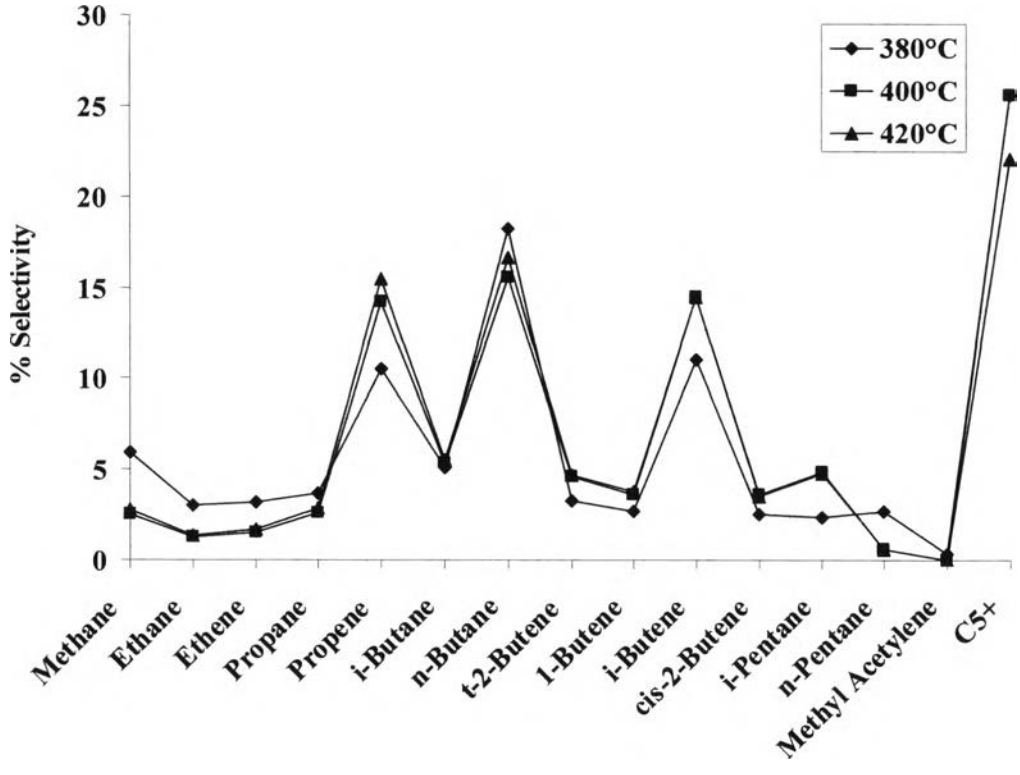

Figure 4.45 Product distribution of gas fractions obtained by catalytic cracking of HDPE using zeolite beta (SBA-15/AIP = 60, Run No.5) at various reaction temperatures.

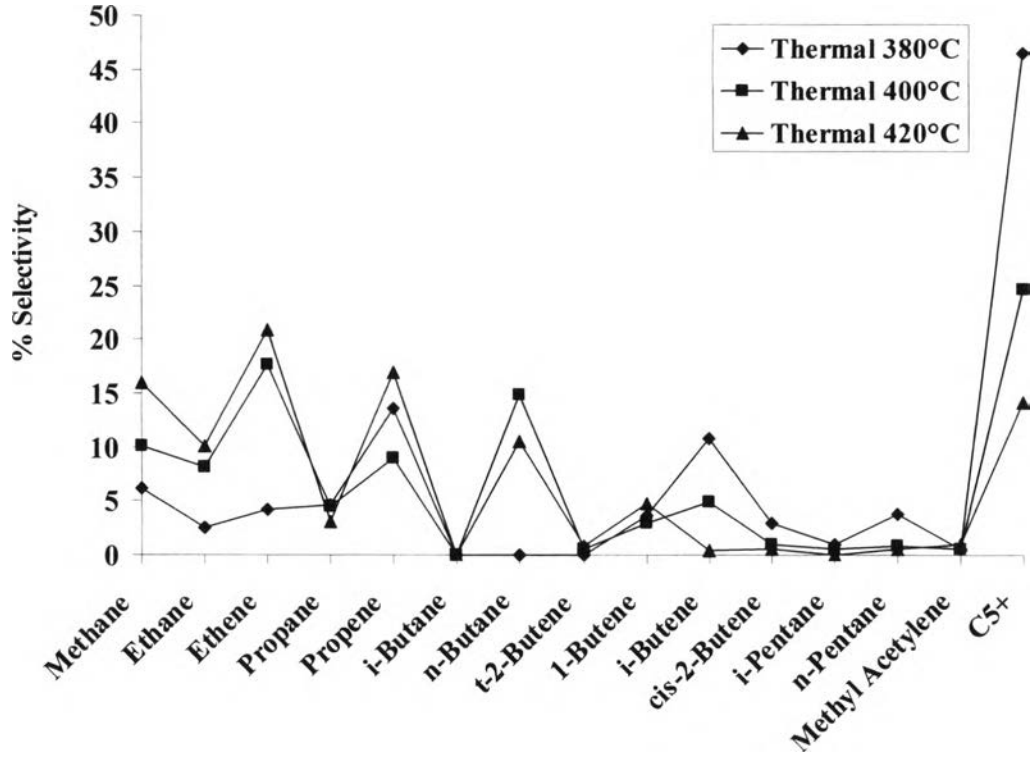

Figure 4.46 Product distribution of gas fractions obtained by thermal cracking of HDPE at various reaction temperatures.

Figure 4.47 shows product distribution of the liquid fractions obtained by catalytic cracking of HPDE waste using zeolite beta with SBA-15/AIP ratio of 60 with different temperature. For catalytic cracking at 380°C, the liquid fraction is mainly C_7 C_8 and C_9 components. Catalytic cracking at 400°C, the liquid fraction is mainly C_7 and C_8 components while at 420°C, liquid fraction is mainly C_7 components. When the temperature increases, the amount of lighter hydrocarbon increases while that of heavier hydrocarbon of C_8 and C_9 decreases. It can conclude that not only the presence of catalysts, but also the temperature affects the gases and liquid components.

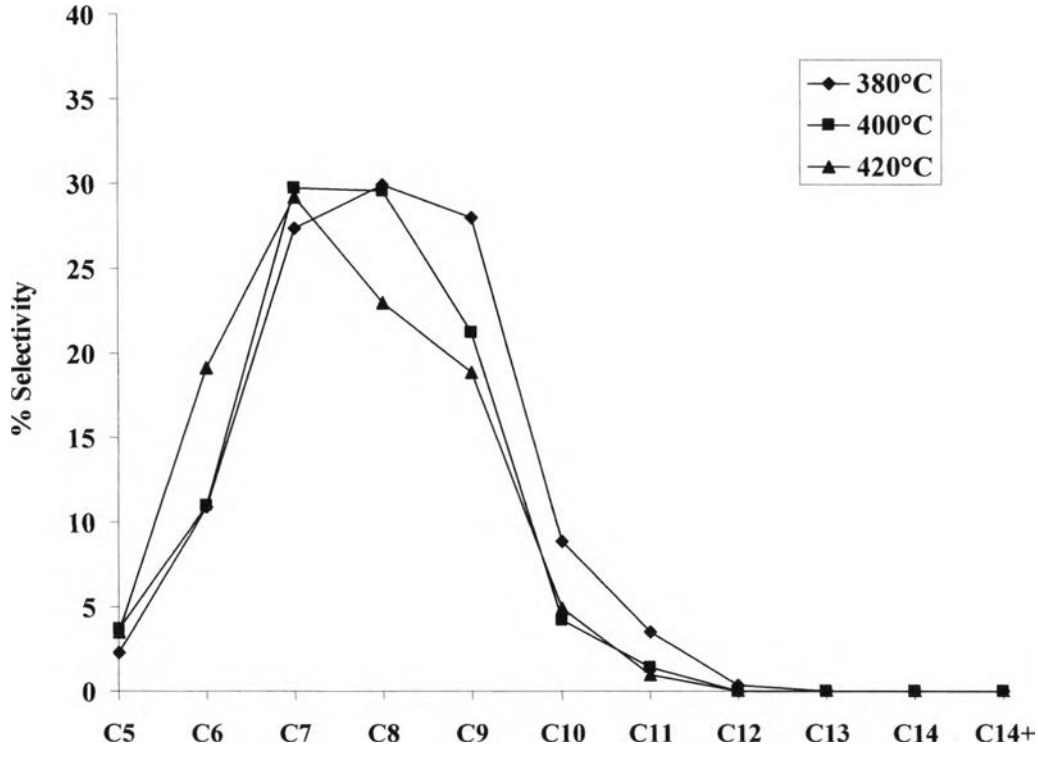

Figure 4.47 Carbon number distribution of liquid fractions from catalytic cracking of HDPE using zeolite beta (SBA-15/AIP = 60, Run No.5) at various reaction temperatures.

4.4.3 Effect of HDPE Waste to Catalyst Ratios

Table 4.10 shows the %conversion and product yield formed catalytic cracking of HDPE waste at 400°C over zeolite beta with SBA-15/AIP ratio of 60 catalyst with different catalyst amount of 0.5, 1, 3, 5 and 10 wt% to HDPE waste. The high conversion value of 95.0 % is obtained when using 1 wt% catalyst amount. Increasing of catalyst amount to 10 wt% leads the %conversion slightly increases to 96.2 %, indicating that the % conversion slightly depends on the catalyst content and the effect of high temperature. However, the catalyst amount of 0.5 wt% gives smallest % conversion due to the small amount of acid site of catalyst.

Table 4.10 Values of % conversion and % yield obtained by thermal cracking and catalytic cracking of HDPE waste over zeolite beta (SBA-15/AIP = 60, Run No.5) various catalyst amounts at 400°C (Conversion: N_2 flow of 20 cm^3/min. and reaction time of 40 min).

	Catalyst amount					
	0.5%	**1%**	**3%**	**5%**	**10%**	**Thermal 400°C**
%conversion	63.9	95.0	96.2	95.7	95.5	2.4
%yield						
1. gas fraction	30.9	36.5	38.2	35.4	37.9	2.4
2.liquid fraction	36.1	58.5	58.0	60.3	57.6	-
- distillate oil		43.2	42.7	45.7	43.3	-
- heavy oil		15.3	15.3	14.6	14.3	-
3. residue	32.9	5.0	3.7	4.3	4.5	97.6
- wax	-	4.2	1.86	3.6	2.8	-
- solid coke	-	0.8	1.84	0.7	1.7	-
4. Total volume of liquid fraction (ml)	2.28	3.97	4.12	4.20	4.02	-
5.Liquid faction density (g/cm^3)	0.71	0.71	0.70	0.72	0.71	-

[a] *Deviation within 0.20%,* [b] *Deviation within 0.40%*
[c] *Deviation within 0.30%,* [d] *Deviation within 0.20%*

131

The accumulated volume of liquid fractions obtained by catalytic cracking of HDPE waste over zeolite beta with SBA-15/AIP ratio of 60 catalyst with different catalyst amount at 400°C is shown in Figure 4.48. The initial rate of liquid fractions formation in the reaction using 1.0-10.0 wt% catalyst content is not significant different except 0.5 wt% catalyst content shows slowly initial rate.

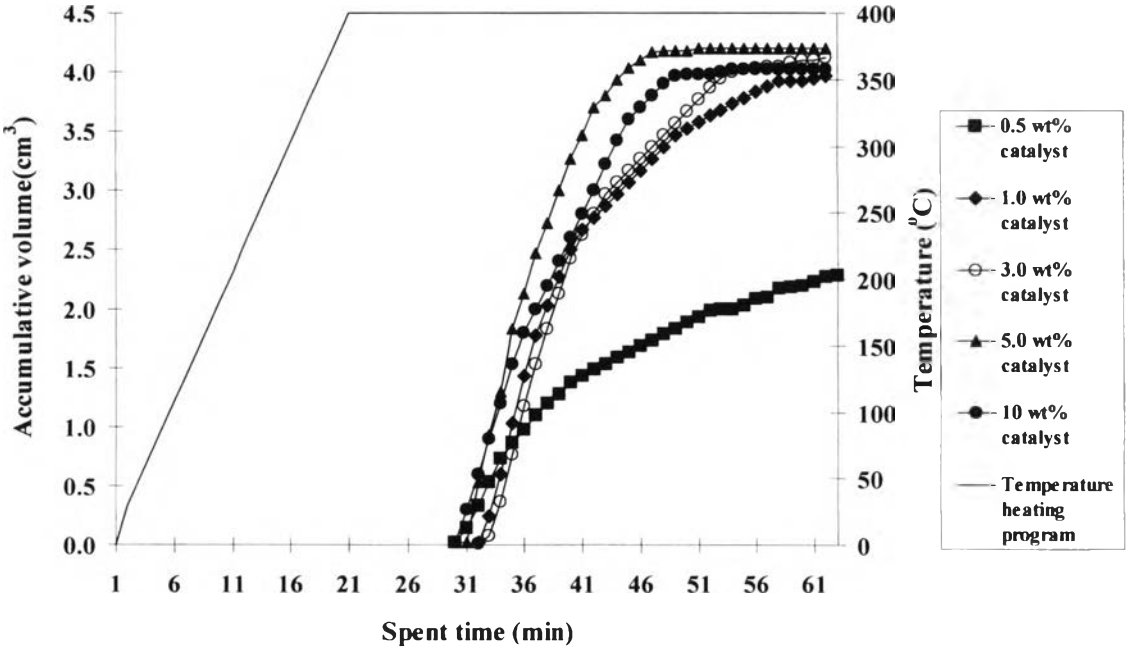

Figure 4.48 Accumulative volume of liquid fractions from catalytic cracking of HDPE waste over zeolite beta (SBA-15/AIP = 60, Run No.5) various catalyst amounts.

Figure 4.49 shows distribution plot of gas fractions obtained by catalytic cracking of HDPE waste over zeolite beta with SBA-15/AIP ratio of 60 catalyst with different catalyst amount at 400°C. The mainly gas fractions from HPED waste cracking are propene, *n*- butane, *i*-butene and C_5^+. Although the product distributions in gaseous phase for 3 wt%, 5 wt% and 10 wt% catalyst content are slightly different. As the catalysts amount to 1 wt% and 0.5 wt% the propene, *n*- butane and *i*-butene are decreased. The product distributions of distillated oil obtained by catalytic cracking of HDPE waste over zeolite beta with SBA-15/AIP ratio of 60 catalyst with different catalyst amount at 400°C are shown in Figure 4.50. The product distributions in liquid phase for all catalyst are slightly different. The C_7 and C_8 are mainly product on

cracking HDPE waste using all catalyst. When catalyst amount is 10 wt% gives highest the C_7 and C_8. In this work, using 1, 3, 5 and 10 wt% catalyst content in HDPE waste cracking at 400°C give the high %conversion due to thermal cracking is occurred together with catalytic cracking.

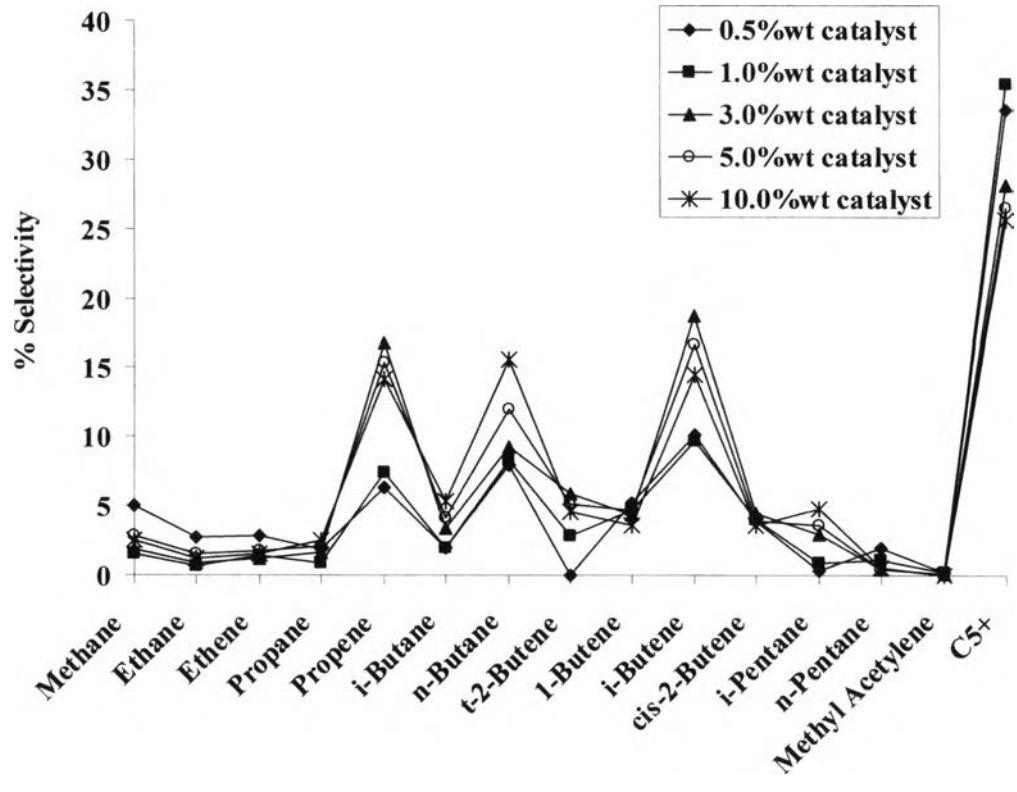

Figure 4.49 Distribution of gas fractions obtained by catalytic cracking of HDPE waste using zeolite beta (SBA-15/AIP = 60, Run No.5) various catalyst amounts.

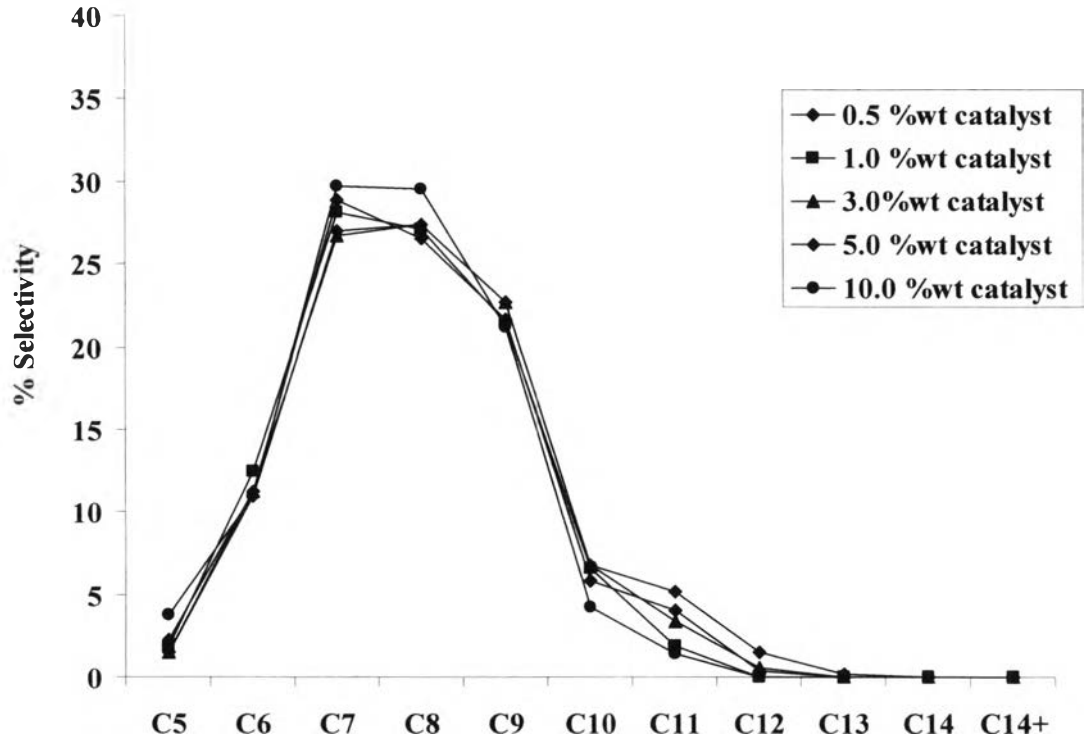

Figure 4.50 Distribution of liquid fractions obtained by catalytic cracking of HDPE waste using zeolite beta (SBA-15/AIP = 60, Run No.5) various catalyst amounts.

In this work, we need to studies the effect of catalyst amount on HDPE waste cracking so we must reduce the reaction temperature to avoid thermal effect. Table 4.11 shows values of % conversion and % yield obtained by catalytic cracking of HDPE waste over zeolite beta with SBA-15/AIP ratio of 60 catalysts at different catalyst amount at 380°C. The % conversion values are not different from catalyst content 3 wt% to 10 wt%, the value are in the range from 85.7 to 88.1%. The %conversion decreases when using catalyst content of 1 wt% and increases residue. Due to the high %conversion and low residue of catalyst content 3, 5 and 10 wt%, the results are not different so the optimum catalyst amount that we choose is the 3 wt% catalyst to HDPE. Due to it gives a high % conversion and uses small amount of catalyst.

Table 4.11 Values of % conversion and % yield obtained by thermal cracking and catalytic cracking of HDPE waste over zeolite beta (SBA-15/AIP = 60, Run No.5) various catalyst amounts at 380°C (Conversion: N_2 flow of 20 cm^3/min. and reaction time of 40 min).

	Catalyst amount				
	1%	**3%**	**5%**	**10%**	**Thermal 380°C**
%conversion[a]	71.2	85.7	89.4	88.1	0.3
%yield					
1. gas fraction[b]	29.1	38.1	36.1	39.6	0.3
2. liquid fraction[c]	41.9	47.6	53.3	48.4	-
- distillate oil	32.0	35.1	39.5	37.2	-
- heavy oil	9.9	12.5	13.8	11.2	-
3. residue	28.8	14.3	10.6	11.9	99.7
- wax	-	-	6.9	9.9	-
- solid coke	-	-	3.7	2.0	-
4. Total volume of liquid fraction (ml)	2.55	2.95	3.25	3.15	-
5.Liquid faction density (g/cm^3)	0.75	0.72	0.73	0.72	-

[a] *Deviation within 0.30%,* [b] *Deviation within 0.23%*
[c] *Deviation within 0.30%,* [d] *Deviation within 0.30%*

The accumulated volume of liquid fractions by catalytic cracking of HDPE waste over zeolite beta with SBA-15/AIP ratio of 60 catalysts with different catalyst amounts at 380°C is show in Figure 4.51. The initial rates of liquid factions formation in reaction using 5 wt% and 10 wt% catalyst content is slightly different, as well as total liquid volumes. The initial rates of liquid factions formation in reaction using 3 wt% and 1 wt% catalyst content is not significant different.

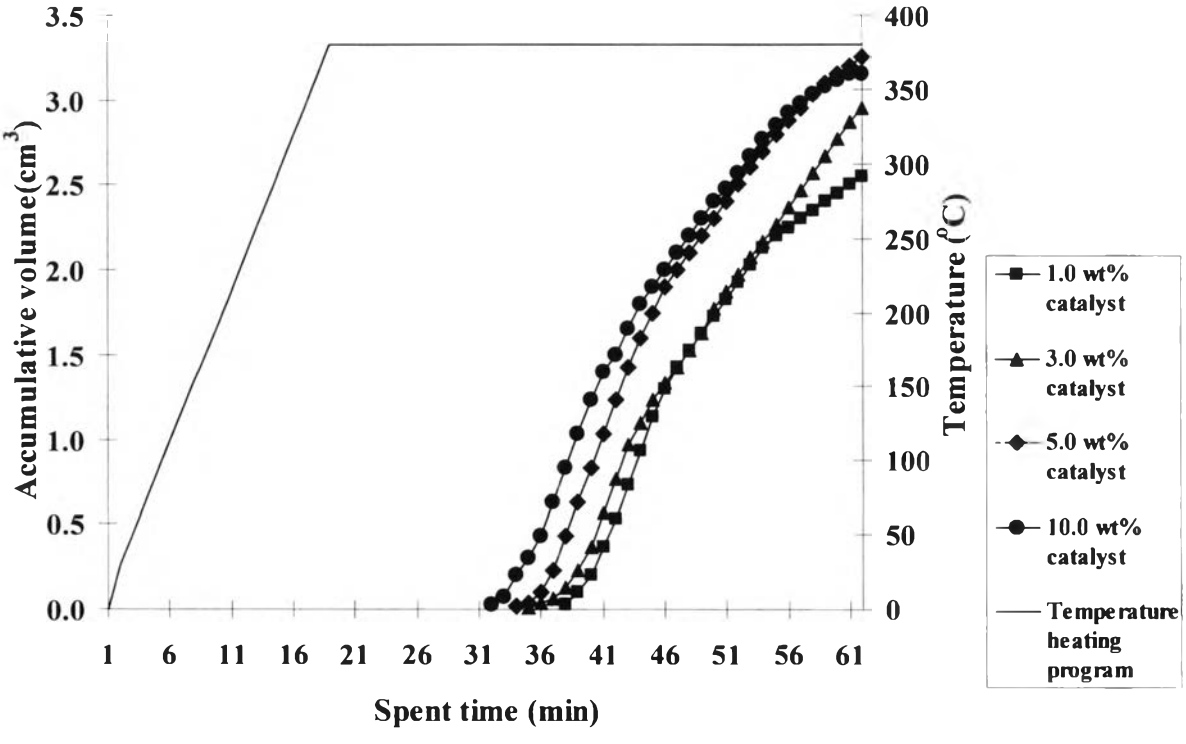

Figure 4.51 Accumulative volume of liquid fractions from catalytic cracking of HDPE waste over zeolite beta (SBA-15/AIP = 60, Run No.5) various catalyst amounts.

Figure 4.52 shows distribution of gas fractions obtained by catalytic cracking of HDPE waste over various zeolite beta with SBA-15/AIP ratio of 60 catalysts at catalyst amount at 380°C. The mainly gas fractions from HDPE waste cracking are propene, *n*-butane, *i*-butene and C_5^+. Increasing the catalyst amount to 10 wt% decrease the heavy hydrocarbon (i-butene) and increase lighter hydrocarbon (methane, ethane and ethane). The distribution of liquid fractions obtained by catalytic cracking of HDPE waste over various zeolite beta with SBA-15/AIP ratio of 60 catalysts at catalyst amount at 380°C are shown in Figure 4.53. The mainly product distribution in liquid phase for all catalyst amounts are C_7 and C_8 on cracking of HDPE waste.

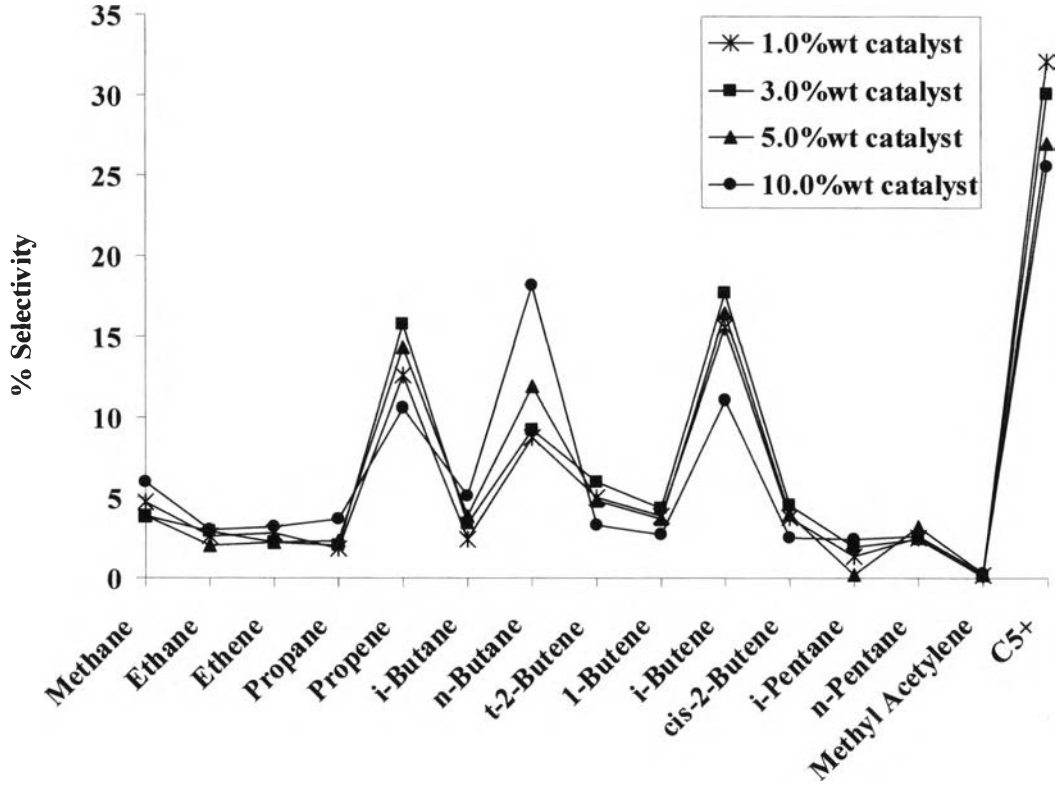

Figure 4.52 Distribution of gas fractions obtained by catalytic cracking of HDPE waste using zeolite beta (SBA-15/AIP = 60, Run No.5) various catalyst amounts.

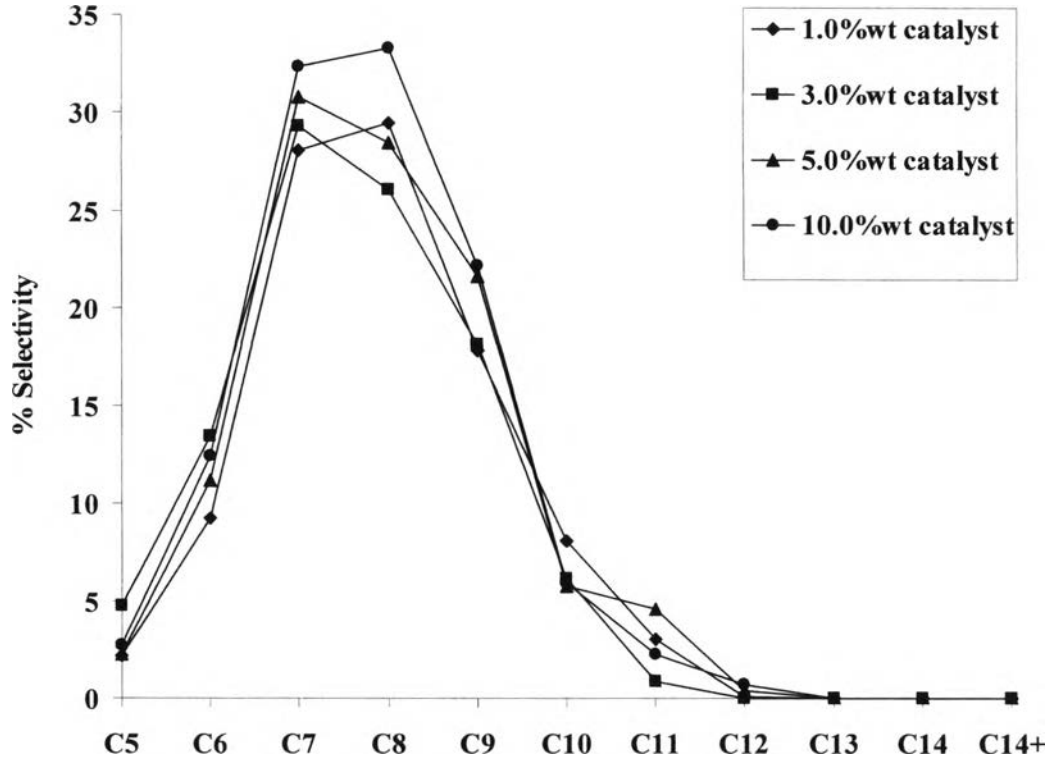

Figure 4.53 Distribution of liquid fractions obtained by catalytic cracking of HDPE waste using zeolite beta (SBA-15/AIP = 60, Run No.5) various catalyst amounts.

4.4.4 Activities of Regenerated BEA in HDPE Waste Cracking

Table 4.12 shows the values of % conversion and % yield obtained by catalytic cracking of HDPE waste using the fresh and regenerated catalyst at 400°C. The value of %conversion obtained in the first regenerated is not different from the fresh catalyst, whereas the third regenerated are significantly from fresh catalyst. The % conversion and products yield are decreased from fresh catalyst when the regenerated over 2 cycles. These results suggest the regenerated catalyst have less acidity and specific surface area than fresh catalyst. Due to the several calcinations before used produce Al in framework migration to non-framework. It illustrious that in the cracking of C-C bonds the acidity of catalysts plays an important role; primary cracking reaction of polymer chain proceed on macroporous surface area of catalyst,

while the smaller fragment are cracked on their micropore surface. The second and third regenerated catalysts have the lower acidity and specific surface area than fresh and first regenerated resulting in the low gas fraction yield.

Table 4.12 Values of % conversion and % yield obtained by catalytic cracking of HDPE waste using the fresh and the regenerated catalysts at 400°C (Conversion: 3 wt% catalyst of plastic, N_2 flow of 20 cm^3/min. and reaction time of 40 min).

	Fresh BEA60	**1st Regenerated Run No.5**	**2nd Regenerated Run No.5**	**3rd Regenerated Run No.5**
%conversion[a]	96.2	96.9	95.8	90.9
%yield				
1. gas fraction[b]	38.2	32.3	34.3	32.8
2.liquid fraction[c]	58.0	64.6	61.5	58.9
- distillate oil	42.7	48.0	44.5	41.6
- heavy oil	15.3	16.6	17.0	17.3
3. residue[d]	3.7	3.1	4.2	9.1
- wax	1.86	1.2	2.0	5.6
- solid coke	1.84	1.9	2.2	3.5
4. Total volume of liquid fraction (ml)	4.12	4.40	4.30	3.75
5. Liquid faction density (g/cm^3)	0.70	0.72	0.72	0.72

[a] *Deviation within 0.45%,* [b] *Deviation within 0.71*
[c] *Deviation within 0.71%,* [d] *Deviation within 0.71%*

Figure 4.54 shows the accumulative volume of liquid fractions. The initial rates of liquid formation are slightly different when using the fresh and the first regenerated catalyst. For the second and the third regenerated the initial rate are slower than fresh and first regenerated due to the less acidity and specific surface area.

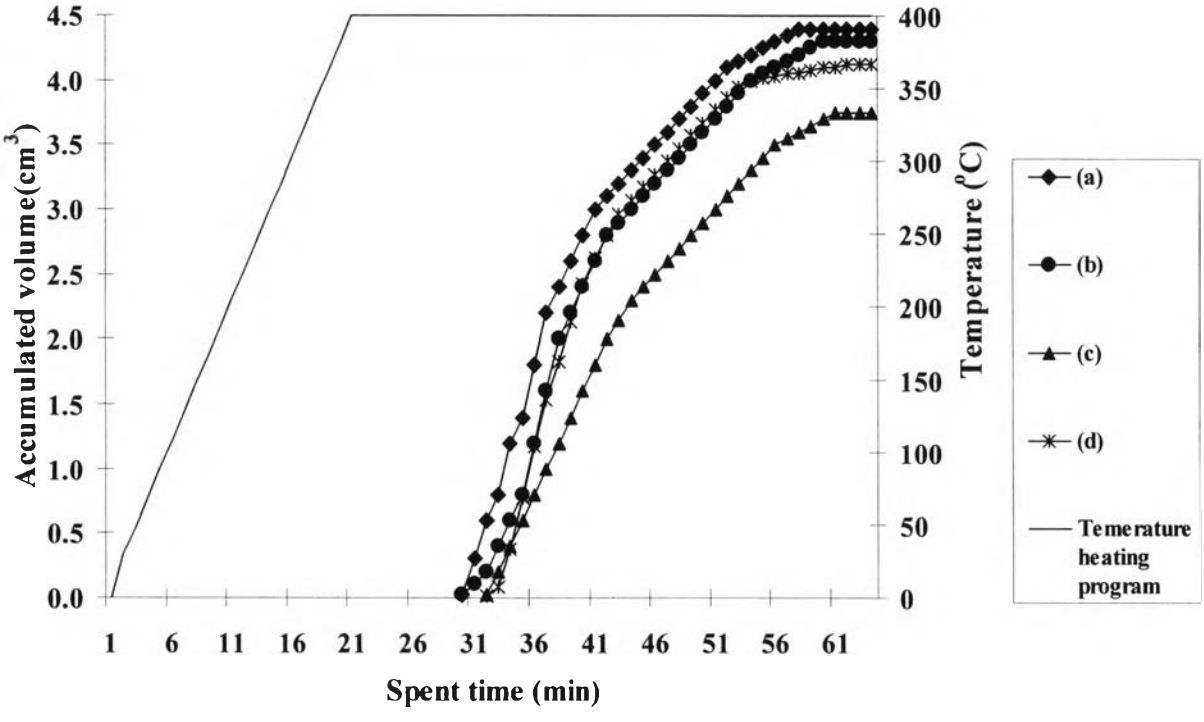

Figure 4.54 Accumulative volume of liquid fractions from catalytic cracking of HDPE waste using the fresh and the regenerated catalysts (SBA-15/AIP = 60, Run No.5): (a) the 1st regenerated; (b) 2nd regenerated; (c) 3rd regenerated catalyst and (d) fresh catalyst.

The distribution of gases component formed in HDPE cracking over the fresh and regenerated zeolite beta with SBA-15/AIP ratio of 60 catalysts at 400°C is shown in Figure 4.55. The gas fraction composes the same product distribution but there are slightly differences in selectivity of gas fractions between the four catalysts. The mainly gas fraction from HDPE waste cracking are propene, *i*-butene and C_5^+.

Figure 4.56 shows product distribution of liquid fractions obtained by the HDPE waste cracking using the fresh and the regenerated zeolite beta with SBA-15/AIP ratio of 60 catalysts at 400°C. The liquid fraction distributions of all catalyst are slightly different and provide mainly C_7 and C_8 in liquid fraction.

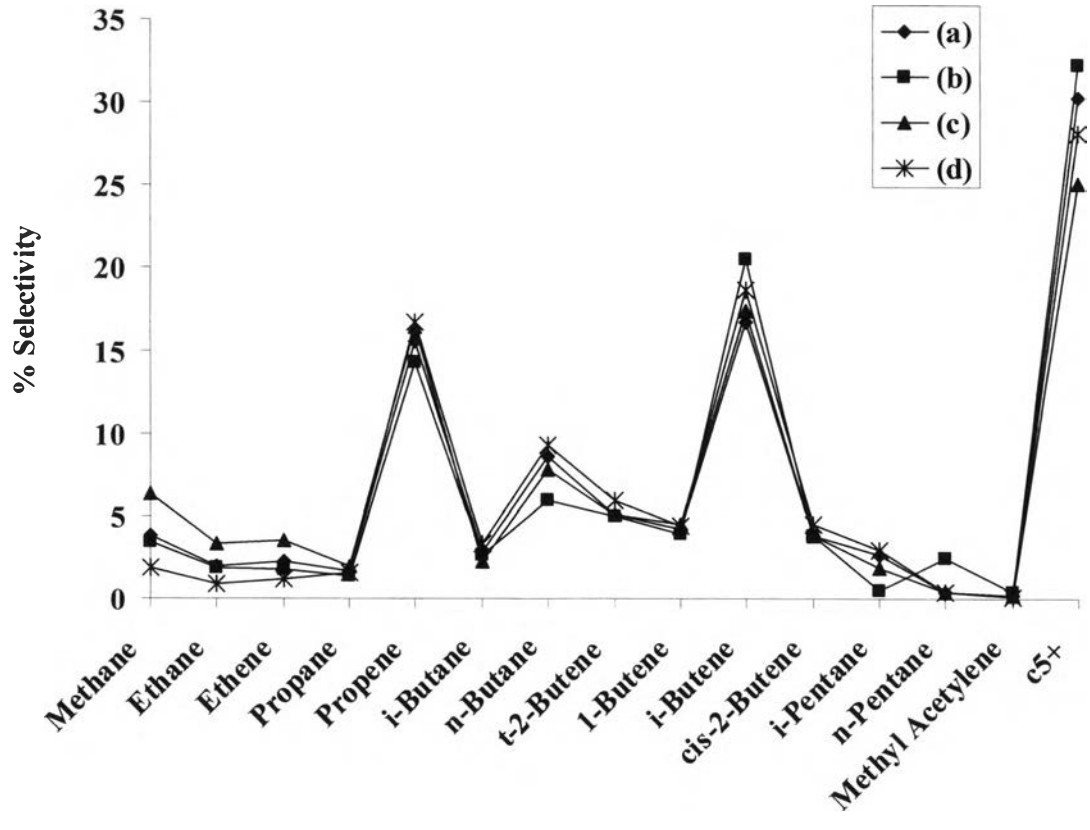

Figure 4.55 Distribution of gas fractions obtained by catalytic cracking of HDPE waste using the fresh and the regenerated catalysts (SBA-15/AIP = 60, Run No.5): (a) the 1st regenerated; (b) 2nd regenerated; (c) 3rd regenerated catalyst and (d) fresh catalyst.

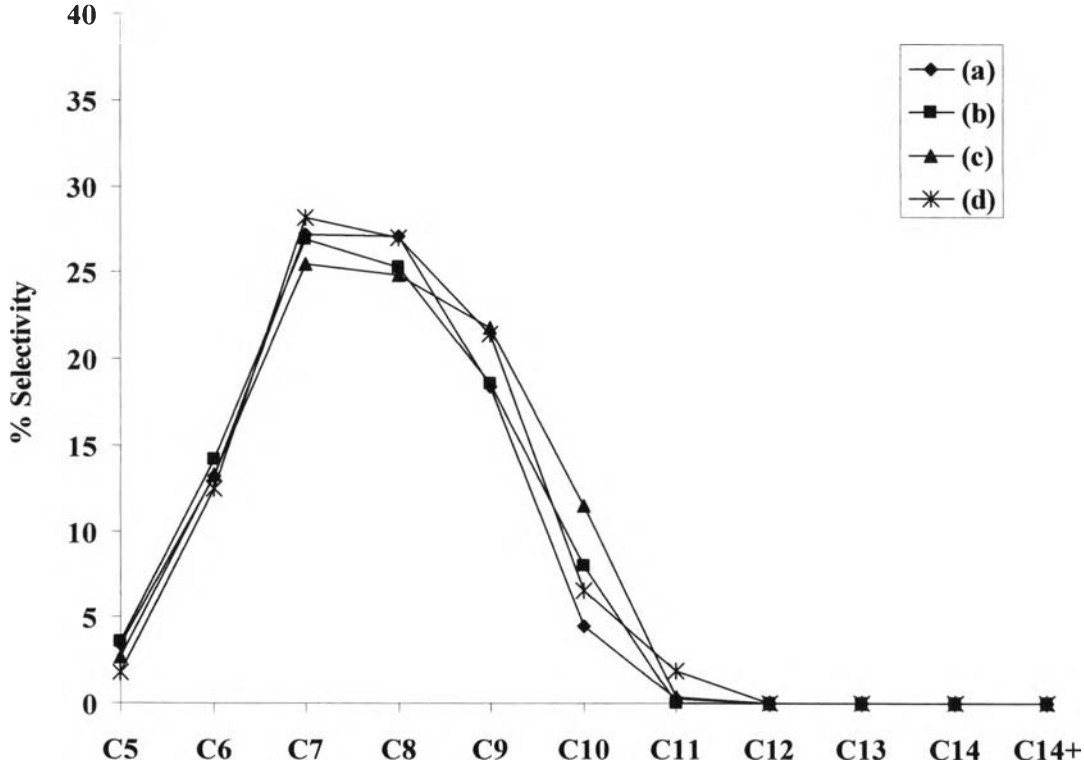

Figure 4.56 Distribution of liquid fractions obtained by catalytic cracking of HDPE waste using the fresh and the regenerated catalysts (SBA-15/AIP = 60, Run No.5): (a) the 1st regenerated; (b) 2nd regenerated; (c) 3rd regenerated catalyst and (d) fresh catalyst.

4.4.5 Regenerated Catalyst (HDPE)

4.4.5.1 XRD Results

The used zeolite beta with SBA-15/AIP ratio of 60 catalysts became black after use due to coke deposit on the surface and in pores. However, it easily turned to white after regeneration by calcinations in muffle furnace at 550°C for 5 h due to the complete removal coke. XRD patterns of the calcined unused and regenerated zeolite beta with SBA-15/AIP of 30 catalysts are shown in Figure 4.57. After catalytic run, the structure of zeolite beta was still remained for the 1st regenerated (firstly regenerated), 2nd regenerated (secondly regenerated) and 3rd

regenerated (thirdly regenerated) catalysts with almost the same crystallinity as the unused catalyst. It Indicates that the high stability of zeolite beta structure.

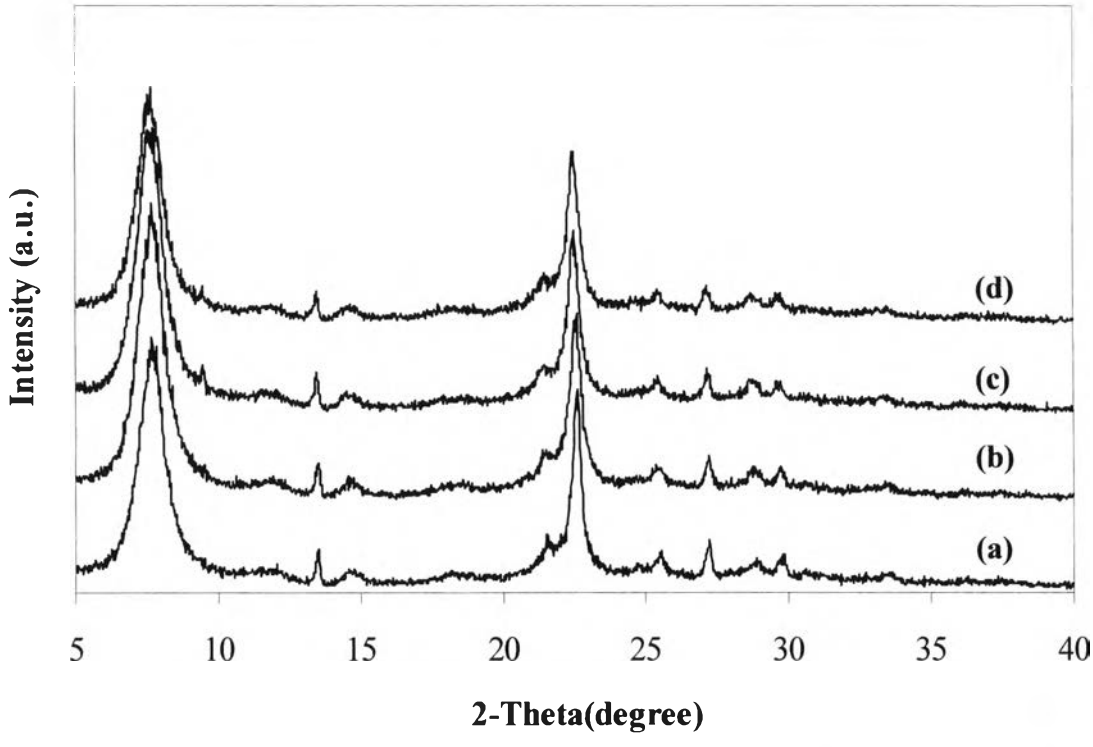

Figure 4.57 XRD pattern of (a) the calcined unused; (b) the 1st regenerated; (c) 2nd regenerated and (d) 3rd regenerated catalyst.

4.4.5.2 SEM Images

Figure 4.58 shows SEM images of the 3rd regenerated catalyst with different magnification. After the third regenerated catalytic run, it is obvious that the regenerated catalyst particle are not changed morphology with similar particle size compared to the fresh catalyst picture of which has been shown in Figure 4.20(c).

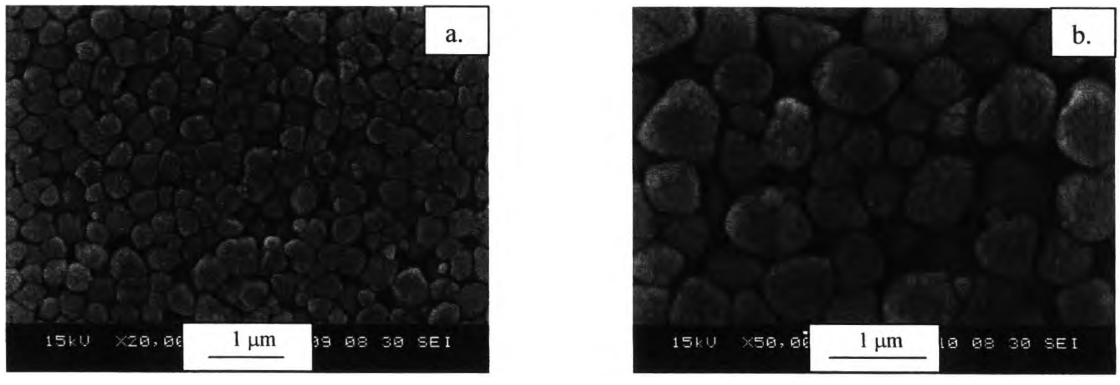

Figure 4.58 SEM images of 3rd regenerated Run No.5 sample with different magnification (a) x20,000 and (b) x 50,000.

4.4.5.3 Nitrogen Adsorption-Desorption

The adsorption-desorption isotherms of fresh and regenerated catalysts are shown in Figure 4.59. The calcined unused, 1st regenerated, 2nd regenerated, 3rd regenerated and fresh catalyst exhibits the characteristic isotherm of microporous material with the specific surface area of 704, 679, 601 and 781 m^2/g. It was sharply decreased compared with the fresh catalyst.

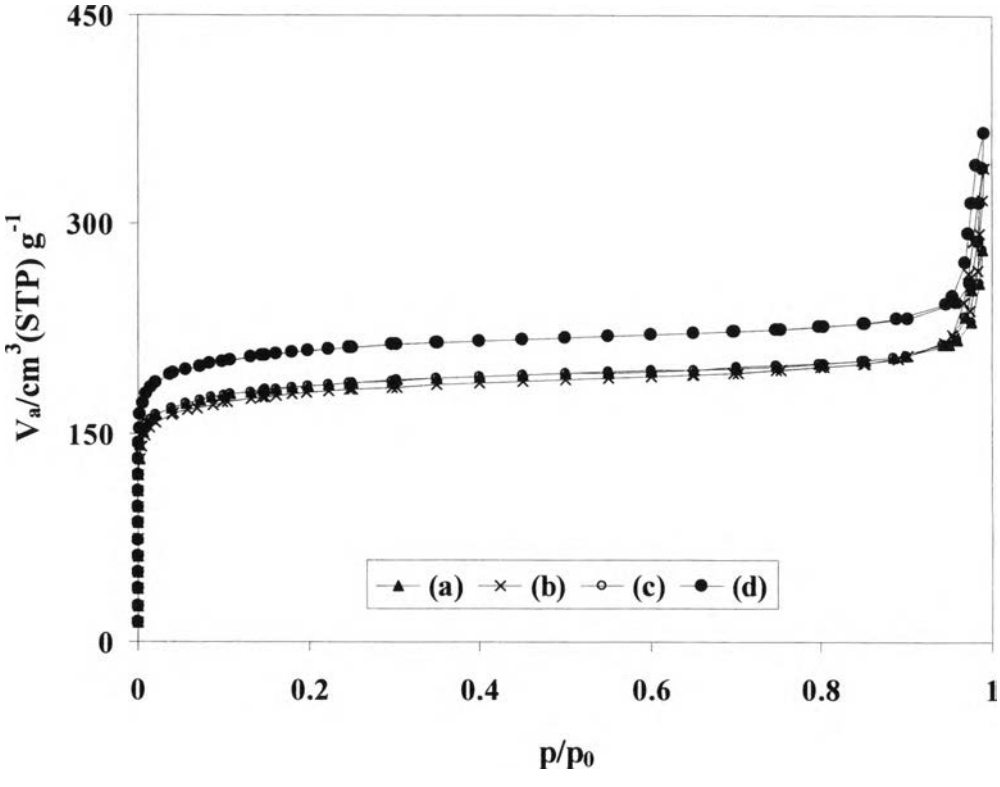

Figure 4.59 N_2 adsorption-desorption isotherms of the regenerated and fresh catalyst: (a) the 1st regenerated; (b) 2nd regenerated; (c) 3rd regenerated catalyst and (d) fresh catalyst.

4.5 Activities of Various Zeolite Beta Catalysts in PP-Derived Crude Oil Cracking

4.5.1 Effect of PP-Derived Crude Oil to Catalyst Ratios

Values of conversion and product yield from PP-Derived crude oil cracking over zeolite beta with the SBA-15/AIP ratio of 30 at 300°C with different catalyst amounts of 1.0, 3.0, 5.0 and 10.0 wt% to PP-Derived crude oil are shown in Table 4.13. The high conversion value of 87.4, 88.1, 89.6% and 87.4 are obtained in the cases of using 3.0 wt%, 5.0 wt% and 10.0 wt% catalyst amounts. Reducing of catalyst amount to 1 wt% leads the %conversion drops to 67.1%, indicating that the

conversion strongly depends on the catalyst amount. The product yield, the gas fraction yield decrease when the amount of catalyst reduces. Basically, the less catalyst amount, the less acidity resulting in the less gas fraction yield. The optimum catalyst amount is the 5.0 wt% catalyst to PP-Derived crude oil due to the high %conversion and highest distillated oil.

Table 4.13 Values of % conversion and % yield obtained by catalytic cracking of PP-Derived crude oil over zeolite beta (SBA-15/AlP = 30, Run No.9) various catalyst amounts at 300°C (Conversion: N_2 flow of 20 cm^3/min. and reaction time of 40 min).

	Catalyst amount				
	Thermal				
	300°C	**1.0%**	**3.0%**	**5.0%**	**10.0%**
%conversion	58.7	67.1	87.4	88.1	89.6
%yield					
1. gas fraction	6.7	9.6	14.3	13.6	13.7
2. liquid fraction	52.0	57.5	73.1	74.5	75.1
- distillate oil	45.6	50.2	58.9	63.0	61.8
- heavy oil	6.4	7.3	14.2	11.5	13.3
3. residue	41.3	32.9	12.6	11.9	10.5
- wax	-	30.3	11.2	10.5	8.9
- solid coke	-	2.6	1.4	1.34	1.6
4. Total volume of liquid fraction (ml)	3.50	3.88	5.07	5.02	5.42

[a] *Deviation within 0.30* [b] *Deviation within 0.40%*
[c] *Deviation within 0.35* [d] *Deviation within 0.30%*

Figure 4.60 shows the kinetic rate in catalytic cracking of PP-Derived crude oil over various amounts of zeolite beta catalyst at 300°C. The initial rates of liquid fraction in the reaction using 3.0 wt%, 5.0 wt% and 10.0 wt% catalyst amounts are not different except 1.0 wt%. The predominant competitive rate of dissociation of liquid molecules to gas molecules compared to the rate of liquid formation.

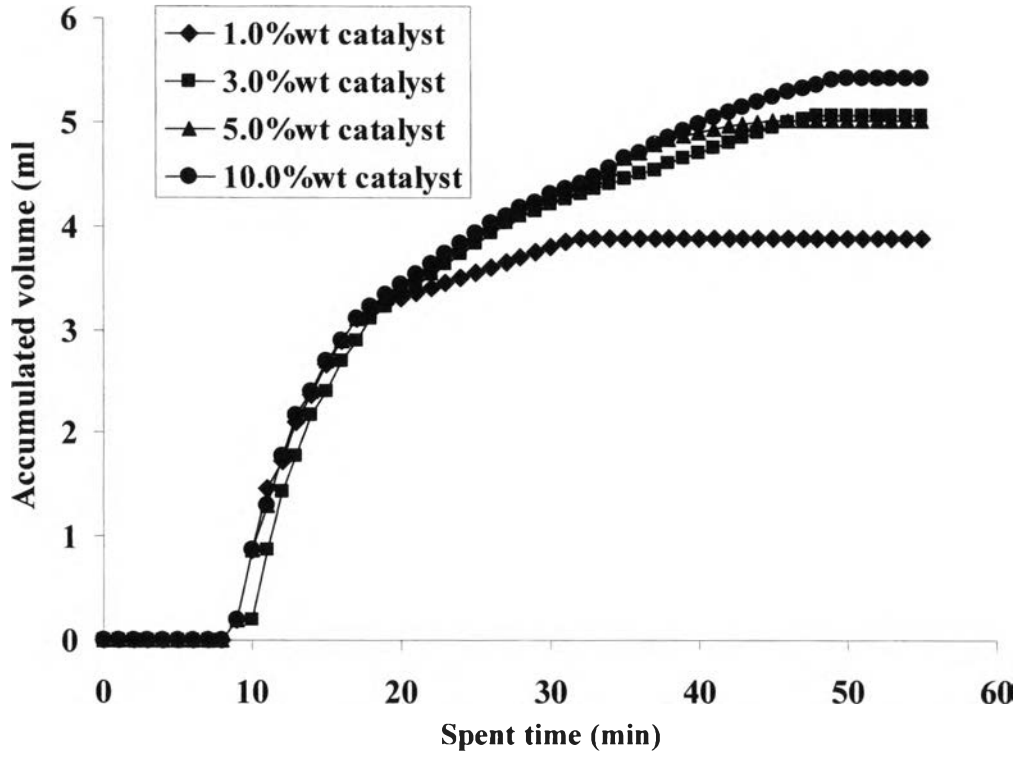

Figure 4.60 Accumulative volume of liquid fractions from catalytic cracking of PP-Derived crude oil over zeolite beta (SBA-15/AIP = 30, Run No.9) various catalyst amounts.

Figure 4.61 shows distribution plots of gas fraction obtained by catalytic cracking and thermal cracking of PP-Derived crude oil over zeolite beta with SBA-15/AIP ratio of 30 catalyst with different catalyst amount at 300°C. The favored gaseous products are *i*-butene, *n*-pentane and C_5+. The selectivity of gas fraction for 5.0 wt% and 10.0 wt% catalyst amounts are similar but different from that for the 1.0 wt% and 3.0 wt% catalyst amounts. However, the methane, ethane, propene and *n*-butane of all catalyst decrease due to PP-Derived crude oil are easy to crack completely, the result show high solid coke. The product distributions of light oil

obtained by catalytic cracking and thermal cracking of PP-Derived crude oil over zeolite beta catalysts with different catalyst amounts at 300°C are shown in Figure 4.62. The product distributions in liquid phase for all catalysts are not significantly different. For the major products are C_9 until C_6-C_8 (gasoline rang) decrease because of the many solid coke are occurred during reaction. The pores of catalyst are filled with solid coke as a result of gasoline decrease.

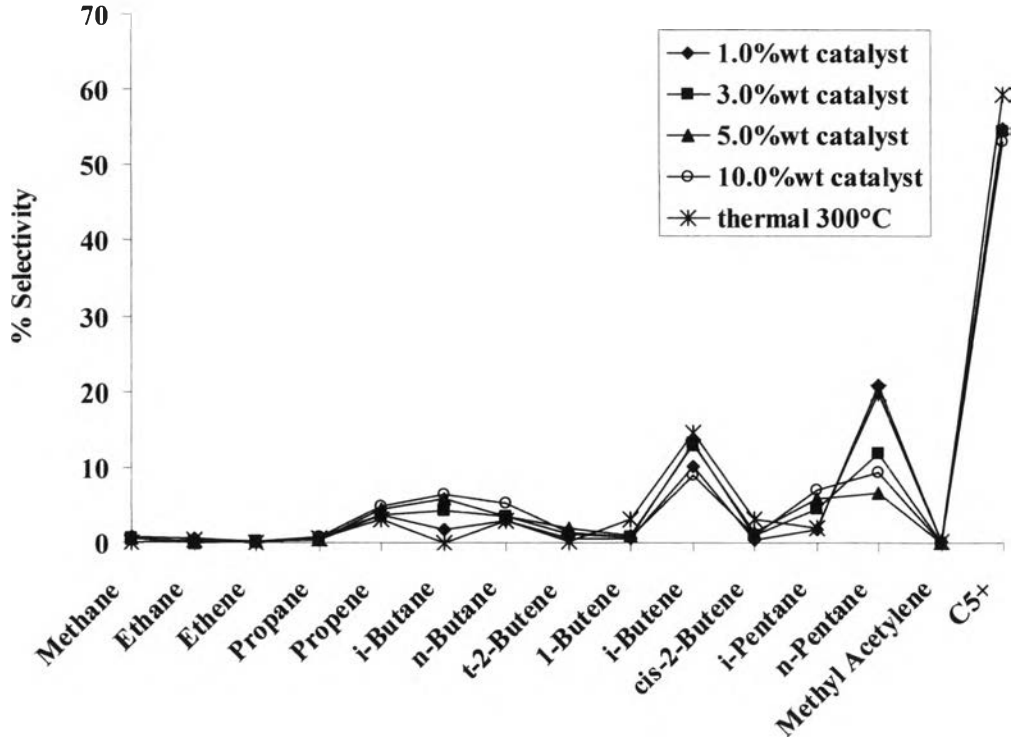

Figure 4.61 Distribution of gas fractions obtained by catalytic cracking of PP-Derived crude oil using zeolite beta (SBA-15/AIP = 30, Run No.9) various catalyst amounts.

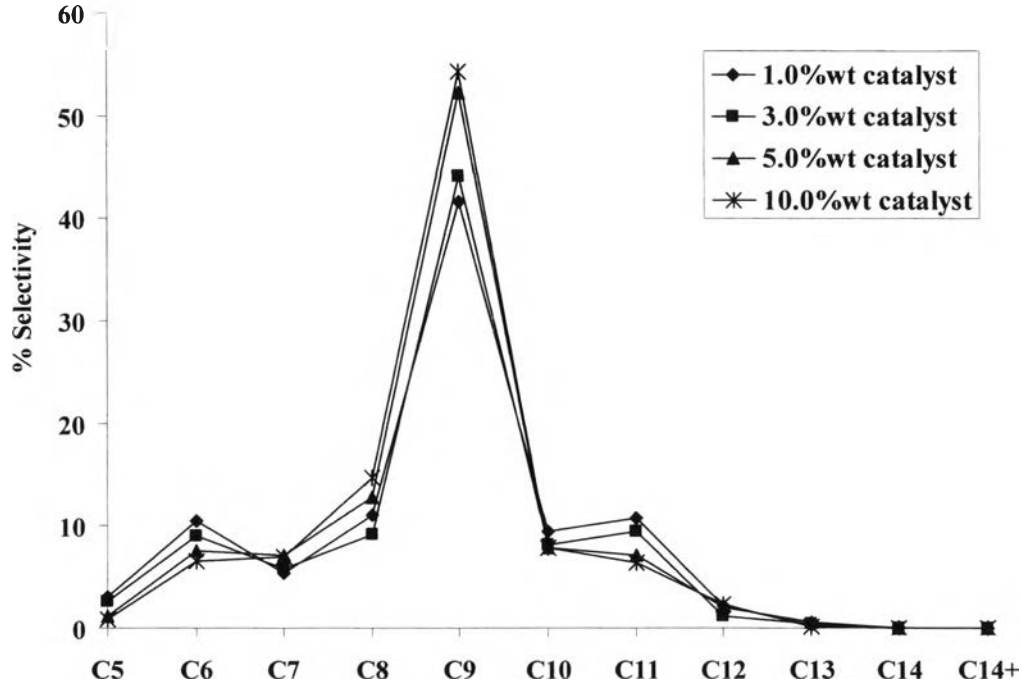

Figure 4.62 Distribution of liquid fractions obtained by catalytic cracking of PP-Derived crude oil using zeolite beta (SBA-15/AIP = 30, Run No.9) various catalyst amounts.

4.5.2 Effect of Reaction Temperature

Zeolite beta with the SBA-15/AIP of 30 was used as a catalyst for studying the influence of temperature on its activity and the thermal cracking was tested in comparison. The values of %conversions and product distribution for thermal and catalytic cracking of PP-Derived crude oil at 300, 350 and 400°C are shown in Table 4.14.

Table 4.14 Values of % conversion and % yield obtained by thermal cracking and catalytic cracking of PP-Derived crude oil over zeolite beta (SBA-15/AIP = 30, Run No.9) various temperatures. (Conversion: 5 wt% catalyst of plastic, N_2 flow of 20 cm^3/min. and reaction time of 40 min).

	Thermal 300°C	**300°C**	**Thermal 350°C**	**350°C**	**Thermal 380°C**	**380°C**	**Thermal 400°C**	**400°C**
%conversion	58.7	87.4	72.7	94.8	88.8	94.7	91.5	95.0
%yield								
1. gas fraction	6.7	14.3	12.9	16.6	12.3	15.5	12.5	15.0
2.liquid fraction	52.0	73.1	59.8	78.2	76.5	79.2	79.0	80.0
- distillate oil	45.6	58.9	48.1	63.2	62.5	65.6	66.4	66.9
- heavy oil	6.4	14.2	11.7	15.0	14.0	13.6	12.6	13.1
3. residue	41.3	12.6	27.3	5.2	11.1	5.3	8.5	5.0
- wax	-	11.2	-	3.78	-	3.78	-	3.44
- solid coke	-	1.4	-	1.42	-	1.52	-	1.56
4. Total volume of liquid fraction (ml)	3.50	5.02	4.35	5.23	5.18	5.38	5.28	5.42

[a] *Deviation within 0.20* [b] *Deviation within 0.23*
[c] *Deviation within 0.30* [d] *Deviation within 0.20*

The activities of PP-Derived crude oil in term of %conversion and product distribution are very high up to 94% at all temperature from 350 to 400°C and are temperature independent. Below the temperature of 350°C the %conversion is affected by the temperature, the conversion decreases with decreasing the cracking temperature. Considering at temperature in the range 350°C to 400°C, the products are mainly in liquid fraction at the high yield about 78.2-80.0 % with minor product in gas fraction at the yield about 15.0-16.6 %. The effect of zeolite beta on PP-Derived crude oil cracking clearly observes at the residue of catalytic cracking dramatically reduces from 27.3% to 5.0% compared with thermal cracking and solid coke increase with increasing the temperature. The only difference is the initial rate of liquid formation as interpreted from Figure 4.63 which shows the plots of accumulative volume of liquid fraction versus lapsed time for PP-Derived crude oil cracking over zeolite beta with SBA-15/AlP ratio of 30 at various reaction temperatures. When the temperature is increased, the initial rate of liquid formation is not difference. But the accumulated volumes are increase with increasing the temperature. Figure 4.64 shows the plots of accumulative volume of liquid fraction versus lapsed time of PP-Derived crude oil from thermal cracking. The initial rate of liquid formation is slightly difference but the accumulate volumes increase with increasing the temperature.

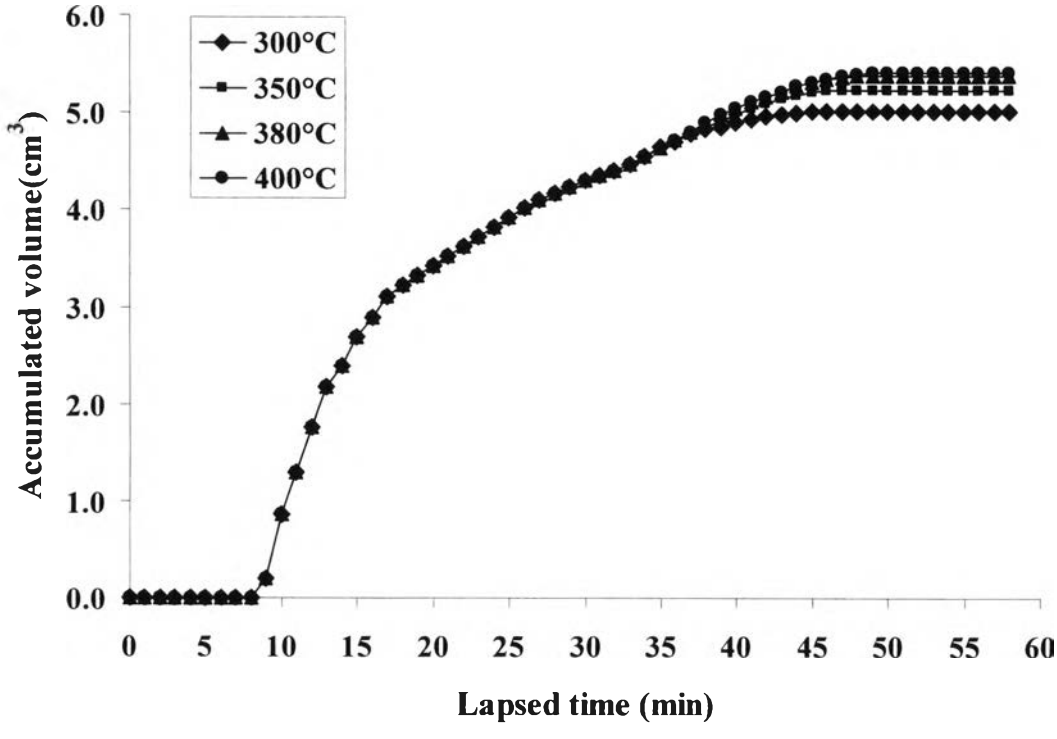

Figure 4.63 Accumulative volume of liquid fractions from catalytic cracking of PP-Derived crude oil over zeolite beta (SBA-15/AIP = 30, Run No.9) various temperatures.

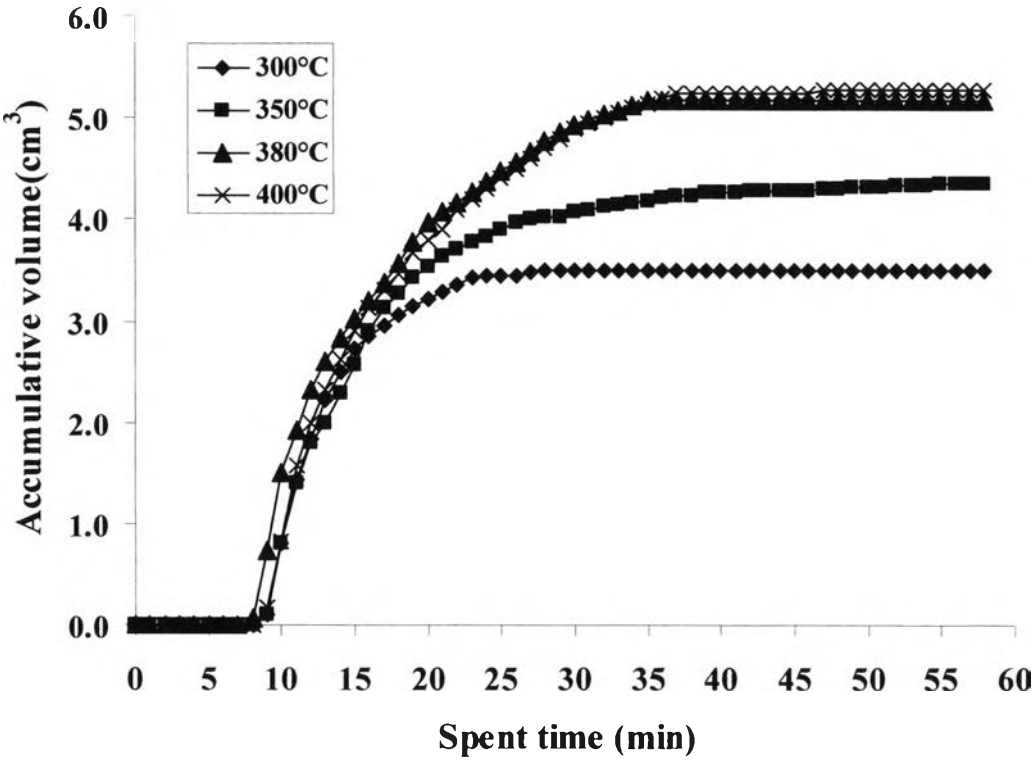

Figure 4.64 Accumulative volume of liquid fractions from thermal cracking of PP-Derived crude oil various temperatures.

Figure 4.65 and 4.66 shows distribution of gas fraction provided by catalytic cracking of PP-Derived crude oil over zeolite beta with the SBA-15/AIP ratio of 30 and thermal cracking at 300, 350, 380 and 400°C. The major component for catalytic cracking is propene, *n*-butane, *i*-butene and C_5^+. Considering of PP-Derived crude oil at ambient condition which are C_1 through C_5, major component for thermal cracking are propene, i-butene and C_5^+. The growing yield of volatile components as function of temperature could be caused by the differences in the thermal stability of polymer chain, because hydrocarbon have reducing thermal stability with increasing temperature. Figure 4.67 and 4.68 shows distribution of liquid fraction provided by catalytic cracking and thermal cracking of PP-Derived crude oil over zeolite beta with the SBA-15/AIP ratio of 30 at various temperatures. The distillate oil major component is C_9 for reaction temperatures at 300-400°C. This result indicates that liquid product distribution not depends on temperature. The

conversion and product distribution obtained at the temperatures of 300°C and 400°C are not different. For thermal cracking at 300-400°C, the liquid fraction is rich of C_9. For the thermal cracking the major product of liquid hydrocarbon fractions are not differences from catalytic cracking.

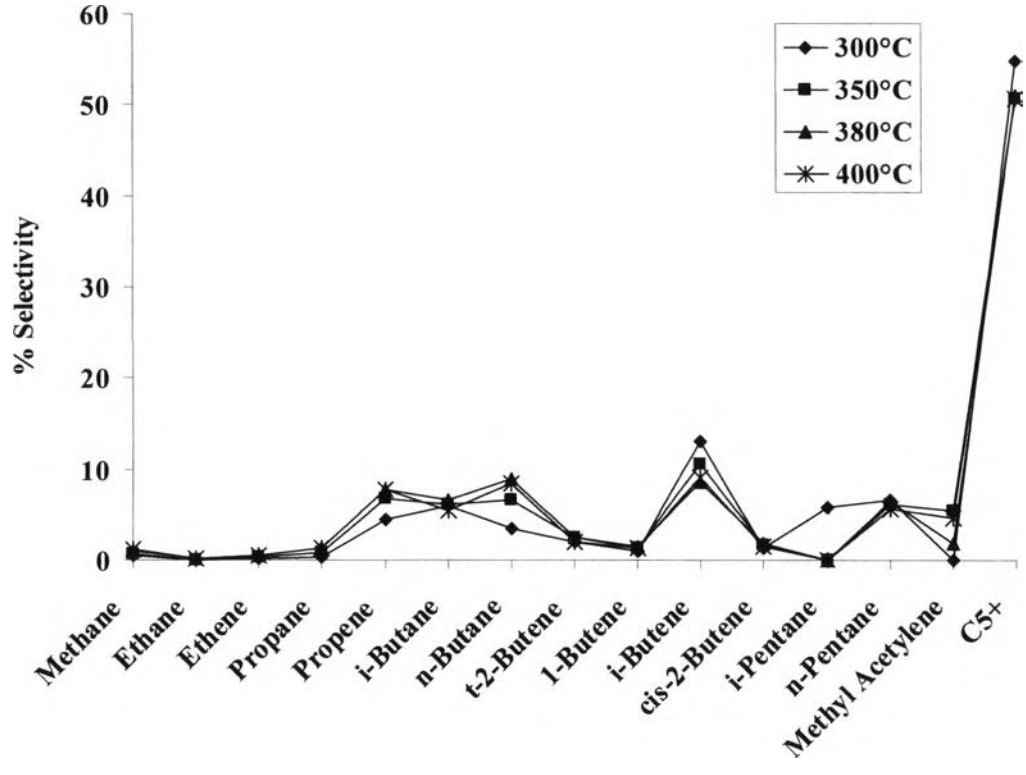

Figure 4.65 Distribution of gas fractions obtained by catalytic cracking of PP-Derived crude oil using zeolite beta (SBA-15/AIP = 30, Run No.9) various temperatures.

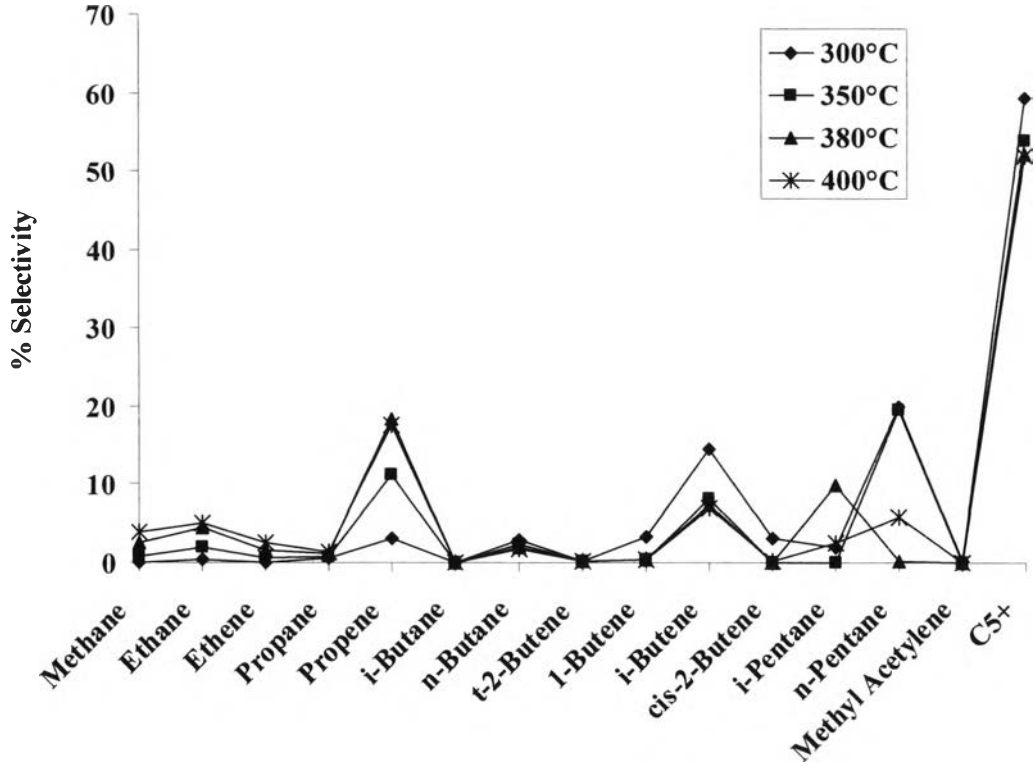

Figure 4.66 Distribution of gas fractions obtained by thermal cracking of PP-Derived crude oil various temperatures.

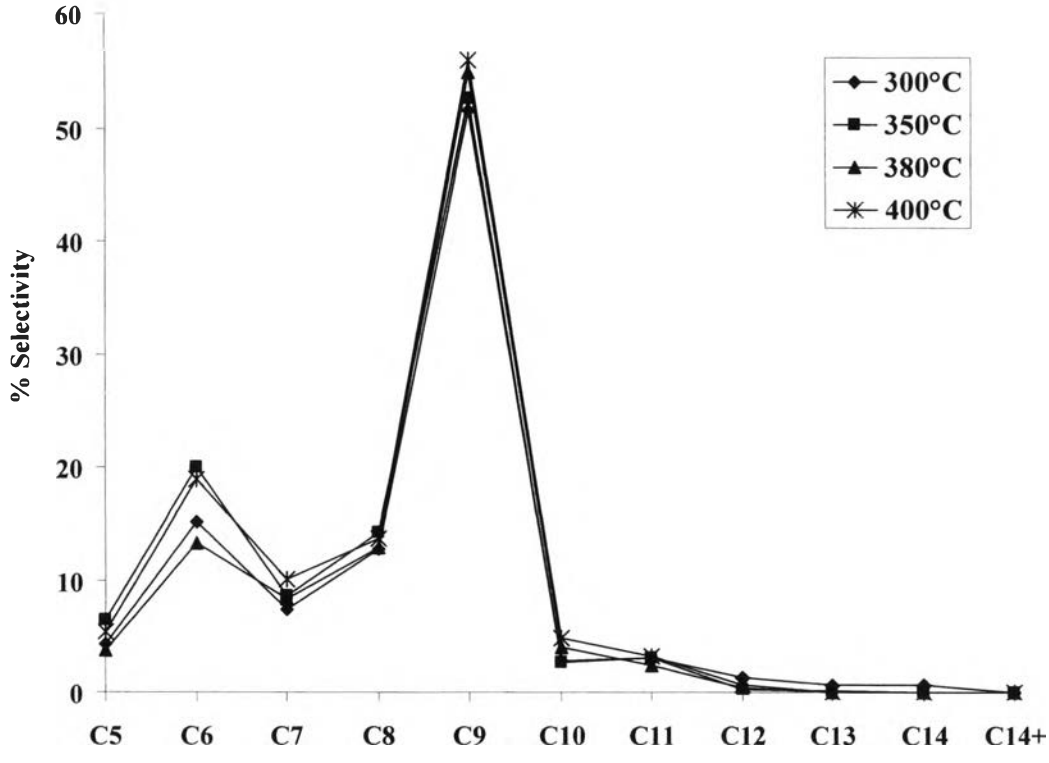

Figure 4.67 Distribution of liquid fractions obtained by catalytic cracking of PP-Derived crude oil using zeolite beta (SBA-15/AIP = 30, Run No.9) various temperatures.

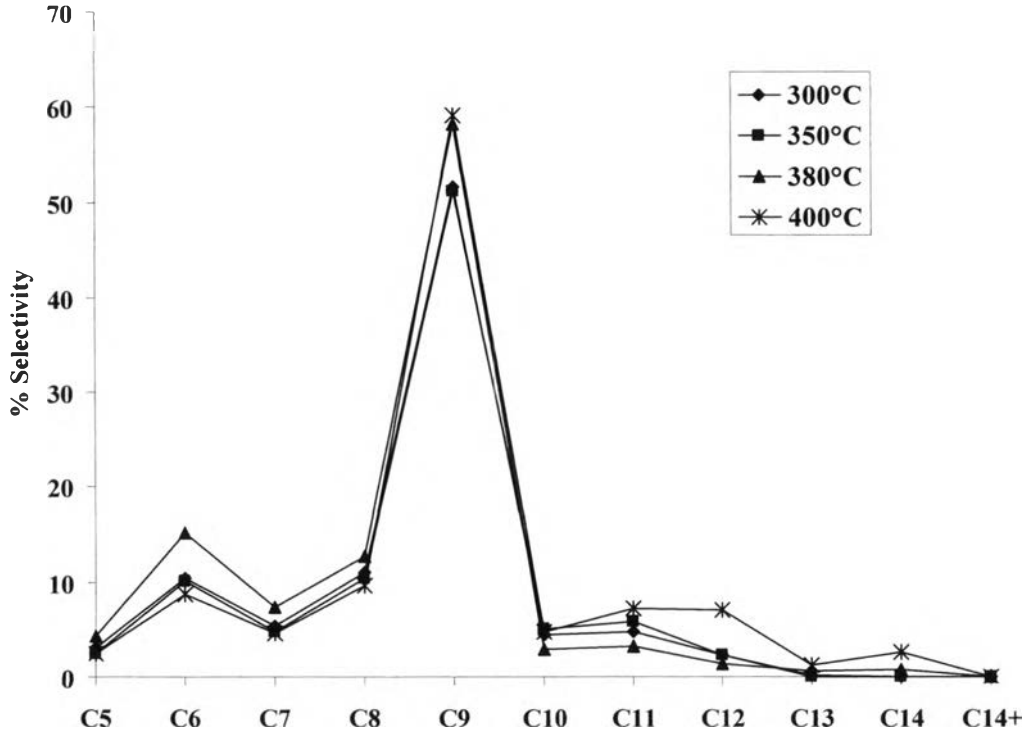

Figure 4.68 Distribution of liquid fractions obtained by thermal cracking of PP-Derived crude oil various temperatures.